AN ALGORITHM FOR THE EXTRACTION OF OCEAN WAVE PARAMETERS FROM WIDE BEAM HF RADAR (CODAR) BACKSCATTER

ERIC WILLIAM GILL, B.Sc., B.Ed.

NOTICE

The quality of this microform is heavily dependent upon the quality of the original thesis submitted for microfilming. Every effort has been made to ensure the highest quality of reproduction possible.

If pages are missing, contact the university which granted the degree.

Some pages may have indistinct print especially if the original pages were typed with a poor typewriter ribbon or if the university sent us an inferior photocopy.

Reproduction in full or in part of this microform is governed by the Canadian Copyright Act, R.S.C. 1970, c. C-30, and subsequent amendments.

AVIS

La qualité de cette microforme dépend grandement de la qualité de la thèse soumise au microfilmage. Nous avons tout fait pour assurer une qualité supérieure de reproduction.

S'il manque des pages, veuillez communiquer avec l'université qui a conféré le grade.

La qualité d'impression de certaines pages peut laisser à désirer, surtout si les pages originales ont été dactylographiées à l'aide d'un ruban usé ou si l'université nous a fait parvenir une photocopie de qualité inférieure.

La reproduction, même partielle, de cette microforme est soumise à la Loi canadienne sur le droit d'auteur, SRC 1970, c. C-30, et ses amendements subséquents.

AN ALGORITHM FOR THE EXTRACTION OF OCEAN WAVE PARAMETERS FROM WIDE BEAM HF RADAR (CODAR) BACKSCATTER

by

©Eric William Gill, BSc., BEd.

A thesis submitted to the School of Graduate Studies
in partial fulfillment of the requirements for the
degree of Master of Engineering

Faculty of Engineering and Applied Science
Memorial University of Newfoundland
February, 1990
St. John's Newfoundland

ISBN 0-315-59211-7

MEMORIAL UNIVERSITY OF NEWFOUNDLAND

This is to authorize the Dean of Graduate Studies to deposit two copies of my thesis/report entitled

An Algorithm for the Extraction of Ocean Wave Parameters from Wide Beam HF Radar (CODAR) Backscatter

in the University Library, on the following conditions. I understand that I may choose only ONE of the Options here listed, and may not afterwards apply for any additional restriction. I further understand that the University will not grant any restriction on the publication of thesis/report abstracts.

(After reading the explanatory notes at the foot of this form, delete TWO of (a), (b) and (c), whichever are inapplicable.)

The conditions of deposit are:

(a) that two copies are to be made available to users at the discretion of their custodians,

OR

(b) that access to, and quotation from, this thesis/report is to be granted only with my written permission for a period of one year from the date on which the thesis/report, after the approval of the award of a degree, is entrusted to the care of the University, namely, _____ 19 ____, after which time the two copies are to be made available to users at the discretion of their custodians,

OR

(c) that access to, and quotation from, this thesis/report is to be granted only with my written permission for a period of _____ years from the date on which the thesis/report, after approval for the award of a degree, is entrusted to the care of the University; namely, _____, 19 ____; after which time two copies are to be made available to users at the discretion of their custodians.

Date Feb. 9, 1990

Signed Eric W Gill

Dean of Graduate Studies

Witnessed by Agnes Reuss

NOTES

1. *Restriction (b) will be granted on application, without reason given.*

   However, applications for restriction (c) must be accompanied with a detailed explanation, indicating why the restriction is thought to be necessary, and justifying the length of time requested. Restrictions required on the grounds that the thesis is being prepared for publication, or that patents are awaited, will not be permitted to exceed three years.

   Restriction (c) can be permitted only by a Committee entrusted by the University with the task of examining such applications, and will be granted only in exceptional circumstances.

2. *Thesis writers are reminded that, if they have been engaged in contractual research, they may have already agreed to restrict access to their thesis until the terms of the contract have been*

Abstract

The remote monitoring of the coastal ocean has been a topic receiving much attention from both the scientific and industrial communities in recent years. Among the many devices which have come to the forefront in providing comprehensive information on ocean surface paramenters is the HF radar operating in the ground wave mode. In particular, a four-element square array known as a CODAR (Coastal Oceans Dynamics Applications Radar) has successfully produced near-shore current maps. The problem addressed in this thesis is that of molding existing theory so as to create an algorithm which would extend the capabilities of this CODAR to include the yielding of directional waveheight spectra from backscattered radiation.

General expressions for the first- and second-order broad beam radar cross sections of the ocean surface presented by Barrick and Lipa (1979b) are applied to the four-element CODAR. Fourier coefficients of both the first- and second-order portions of the *radar* spectrum are developed with all but one of the various required integrations being carried out in closed form. The Fourier basis function approach allows the broad beam cross sections to be written as a system of integral equations. The second-order radar return involves a double integral whose integrand contains nonlinear combinations of the unknowns, namely the Fourier coefficients of the *ocean wave* directional spectrum. The first-order portion of the radar spectrum is used to linearize this integral, thus allowing the system of equations to be formulated in terms of matrices. The matrix system is solved using a singular value decomposition approach.

The analysis is carried out in its entirety for simulated data only. However, Appendix D outlines the procedure for calculating the four-element square array cross sections from measured data. These may be used in the algorithms developed here to extract directional waveheight information from the backscatter of high frequency radiation from the ocean surface.

Acknowledgements

The author wishes to thank the Department of Engineering and Applied Science for affording him the opportunity of conducting this work. Particularly, the supervision of Dr. John Walsh and his suggestion of an exciting research topic in the author's field of interest is greatly appreciated.

The insight into the early stages of the research provided by Mr. Randy Howell is worthy of special thanks. Members of the Remote Sensing Group at C-CORE, in particular Mr. Ken Hickey, Dr. Rafaat Khan, Mr. Wayne Pearson, and Mr. William Winsor, have also provided valuable assistance at various stages of this work.

The author wishes to thank the administration of Cabot Institute for the provision of an extra year of educational leave so that the present work could be completed.

The author is grateful for financial support in the forms of (1) a Career Award and a Faculty Award from the provincial Department of Career Development and Advanced Studies; (2) a C-CORE graduate fellowship and (3) graduate student support from a Natural Sciences and Engineering Research Council (NSERC) Strategic Grant to Dr. John Walsh.

Finally, the patience and understanding of the author's wife and family during the research period is deeply appreciated.

Contents

Abstract ii
Acknowledgements iii
Table of Contents iv
List of Tables vi
List of Figures vii
Table of Symbols ix

1 Introduction **1**

1.1 Research Rationale 1

1.2 Literature Review 2

1.3 Scope of Thesis 7

2 Formulation of the Problem and Development of Simulated Wide Beam Radar Spectral Coefficients **9**

2.1 The First-Order Narrow Beam Radar Cross Section of the Ocean Surface 9

2.2 The Second-Order Narrow Beam Cross Section of the Ocean Surface . 11

2.2.1 Normalization of the Second-order Cross Section 11

2.2.2 Reduction of the Second-order Cross Section to a Single Integral 14

2.2.3 Solution of the Delta-function Constraint 15

2.2.4 The Coupling Coefficient 17

2.3 The Wide Beam Cross Sections of the Ocean for a Four-Element Square Array 20

2.3.1 The Beam Pattern and its Fourier Coefficients 22

2.3.2 The Ocean Model and its Fourier Coefficients 27
2.3.3 A Fourier Formulation of the Wide Beam Second-order Cross Section 29
2.4 Calculation of Simulated Normalized Radar Spectral Coefficients . . . 31
2.4.1 Simulated First-order Radar Spectral Coefficients 32
2.4.2 Simulated Second-Order Radar Spectral Coefficients 35
2.4.3 Illustration of Radar Spectral Coefficients 40

3 The Integral Inversion **47**
3.1 The Linearization Scheme 47
3.2 Discretization of the Second-order Equation 50
3.3 Solution of the Matrix Equation 54
3.4 Calculation of Ocean Spectra from Simulated Radar Data 56
3.4.1 Illustrations of Typical Ocean Spectra 57
3.4.2 Normalized RMS Waveheight 61
3.4.3 Dominant Direction of the Ocean Wavefield 63
3.4.4 Recovery of the Spread Parameter 63

4 Conclusions **69**
4.1 General Summary 69
4.2 Suggestions for Future Work 71

Bibliography **73**

A Calculation of the Beam Pattern Coefficients **77**

B Inversion of the First-Order Return **82**

C FORTRAN Code for the Inversion of the Second-order Backscatter **85**

D Creation of the Four-element Square Array Cross Sections from Measured Data **112**

List of Tables

1 The four-element square array beam pattern coefficients for array radius of 2.54 m 25

2 Normalized waveheights for various wavefield conditions 62

List of Figures

1 Behaviour of coupling coefficient with depth 19

2 Operational set-up of a four-element square array from a coastal site . 21

3 Wave vectors associated with the broad beam analysis 23

4 Comparison of beam pattern with its truncated Fourier series 26

5 A typical real four-element square array spectrum 34

6 Simulated radar spectral coefficients with dominant wavefield direction of 0° 41

7 Simulated radar spectral coefficients with dominant wavefield direction of 45° 42

8 Simulated radar spectral coefficients with dominant wavefield direction of 90° 43

9 Zero-order radar spectral coefficients showing the effect of water depth on the radar spectrum 44

10 Zero-order radar spectral coefficients showing the effect of increasing sea state on the radar spectrum 46

11 Normalized ocean spectra obtained from inversion for wind speed of 10 m/s 58

12 Normalized ocean spectra obtained from inversion for wind speed of 15 m/s 59

13 Behaviour of the singular values used in the inversion algorithm . . . 60

14 Dominant directions for wind speed of 10 m/s 64

15 Dominant directions for wind speed of 15 m/s 65
16 Spread parameters for wind speed of 10 m/s 67
17 Spread parameters for wind speed of 15 m/s 68
18 The complete surface of $D(\phi, \phi)$ and its approximation 81

Table of Symbols

$\sigma_1(\omega, \phi)$: First-order narrow beam cross section (p. 9).

ω : Angular Doppler frequency (p. 9).

ϕ : Narrow beam look direction (p. 9).

m' : Sign of the Doppler shift (p. 9).

$\vec{k_0}$: Radar wave vector (p. 9).

S : Ocean directional spectrum (p. 9).

δ : Delta function (p. 9).

ω_B : Angular frequency of the Bragg wave (p. 9).

ω_W : Angular frequency of water wave (p. 10).

g : Gravitational acceleration (p. 10).

$\vec{k}$: Wavevector of first ocean scatterer (p. 10).

k_B : Wavenumber of the Bragg wave (p. 10).

η : Normalized Doppler frequency (p. 10).

Z : Normalized ocean directional spectrum (p. 10).

$\vec{K}$: Normalized wavevector of the first ocean scatterer (p. 10).

$\sigma_1(\eta, \phi)$: Normalized first-order cross section (p. 10).

$\sigma_2(\omega, \phi, d)$: Second-order narrow beam cross section (p. 11).

d : Water depth (p. 11).

$\vec{k'}$: Wavevector of the second scatterer (p. 11).

m : Direction indicator for first ocean scatterer (p. 11).

ω_W : Angular frequency of second ocean scatterer (p. 11).

ω'_W : Angular frequency of second ocean scatterer (p. 11).

$\hat{k}_0$: Unit vector in direction of the narrow beam (p. 11).

Γ : Coupling coefficient (p. 11).

θ : Direction of first ocean scatterer (p. 11).

Γ_H : Hydrodynamic coupling coefficient (p. 12).

Γ_E : Electromagnetic coupling coefficient (p. 12).

Γ_N : Normalized coupling coefficient (p. 12).

$\vec{K}'$: Normalized wavevector of second ocean scatterer (p. 12).

η_W : Normalized angular frequency of first ocean scatterer (p. 12).

η'_W : Normalized angular frequency of second ocean scatterer (p. 12).

D : Normalized water depth (p. 12).

$\sigma_2(\eta, \phi, D)$: Normalized second-order narrow beam cross section (p. 12).

y : $\sqrt{K}$ (p. 14).

L : The product of mm' (p. 15).

y^* : Solution to the delta-function constraint (p. 15).

$g(y)$: Function associated with the delta function constraint (p. 15).

Γ_{e_N} : Normalized electromagnetic coupling coefficient (p. 17).

Δ : Normalized surface impedance (p. 17).

Γ_{H_N} : Normalized hydrodynamic coupling coefficient (p. 18).

$\Gamma_{H_{N_{\text{deep}}}}$: Normalized deep water hydrodynamic coupling coefficient (p. 18).

$\Gamma_{N_{\text{deep}}}$: Normalized deep water coupling coefficient (p. 18).

ψ : Wide beam scan angle (p. 20).

$\sigma_j(\omega, \psi)$: Wide beam cross section of ocean (p. 20).

γ : Angle between 2–4 axis of array and the shoreline (p. 20).

$G(\psi, \phi)$: Wide beam pattern (p. 20).

c : Speed of light in air (p. 20).

τ_R : Pulse width of Doppler radar transmit signal (p. 20).

$\vec{K}_\psi$: Wavevector of magnitude k_0 and direction ψ (p. 22).

$\vec{K}_\phi$: Wavevector of magnitude k_0 and direction ϕ (p. 22).

r : Radius of the four-element square array (p. 22).

g_{tpc} : Cos-cos Fourier coefficients of wide beam (p. 24).

g_{tps} : Sin-sin Fourier coefficients of wide beam (p. 24).

J_t, J_p : Bessel functions of the first kind (p. 24).

ζ : $\frac{2k_0 r}{\sqrt{2}}$ (p. 24).

$f(k)$: Pierson-Moskowitz non-directional ocean spectrum (p. 27).

$g(\theta + \phi)$: Directional factor of ocean spectrum (p. 27).

k_c : Cutoff ocean wavenumber (p. 27).

u : Wind speed (p. 27).

α^* : Dominant direction of ocean wavefield (p. 28).

$a_n(k)$: Fourier coefficient of ocean wave of wavenumber k (p. 28).

$b_n(k)$: Fourier coefficient of ocean wave of wavenumber k (p. 28).

s : Spread parameter of ocean wavefield (p. 28).

$\alpha_t(\omega)$: Abbreviation for cosine portion of ϕ integration (p. 30).

$\beta_t(\omega)$: Abbreviation for sine portion of ϕ integration (p. 30).

$b_t(\omega)$: Fourier coefficients of wide beam cross section (p. 30).

$B_t(\eta)$: Normalized Fourier coefficients of wide beam cross section (p. 30).

$W(\eta)$: Gaussian function of normalized Doppler frequency (p. 33).

$B_{t_c}(\eta)$: Smeared coefficients of normalized first-order cross section (p. 30).

τ : Normalized width of $W(\eta)$ (p. 33).

E_c : The first-order radar coefficients excluding delta function (p. 33).

$\Delta\eta$: Width of the normalized first-order peaks (p. 35).

$T(\vec{K},\vec{K}')$: Product of two normalized ocean spectra (p. 36).

$T_1(\vec{K},\vec{K}')$: Simplified product of two normalized ocean spectra (p. 37).

s_{nlpj} : Various ϕ integrations for $j = 1,\ldots,8$ (p. 38).

d_j : Various ϕ integral sums (p. 38).

$C_{1_{anlpt}}$: Terms containing all integrations but the θ integral (p. 39).

$C_{2_{anlpt}}$: Terms containing all integrations but the θ integral (p. 39).

$C_{1_{bnlpt}}$: Terms containing all integrations but the θ integral (p. 39).

$C_{2_{bnlpt}}$: Terms containing all integrations but the θ integral (p. 39).

h : *rms* waveheight (p. 39).

f_P : Phillip's equilibrium spectrum (p. 48).

$\alpha_{nlpt}(\theta,\eta)$: θ-integrand excluding wave coefficients $a_n(K)$ (p. 50).

$\beta_{nlpt}(\theta,\eta)$: θ-integrand excluding wave coefficients $b_n(K)$ (p. 50).

K_j : Endpoints of wavenumber bands (p. 51).

K_{m_j} : Midpoints of wavenumber bands (p. 51).

$\Psi_{a_{nit}}$: Contribution to radar coefficient by coefficient a_n in band i (p. 52).

$\Psi_{b_{nit}}$: Contribution to radar coefficient by coefficient b_n in band i (p. 52).

η_p : Any particular value of normalized Doppler frequency (p. 52).

$\underline{\underline{A}}_p$: Matrix multiplying ocean wave coefficients when $\eta = \eta_p$ (p. 53).

$\underline{B}_p$: Column vector of radar spectral coefficients with $\eta = \eta_p$ (p. 53).

$\underline{X}$: Column vector of ocean spectral coefficients (p. 53).

$\underline{\underline{A}}$: Same as $\underline{\underline{A}}_p$ but for all η (p. 54).

$\underline{B}$: Same as $\underline{B}_p$ but for all η (p. 54).

$\underline{\underline{U}}$, $\underline{\underline{V}}$: Orthogonal matrices used in singular value decomposition of $\underline{\underline{A}}$ (p. 55).

$\sum$: Diagonal matrix of singular values (p. 55).

Σ^{-1} : The inverse of Σ (p. 55).

$\mu_1, \ldots, \mu_r$: The diagonal elements of Σ (p. 55).

$\underline{\underline{A}}^{-1}$: The inverse of $\underline{\underline{A}}$ (p. 55).

$\underline{\underline{A}}^{+}$: The pseudo-inverse of $\underline{\underline{A}}$ (p. 55).

$\underline{X}_r$: Optimal linear least squares solution for ocean spectral coefficients (p. 55).

H : Normalized *rms* waveheight (p. 61).

g_{tpcs} : Cos-sin Fourier coefficients of beam pattern (p. 79).

g_{tpsc} : Sin-cos Fourier coefficients of beam pattern (p. 79).

$f_1(\psi, \phi)$, $f_2(\psi, \phi)$: Pieces of the broad beam pattern (p. 80).

$\underline{\underline{A}}_B$: Same as $\underline{\underline{A}}$ but for frequency range $\Delta\eta$ only (p. 84).

$\underline{X}_B$: Same as $\underline{X}$ but for frequency range $\Delta\eta$ only (p. 84).

$\underline{\underline{B}}_B$: Same as $\underline{\underline{B}}$ but for frequency range $\Delta\eta$ only (p. 84).

$\underline{X}_{B_r}$: Same as $\underline{X}_r$ but for frequency range $\Delta\eta$ only (p. 84).

$\underline{\underline{A}}_B^{+}$: Same as $\underline{\underline{A}}^{+}$ but for frequency range $\Delta\eta$ only (p. 84).

${}_nV_j(\omega)$: n^{th} sample voltage on the j^{th} antenna element (p. 113).

${}_nV_{x_j}(\omega)$: real part of ${}_nV_j(\omega)$ (p. 113).

${}_nV_{y_j}(\omega)$: imaginary part of ${}_nV_j(\omega)$ (p. 113).

${}_NC_{j\ell}(\omega)$: N-sample-averaged cross spectrum between the j^{th} and ℓ^{th} (p. 113).

${}_nV_\ell^*(\omega)$: n^{th} Complex conjugate of ${}_nV_\ell(\omega)$ (p. 113).

P : Number of elements of a planar array (p. 114).

${}_N\sigma(\omega, \psi)$: Wide beam cross section produced from ${}_NC_{j\ell}(\omega)$ (p. 114).

$Z_1, \ldots, Z_q$: Series of q complex numbers (p. 114).

Chapter 1

Introduction

1.1 Research Rationale

With the burgeoning interest in marine exploration and development, there has arisen the necessity of accurate monitoring of the coastal waters in the vicinity of such activity. Amongst the information required to produce a complete synopsis of oceanic conditions is a knowledge of the wave field itself. Consequently, in recent years, much emphasis has been placed on the remote sensing of ocean wave spectra.

Included in the types of devices used to collect ocean surface data is the HF ground wave radar. Data provided by both narrow and broad beam radar configurations have been subjected to a variety of analysis techniques to give ocean spectral information. The quantity of data which may be obtained by these radars far exceeds that possible by point sensors such as wave buoys. Further, the advantages, in terms of both deployment and maintenance, of shore-based operation over that of in-situ installations is obvious.

At C-CORE (Centre for Cold Ocean Resources Engineering), St. John's, Newfoundland, a CODAR (Coastal Oceans Dynamics Applications Radar) has been used to produce surface current maps for coastal regions. This device, consisting of a four-element square array operating in the ground wave mode at 25.4 MHz, has heretofore been employed strictly as a current measuring device. The problem addressed here is that of developing an algorithm to allow extraction of waveheight spectra from

ocean backscatter received by this array. The process involves simplification and inversion of a two-dimensional Fredholm integral equation of the first kind which is used to represent the second-order radar cross section of the ocean surface. Implementation of such an algorithm will greatly enhance the versatility of the CODAR system. Since the four-element array has a wider aperture than that of an existing broad beam system used for wave measurement (see section 1.2), it is expected that better directional wave information may be obtained by the former.

1.2 Literature Review

The determination of wave conditions from radar backscatter involved, initially, the development of a model for the radar cross section of the ocean surface. This analysis finds its roots in the work of Rayleigh (1896). Rayleigh gave a perturbational treatment of the scattering of acoustic waves from rough surfaces. Rice (1951) adapted and generalized Rayleigh's approach to examine the reflection of plane electromagnetic waves from a 'slightly rough', perfectly conducting surface which could be represented by a double Fourier series. 'Slightly rough' was taken to mean that the product of the incident radiation wavenumber and any surface deviation from the mean was very much less than one.

It was Barrick (1971, parts 1 and 2) who first extended the Rayleigh- Rice procedure to include surfaces of finite, but high, conductivity. He developed the effective surface impedance for such a case at grazing incidence and subsequently applied the results in his study (1971) of propagation losses due to sea state of HF and VHF radiation travelling above the ocean surface. Wait (1971) and Rosich and Wait (1977) provided a similar treatment for two-dimensional surfaces without requiring the restrictions of high conductivity and grazing incidence.

Crombie (1955) had explained that the physical mechanism producing backscatter from the ocean surface was 'Bragg scatter'. That is, the discrete frequency shifts

above and below the carrier frequency observed in the radar spectrum corresponded uniquely with the deviations which would be produced by ocean waves having lengths exactly one-half the radio wavelength and moving toward or away from the radar. Barrick(1972) produced from the Rice theory a first-order scatter cross section of the ocean which supported Crombie's experimental deductions.

Hasselman (1971) proposed the concept of second-order hydrodynamic and electromagnetic interactions giving rise to the observed continuum beyond and between the 'Bragg lines' in the Doppler power spectrum obtained from sea echo. Then, Barrick (1972b) derived an expression for the average second-order backscatter cross section per unit surface area per rad/s bandwidth. His perturbation analysis showed that this expression is related to the ocean wave directional spectrum through a nonlinear, two-dimensional, Fredholm type integral equation. He assumed grazing incidence with vertical polarization over a perfectly conducting sea. The result represented an extension of the previous work to include (1) second-order terms arising from the Rice perturbation theory and (2) second-order terms from the hydrodynamic equations describing the water surface height. The latter are given by Kinsman (1965). A delta function in the integral equation indicated constraints on the ocean wave vectors which were necessary to produce this higher order scatter. The physical second-order scatter mechanisms, advanced by Hasselman, are summarized by Shearman (1983).

Srivastava (1984), based on the Walsh (1980b) formulation in the spatial Fourier transform domain for scattering from a general time invariant surface, also developed first- and second-order radar cross section equations of the ocean surface. Srivastava's first-order proved to be the same as Barrick's. However, his second-order involved terms arising from surface and incident field interactions between the source and primary ocean scattering patch and from off-patch double scatter.

With the first- and second-order backscatter cross section equations developed,

Barrick and Snider (1976) turned to statistical analysis of the Doppler echo received and to the application of this analysis to system design.

Subsequently, Barrick (1977a, 1977b) presented the first general model for extracting wave height and wave period from HF echo received from the surface of the deep ocean. Only one of the four second-order sidebands of the radar spectrum was used. This was divided by a dimensionless weighting function and then by the first-order spectral energy to remove unknown path losses and gain factors and to eliminate the need for previous knowledge of wave or radar directionality. Preliminary results for *rms* waveheight obtained from the inversion of the integral equation differed from those measured simultaneously by a Waverider data buoy by about 23%.

Lipa (1977), using the cross sections developed by Barrick, reduced the second-order cross section to a system of linear equations. This system was solved using a stabilization technique developed by Phillips (1962) and Twomey (1963). The stabilization method, which involved minimizing the deviation of an ultimate solution from an initial guess, was required because small changes in the data due to random noise could lead to severe distortion in the result. Lipa (1978) showed that this procedure applied to real data obtained by a narrow beam radar operating in the ground wave mode was an improvement over Barrick's earlier efforts. She also obtained results for the directional features of the ocean spectrum. Barrick and Lipa (1979a) consolidated this process and discussed the mapping of ocean currents from the first-order portion of the radar return.

Again, Barrick and Lipa (1979b) presented an algorithm for extraction of directional spectra from sea echo received by a compact broad beam three-element crossed-loops/monopole antenna (the crossed-loops CODAR). This involved the representation of the broad beam cross section as the convolution of the antenna pattern with the narrow beam cross section. A Fourier basis formulation of the cross section led to a matrix equation. The matrix system was solved, as before, to give the ocean

wave directional spectrum. Lipa and Barrick (1983) also gave details of the cross spectral analysis of the echo required for the calculation of the broad beam cross section. The procedure was rigorously applied to the crossed-loops CODAR, and an outline of how the technique could be used for an n-element array was supplied.

Lipa et al. (1981) and Lipa and Barrick (1982) provided further refinement in both experimental results and theoretical analysis for pulsed Doppler radar sea echo received by narrow beam systems. The latter work presented an application of the inversion of the second-order radar return using a linearization scheme proposed by Barrick (1977b) and a 'bands' approximation similar to that suggested by Barrick and Lipa (1979b). The 'bands' approximation assumes that the ocean spectral energy is constant over narrow ranges (or 'bands') of wavenumbers. This is what allowed the integral equation associated with the second-order echo to be converted to a linear system. The system, in which the unknowns were Fourier coefficients of the ocean wave directional spectrum, was solved using the stabilization technique already cited.

Work by Shearman et al. (1982, 1982b) and Wyatt et al. (1985) applied the theory of Lipa and Barrick to FMICW (frequency-modulated interrupted continuous wave) radar operation with no new insights into inversion techniques. Shearman's group did, however, provide experimental results which suggested that modifications in the echo pattern due to shadowing effects by objects or land were far more prominent than any perturbation of the antenna characteristics due to general irregularities in the coastline from which the operations occurred.

Wyatt (1986a) and Wyatt et al. (1986), using an extension of a model fitting technique described by Lipa and Barrick (1982), sought to extract information from a greater range of frequencies in the Doppler echo spectrum. Basically, Wyatt produced a large number of detailed calculations of simulated Doppler spectra for a variety of modelled and measured ocean wave spectra. Real radar returns were then matched with the simulations in 'look-up table' fashion. As did Lipa and Barrick,

Wyatt showed that a two-radar narrow beam system provided better accuracy than the single-radar configuration in obtaining ocean wave directional information. This resulted from the elimination of the left-right ambiguity associated with returns received by a single radar.

Based on work by Barrick (1986) on the hydrodynamic coupling coefficient, Lipa and Barrick (1986) extended their previous theory and modelling to include ocean regions of general depth. The modified cross section equations allowed for the sensing of surface conditions in the coastal ocean by both wide and narrow beam antennas.

Among the most recent approaches to extraction of directional wave spectra from narrow beam radar sea echo is that by Howell (1990). Similar to previous investigators, he initially developed simulated radar spectra using a Pierson-Moskowitz ocean model with a cardioid directional distribution. Using the linearization scheme of Barrick (1977b), and a discretization approach for the temporal ocean spectrum in which wave energy was considered constant over small ranges of frequency, Howell also formed a matrix equation. He then performed the necessary inversion by a singular value decomposition approach. This allowed for the direct extraction of the wave information without having to make an initial guess. Howell has implemented the cross sections of Barrick as well as new estimates recently developed by Walsh and Howell (1990). His method, using Barrick's cross section, applied to real data from both single and double narrow beam systems, has produced results at least comparable to those of other investigators and to similar measurements obtained by directional wave buoys. Results based on the new estimate provide even better agreement with the buoy data.

To date, the literature has dealt with the extraction of non-directional and directional waveheight spectra from either narrow beam radar data or from the crossed-loops CODAR wide beam system. Also, the latter as well as a four-element square

array have been employed by Lipa and Barrick (1983) as ocean current measuring instruments. However, an algorithm to deduce wave information from the square antenna was never developed. This, according to Lipa and Barrick (1983), was primarily due to the increased complexity of the data analysis over that of the smaller crossed-loops system.

1.3 Scope of Thesis

This work presents an analysis for the retrieval of waveheight spectra from data collected by a four-element square array. The ocean surface is assumed to be 'illuminated' with a HF signal from either an omnidirectional transmitter or an antenna whose radiation pattern is approximately the same in all seaward directions. As well, the region of ocean viewed by the array is taken to be homogeneous in its wave spectral characteristics. For operation from a straight shoreline, as contained in the illustrations within this thesis, the latter assumption can be sometimes restrictive due to depth variations. The analysis itself, however, may be used for any size ocean sector, including the open ocean. If the view is restricted by headlands or if, in the opposite extreme, the radar operates from an ocean platform, the condition of wave spectral homogeneity is more likely to be realized.

The problem is formulated using a scheme reported by Barrick and Lipa (1979b) for the crossed-loops/monopole receiving antenna. The general wide beam first- and second-order cross section equations are adapted to fit the four-element case. The cross sections are expressed as an angular Fourier series in which all but one of several integrations are carried out in closed form. The closed form feature allows the analysis to be immediately transferred to four-element square arrays of any dimension.

Simulated radar spectral coefficients are calculated by assuming a model of the ocean-wave spectrum. The effects of water depth, wind speed and dominant wave direction on the coefficients are examined.

Using a linearization assumption similar to, but not as constrained as, that of Lipa and Barrick (1982) and the discretization approximation of Howell (1990), the second-order cross section expression is converted to matrix form. The unknowns of the matrix system are the Fourier coefficients of the ocean wave directional spectrum.The system is solved using the method of singular value decomposition . Simulated results for several ocean spectra obtained through this inversion process are illustrated.

No attempt has been made to model the effects of noise, ocean currents or third order wave-wave interactions, all of which will smear the HF return from the ocean's surface.

The following chapter contains the formulation of the problem and investigates the various components of the four-element array cross section equations. Chapter 3 contains the inversion process which yields the ocean wave spectrum. Simulated results are examined here. Chapter 4 contains conclusions and suggestions for further work.

In Appendix A, calculation of the beam pattern coefficients is examined in detail. Appendix B provides the method of obtaining the coefficients of the Bragg wave from the first-order radar data. Appendix C supplies the major FORTRAN routines used in inverting the second-order cross section equation. Appendix D outlines how the radar spectral coefficients may be obtained from real data.

Chapter 2

Formulation of the Problem and Development of Simulated Wide Beam Radar Spectral Coefficients

The formulation of the *wide beam* problem is based on the radar cross section equations of the ocean surface for a *narrow beam* receive array given by Barrick (1972b). Because of their importance in this thesis we present these cross sections and indicate any alterations which have been made for the analysis at hand. Here, the ocean is considered to be of arbitrary, but constant, depth within any given radar range cell under observation. Therefore, no consideration is given to wave refraction caused by depth changes.

2.1 The First-Order Narrow Beam Radar Cross Section of the Ocean Surface

In the absence of ocean currents, the first-order cross section , $\sigma_1(\omega, \phi)$, per unit surface area of ocean per radian per second, is given by

$$\sigma_1(\omega, \phi) = 2^6 \pi k_0^4 \sum_{m'=\pm 1} S(-2m'\vec{k_0}) \delta(\omega - m'\omega_B). \tag{2.1}$$

Here m' signifies the sign of the Doppler shift, ω, in the radar spectrum; $\vec{k_0}$ is the radar wave vector pointing in the direction ϕ measured with respect to any convenient reference; $S(-2m'\vec{k_0})$ is the directional waveheight spectrum of the Bragg wave vectors

$\pm 2\vec{k_0}$. The delta-function constraint, $\delta(\cdot)$, representing the Bragg scatter condition, shows that, ideally, the first-order spectral peaks are impulse functions occurring at the Bragg frequencies $\pm\omega_B$. The broadening of these spectral peaks by such factors as currents and system effects is addressed in Section 2.4.1. Gains and losses associated with the radar return need not appear in the cross section equation because of the way the analysis proceeds (see Section 3.1). The only assumption about these factors is that they are the same for both first- and second-order radar spectra.

Taking the dispersion relationship (Kinsmen (1965)) for water of depth d to be

$$\omega_W = \sqrt{gk \tanh kd}, \tag{2.2}$$

with g being the gravitational acceleration, k the wavenumber of the ocean wave and ω_W the angular frequency, we write, for the Bragg wave,

$$\omega_B = \sqrt{gk_B \tanh k_B d}. \tag{2.3}$$

Noting the Bragg resonance condition

$$k_B = 2k_0 \tag{2.4}$$

and the fact that, in the upper HF band, $\tanh k_B d$ will be practically unity for all water depths of interest, equation (2.3) becomes

$$\omega_B = \sqrt{2gk_0}. \tag{2.5}$$

To simplify the analysis, it is convenient to define, after Lipa and Barrick (1982), the following dimensionless quantities:

$$\text{Doppler frequency:} \quad \eta = \omega/\omega_B \tag{2.6}$$

$$\text{wave vector:} \quad \vec{K} = \vec{k}/2k_0 \tag{2.7}$$

$$\text{spatial ocean wavespectrum:} \quad Z(\vec{K}) = (2k_0)^4 S(\vec{k}). \tag{2.8}$$

Defining the normalized first-order cross section as

$$\sigma_1(\eta, \phi) = \omega_B \sigma_1(\omega, \phi) \tag{2.9}$$

and considering that

$$\begin{aligned} \delta(\omega - m'\omega_B) &= \delta(\omega_B(\eta - m')) \\ &= \frac{\delta(\eta - m')}{\omega_B}, \end{aligned} \tag{2.10}$$

equation (2.1) has normalized form

$$\sigma_1(\eta, \phi) = 4\pi \sum_{m'=\pm 1} Z(-m'\hat{k}_0)\delta(\eta - m') . \tag{2.11}$$

Here,

$$\hat{k}_0 = \frac{\vec{k}_0}{|\vec{k}_0|}.$$

2.2 The Second-Order Narrow Beam Cross Section of the Ocean Surface

2.2.1 Normalization of the Second-order Cross Section

With the exception of some notational variation and a change from rectangular to polar coordinates, Barrick (1972b) presents the second order radar cross section of the ocean's surface as

$$\begin{aligned} \sigma_2(\omega, \phi, d) &= 2^7 \pi k_0^4 \sum_{m'=\pm 1} \int_0^\infty \int_{-\theta_0}^{\theta_0} |\Gamma|^2 S(m\vec{k}) S(m'\vec{k}') \\ &\quad \cdot \delta(\omega - m\omega_W - m'\omega'_W)\, k\, dk\, d\theta. \end{aligned} \tag{2.12}$$

In order for second-order backscatter to occur, the wave vectors, $\vec{k}$ and $\vec{k}'$, responsible for the scattering obey the constraint (Barrick (1977b))

$$\vec{k} + \vec{k}' = -2\vec{k}_0 , \tag{2.13}$$

while the delta-function imposes the necessary conditions on the frequencies. Here $\vec{k}' \geq \vec{k}$. The quantities ω, ϕ, $\vec{k}_0$ and $S(\cdot)$ have the same meaning as in equation (2.1) The water depth, d, is assumed constant. The coupling coefficient, Γ, is the sum of

the hydrodynamic and electromagnetic coupling coefficients, Γ_H and Γ_E respectively; i. e.

$$\Gamma = \Gamma_H + \Gamma_E. \tag{2.14}$$

This coefficient represents the second-order interactions of the scattering waves with each other as well as with the incident radiation. Its form and significance are detailed in Section 2.2.4. The values of m and m' (i. e. ± 1) incorporate the four possible directional combinations of the scattering waves, while θ gives the angle, relative to $\vec{k_0}$, of the scatterer whose wavenumber is k (i. e. $\left|\vec{k}\right|$). The integration limits, $\pm\theta_0$, for the ocean wavenumbers of interest can be shown to be $\pm\pi$. The quantities ω_W and ω'_W are angular frequencies corresponding to the wave vectors $\vec{k}$ and $\vec{k'}$ respectively. As shown by Lipa and Barrick (1982), when $mm' = 1$ the Doppler frequency, ω, lies outside the Bragg peaks, and for $mm' = -1$, ω is between those peaks.

As with the first-order cross section, it is convenient to represent equation (2.12) in normalized form. In addition to the normalizations of equations (2.6)–(2.8), we define the following:

$$\text{coupling coefficient:} \quad \Gamma_N = \Gamma/2k_0 \tag{2.15}$$

$$\text{second scatterer wave vector:} \quad \vec{K'} = \vec{k'}/2k_0 \tag{2.16}$$

$$\text{angular frequency of water wave:} \quad \eta_W = \omega_W/\omega_B \tag{2.17}$$

$$\eta'_W = \omega'_W/\omega_B \tag{2.18}$$

$$\text{water depth:} \quad D = 2k_0 d \tag{2.19}$$

$$\text{second-order cross section:} \quad \sigma_2(\eta, \phi, D) = \omega_B \sigma_2(\omega, \phi, d). \tag{2.20}$$

From equations (2.2)–(2.4) and (2.7), (2.17) becomes

$$\begin{aligned} \eta_W &= \frac{\sqrt{gk\tanh(kd)}}{\sqrt{gk_B\tanh(k_B d)}} \\ &= \frac{\sqrt{\frac{k}{2k_0}\tanh\left(2k_0 K \cdot \frac{D}{2k_0}\right)}}{\sqrt{\tanh\left(2k_0 \cdot \frac{D}{2k_0}\right)}} \end{aligned}$$

$$= \frac{\sqrt{K\tanh(KD)}}{\sqrt{\tanh(D)}}. \tag{2.21}$$

Similarly,

$$\eta'_{\rm W} = \frac{\sqrt{K'\tanh(K'D)}}{\sqrt{\tanh(D)}}. \tag{2.22}$$

Considering these normalizations along with the fact that

$$\delta(\omega - m\omega_{\rm W} - m'\omega'_{\rm W}) = \frac{1}{\omega_B}\delta\left(\eta - \frac{m\sqrt{K\tanh(KD)} - m'\sqrt{K'\tanh(K'D)}}{\sqrt{\tanh(D)}}\right), \tag{2.23}$$

equation (2.12) takes on the form

$$\begin{aligned}\sigma_2(\eta,\phi,D) &= 8\pi \sum_{m'=\pm 1} \int_0^{\infty}\int_{-\theta_0}^{\theta_0} |\Gamma_N|^2 \, Z(m\vec{K})Z(m'\vec{K}') \\ &\quad \cdot \delta\left(\eta - \frac{m\sqrt{K\tanh(KD)} - m'\sqrt{K'\tanh(K'D)}}{\sqrt{\tanh(D)}}\right) K\,dK\,d\theta. \end{aligned} \tag{2.24}$$

Equation (2.24) differs from that given by Lipa and Barrick (1986) in that it retains the general form of the dispersion relationship given by equation (2.2) for the second scatterer (i. e. for the wave whose wave vector is $\vec{K}'$). Also, for the sake of completeness, $\sqrt{\tanh(D)}$ is retained in the delta-function argument. It should be noted, however, that this latter quantity is essentially unity for water depths greater than about five metres.

A singularity in the radar spectrum when $|\eta| = \sqrt{2}$, as discussed by Lipa and Barrick (1982), is depicted later in its effect on the the wide beam return (see Section 2.4.3). Other characteristics of this narrow beam cross section in terms of their relation to and effect on the wide beam equation are also therein examined.

2.2.2 Reduction of the Second-order Cross Section to a Single Integral

In the spirit of Lipa and Barrick (1986), and implementing the appropriate alterations due to the assumption of constant but arbitrary water depth, we define the following:

$$y = \sqrt{K} \Rightarrow dK = 2y\,dy \tag{2.25}$$

$$h(y,\theta,D) = \frac{my\sqrt{\tanh(y^2D)} + m'\sqrt{\tanh(K'D)}}{\sqrt{tanh(D)}} \tag{2.26}$$

$$I(y,\theta,D) = 2^4\pi\,|\Gamma_N|^2\,Z(m\vec{K})Z(m'\vec{K'})y^3\ . \tag{2.27}$$

It will be also useful to note that since, in terms of normalized quantities, the constraint given by equation (2.13) becomes

$$\vec{K} + \vec{K'} = -\hat{k}_0\ , \tag{2.28}$$

the law of cosines yields for the second scatter

$$K' = \sqrt{K^2 + 2K\,\cos(\theta) + 1}\ , \tag{2.29}$$

while from the law of sines the direction of $\vec{K'}$ is

$$\theta' = \arcsin(\frac{K}{K'}\sin(\theta)) + \pi\ . \tag{2.30}$$

Using

$$dy = \left|\frac{\partial y}{\partial h}\right|_\theta dh\ , \tag{2.31}$$

the normalized second-order cross section of equation (2.24) may be written as

$$\sigma_2(\eta,\phi,D) = \sum_{m'=\pm1}\int_0^\infty\int_{-\theta_0}^{\theta_0} I(y,\theta,D)\,\delta(\eta - h(y,\theta,D))\left|\frac{\partial y}{\partial h}\right|_\theta d\theta\,dh\ . \tag{2.32}$$

The value of $\left|\frac{\partial y}{\partial h}\right|_\theta$ is easily obtained by differentiating equation (2.26). This gives

$$\left|\frac{\partial y}{\partial h}\right|_\theta = \frac{\sqrt{\tanh(D)}}{\sqrt{\tanh(y^2D)} + \frac{y^2D\,\mathrm{sech}^2(y^2D)}{\sqrt{\tanh(y^2D)}} + \frac{L(y^3+y\cos(\theta))}{K'^{3/2}}(\sqrt{\tanh(K'D)} + \frac{K'D\,\mathrm{sech}^2(K'D)}{\sqrt{\tanh(K'D)}})}\ . \tag{2.33}$$

Here, $L = mm'$, and the expression for K' in terms of K and θ has not been used for the sake of compactness. Next, suppose that y^* is the value of y which provides the solution to the delta-function constraint. This means that equation (2.32) can be immediately written as

$$\sigma_2(\eta, \phi, D) = \sum_{m'=\pm 1} \int_{-\theta_0}^{\theta_0} I(y^*, \theta, D) \left| \frac{\partial y}{\partial h} \right|_\theta |_{y=y^*} d\theta \, . \tag{2.34}$$

The following section shows how to find y^*, the delta-function solution, in terms of η and θ. The θ integral of equation (2.34), when later substituted into the wide beam cross section equation, is calculated numerically.

2.2.3 Solution of the Delta-function Constraint

Obtaining the solution of the delta-function constraint implies solving

$$\eta - h(y^*, \theta, D) = 0 \, . \tag{2.35}$$

This may be done numerically with a Newton-Raphson method (e. g. see James et al. (1977)). The method, applied to the immediate problem, requires the solution of a function

$$g(y) = \eta - h(y, \theta, D) \tag{2.36}$$

for fixed η, θ, and D.

Invoking the relationship between K and K' through equation (2.29) and the definitions of y and $h(y, \theta, D)$ from equations (2.25) and (2.26) respectively, equation (2.36) may be written as

$$\begin{aligned} g(y) &= \eta - h(y, \theta, D) \\ &= \eta - \Big(\frac{my\sqrt{\tanh(y^2 D)}}{\sqrt{\tanh(D)}} + \\ &\qquad \frac{m'(y^4 + 2y^2\cos(\theta) + 1)^{\frac{1}{4}} \sqrt{\tanh((y^4 + 2y^2\cos(\theta) + 1)^{\frac{1}{2}} \cdot D)}}{\sqrt{\tanh(D)}} \Big) \, . \end{aligned} \tag{2.37}$$

From equations (2.35) and (2.36) it is evident that we may write

$$g(y^*) = 0 \,. \tag{2.38}$$

Following the Newton-Raphson method, $g(y)$ is expanded about y^* to give

$$\begin{aligned} g(y) &= g(y^*) + (y - y^*)\left(\frac{\partial g}{\partial y}\right)_{y=y^*} \\ &= (y - y^*)\left(\frac{\partial g}{\partial y}\right)_{y=y^*} \end{aligned}$$

or

$$y^* = y - \frac{g(y)}{\left(\frac{\partial g}{\partial y}\right)_{y=y^*}} \,. \tag{2.39}$$

It is straightforward to show that the expression for $\frac{\partial g}{\partial y}$ required in equation (2.39) is given, on differentiating equation (2.37), as

$$\begin{aligned} \frac{\partial g}{\partial y} = & \frac{-m\sqrt{\tanh(y^2 D)}}{\sqrt{\tanh(D)}} - \frac{my^2 D \operatorname{sech}^2(y^2 D)}{\sqrt{\tanh(D)\tanh(y^2 D)}} \\ & - \frac{m'(y^3 + y\cos(\theta))\sqrt{\tanh((y^4 + 2y^2\cos(\theta) + 1)^{\frac{1}{2}} D)}}{(y^4 + 2y^2\cos(\theta) + 1)^{\frac{3}{4}}\sqrt{\tanh(D)}} \\ & - \frac{m'(y^3 + y\cos(\theta))\operatorname{sech}^2((y^4 + 2y^2\cos(\theta) + 1)^{\frac{1}{2}} D)}{(y^4 + 2y^2\cos(\theta) + 1)^{\frac{1}{4}}\sqrt{\tanh((y^4 + 2y^2\cos(\theta) + 1)^{\frac{1}{2}} D)\tanh(D)}} \end{aligned} \tag{2.40}$$

Then, an initial guess is made for y^* (say y_i^*), and from equation (2.39) a better approximation y_{i+1}^* is calculated. This process is repeated until $\left|y_{i+1}^* - y_i^*\right|$ falls within a specified tolerance. To determine a suitable initial guess, equation (2.37) may be examined in light of the fact that, very near the Bragg peaks of the Doppler spectrum, $y \ll 1$. The resulting information, along with equation (2.38), allows the following approximation to be made for these small values of y:

$$y^*\sqrt{\tanh(y^{*2} D)} \approx m(\eta - m')\sqrt{\tanh(D)} \,. \tag{2.41}$$

For deep water, as discussed by Lipa and Barrick (1982), this reduces to

$$y^* \approx m(\eta - m') \,. \tag{2.42}$$

It has been found by programming (Appendix C) that, in fact, the initial choice of y^* given by equation (2.42) provides the necessary convergence for any values of η and D of interest.

2.2.4 The Coupling Coefficient

The coupling coefficient appearing in the second-order cross section, equation (2.12), and indicated as consisting of two parts in equation (2.14), is sensitive to the water depth and the direction of travel of the ocean waves. Its derivation, for the case of deep water, is carried out by Weber and Barrick (1977). Here we examine how water depth and wave direction affect the magnitude of this coefficient.

The *electromagnetic* portion, which is unaffected by water depth, is given in normalized form by Lipa and Barrick (1982) as

$$\Gamma_{E_N} = \frac{1}{2}\left[\frac{(\vec{K}\cdot\hat{k}_0)(\vec{K'}\cdot\hat{k}_0) - 2(\vec{K}\cdot\vec{K'})}{\sqrt{\vec{K}\cdot\vec{K'}} - \frac{\Delta}{2}}\right] . \tag{2.43}$$

The quantities $\vec{K}$, $\vec{K'}$, and $\hat{k}_0$ are as previously defined while Δ is the impedance of the ocean surface normalized with respect to that of free space. The minus sign appearing in the denominator of the electromagnetic coupling coefficient is a correction to the 1982 presentation and is discussed by Lipa and Barrick (1986). Barrick (1971) showed that a reasonable value of Δ across the HF band is given by

$$\Delta = 0.011 - 0.012\,i \tag{2.44}$$

Also noted by Lipa and Barrick (1982) is a peak in the radar spectrum at $|\eta| = 2^{\frac{3}{4}}$ representing the electromagnetic *corner reflector* condition (i. e. when $\vec{K}\cdot\vec{K} = 0$ in equation (2.43)). The corresponding effect on the broad beam spectrum is noted in Section 2.4.3.

Barrick and Lipa (1986) have given a general expression for the *hydrodynamic* coupling coefficient for water of any depth. Normalizing the expression after the

fashion of equation (2.15) one obtains, on letting $L = mm'$,

$$\begin{aligned}\Gamma_{H_N} &= \frac{-i}{2}\{K\tanh(KD) + K'\tanh(K'D) \\ &+\frac{L(KK'\tanh(KD)\tanh(K'D) - \vec{K}\cdot\vec{K}')}{\sqrt{KK'\tanh(KD)\tanh(K'D)}}\left(\frac{1+\eta^2}{1-\eta^2}\right) \\ &-(\sqrt{K\tanh(KD)} + L\sqrt{K'\tanh(K'D)}) \\ &\cdot\frac{(K\tanh(KD))^{\frac{3}{2}}\mathrm{csch}^2(KD) + L(K'\tanh(K'D))^{\frac{3}{2}}\mathrm{csch}^2(K'D)}{\tanh(D(1-\eta^2))}\Bigg\} \quad (2.45)\end{aligned}$$

For deep water, $\tanh(\cdot) \to 1$ and $\mathrm{csch}^2(\cdot) \to 0$ so that normalized hydrodynamic coupling coefficient becomes

$$\Gamma_{H_N\text{deep}} = \frac{-i}{2}\left[K + K' + \frac{L(KK' - \vec{K}\cdot\vec{K}')}{\sqrt{KK'}}\left(\frac{1+\eta^2}{1-\eta^2}\right)\right]. \quad (2.46)$$

In the spirit of equations (2.14) and (2.15), it is clear that the general normalized coupling coefficient is

$$\Gamma_N = \Gamma_{E_N} + \Gamma_{H_N} \quad (2.47)$$

while the deep water quantity may be written as

$$\Gamma_{N\text{deep}} = \Gamma_{E_N} + \Gamma_{H_N\text{deep}} \quad (2.48)$$

Figure 1 compares the square of the magnitude of the general normalized coupling coefficient with that for deep water for fixed directions of ocean wave with respect to a narrow beam. It is clear from the illustration that, since the electromagnetic coupling coefficient remains constant regardless of depth, the hydrodynamic portion increases in importance for waves of a given wavenumber as the water becomes shallower. It is also evident that the coupling coefficient is greatest when the ocean wave is travelling towards the radar (i. e. direction of 180° to the beam). Finally, it should be noted that the coefficient is symmetric in angle about the beam.

While directions considered here are measured with respect to a *narrow* beam, their significance in the *wide* beam case will become evident when the second-order wide beam cross section of the ocean surface is examined in Sections 2.3 and 2.4.

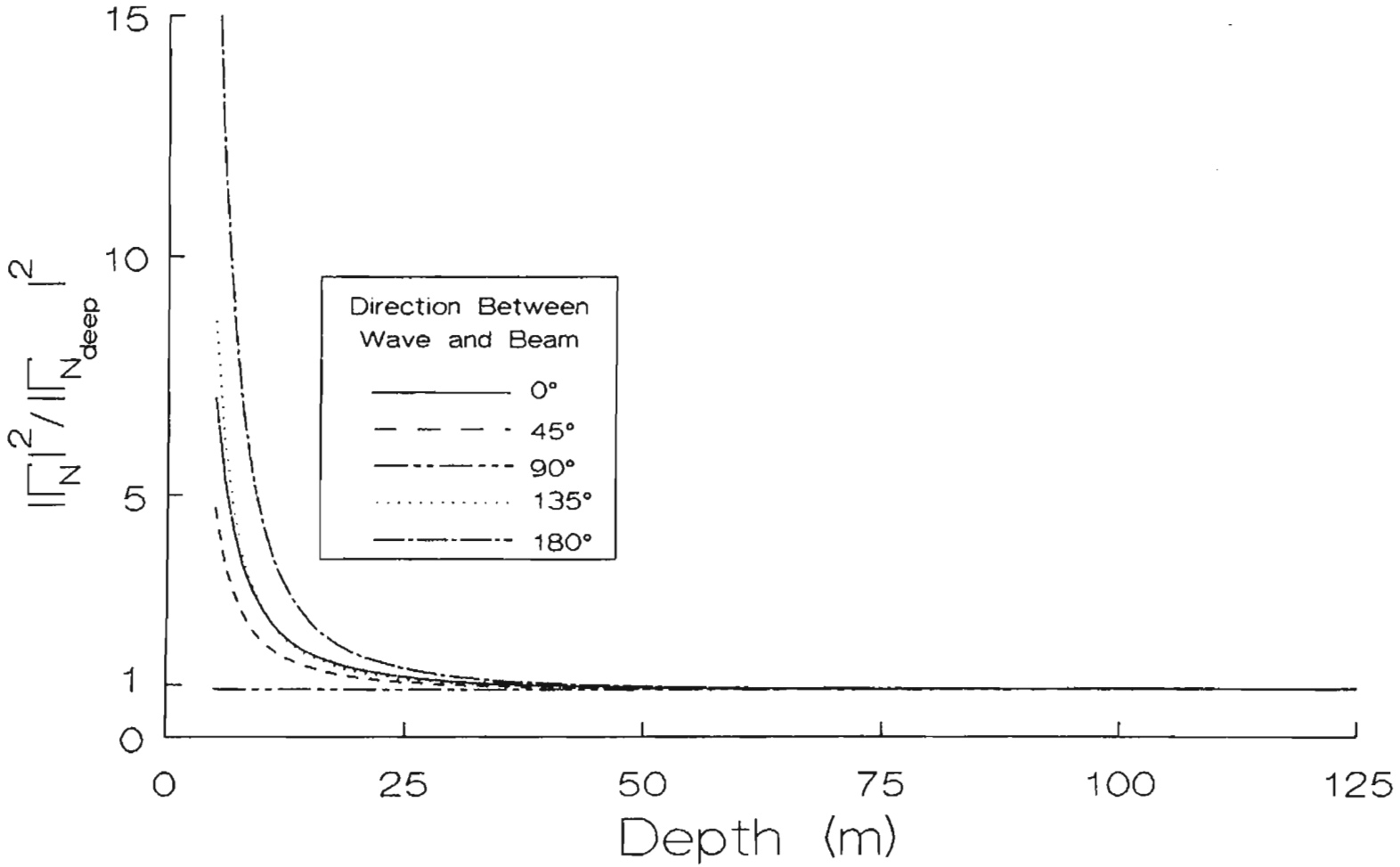

FIGURE 1: The ratio of the square of the magnitude of the normalized coupling coefficient in general-depth water to that in deep water for a 210 m ocean wave travelling in various directions to the beam. The radar operating frequency is 25.4 MHz.

2.3 The Wide Beam Cross Sections of the Ocean for a Four-Element Square Array

Figure 2 depicts the typical operational set-up of a four-element square array from a coastal site. An analysis of the form and properties of the illustrated beam pattern is given in Section 2.3.2. The angle ψ is the direction of the beam maximum (or *scan* angle) with respect to any conveniently chosen reference. Subsequent calculations are simplified by choosing this reference to be the line 'joining' elements 2 and 4 of the array with the centre of the ocean annulus being viewed. The angle ϕ is, as before, the narrow beam *look* direction.

Given by Barrick and Lipa (1979b), the wide beam radar cross section, $\sigma(\omega, \psi)$, at scan angle ψ may be considered as the integration, over narrow beam look direction, of the product of the narrow beam cross section and the power pattern, $G(\psi, \phi)$, of the wide beam array. Referring to Figure 2, we write for water of fixed depth d,

$$\sigma_j(\omega, \psi) = \frac{1}{2\gamma} \int_{-\gamma}^{\gamma} G(\psi, \phi)\, \sigma_j(\omega, \phi, d)\, d\phi \,. \tag{2.49}$$

Equation (2.49) represents the first- or second-order wide beam cross section for $j = 1$ or 2 respectively. The factor $\sigma_j(\omega, \phi, d)$ is defined by equation (2.1) for $j = 1$ and equation (2.12) for $j = 2$. The quantity 2γ is the total angle of sea surface subtended by the coastline for a given annulus of ocean. The annulus width is $\frac{c\tau_R}{2}$ where c is the speed of light and τ_R is the pulse width of the Doppler radar signal.

Equation (2.49) with $j = 2$ is a two-dimensional integral equation of the *first* kind (see, for example, Mciseiwitsch (1977)). The basic task confronted here is that of *inverting* this equation to give the directional ocean wave spectrum, $S(\vec{k})$ (or, equivalently, the normalized form, $Z(\vec{K})$) which is contained in the $\sigma_2(\omega, \phi, d)$ integral. The following subsections give the required components of a Fourier basis approach to this inversion problem.

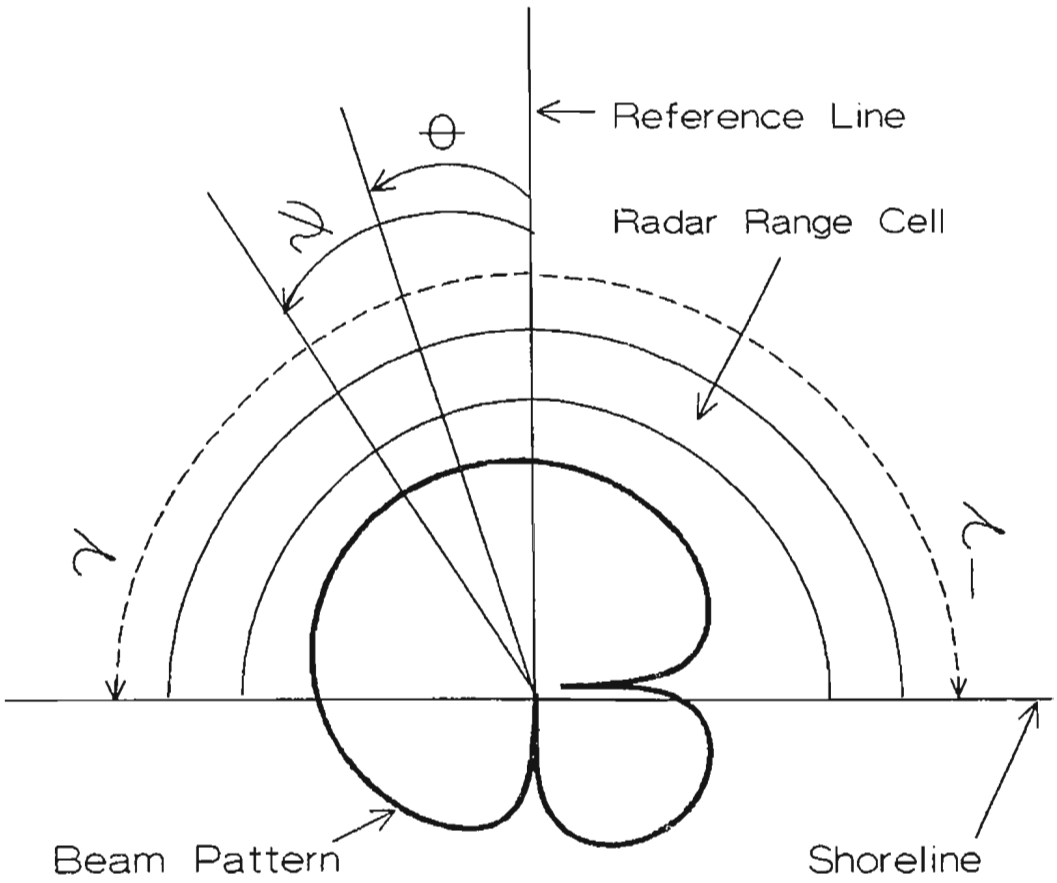

FIGURE 2: Sketch of a four-element square array beam pattern showing a typical semi-circular annulus of ocean from which the antenna receives backscattered radiation when operation occurs from a straight shoreline. The scan angle, ψ, the narrow beam look direction, Φ, and the shore angle, γ, are measured relative to a reference line joining the 2-4 axis of the array. The array is oriented such that the reference line also bisects the ocean annulus.

2.3.1 The Beam Pattern and its Fourier Coefficients

For an n-point receive array, the beam pattern response as given by Capon et al. (1967) and Capon (1969) is

$$G(\psi,\phi) = \left| \frac{1}{n} \sum_{i=1}^{n} a_i e^{i(\vec{K_\psi} - \vec{K_\phi})\cdot\vec{r_i}} \right|^2 \tag{2.50}$$

where a_i is a weighting function for the i^{th} sensor signals and $\vec{r_i}$ is the position vector, relative to an arbitrarily chosen origin, for the i^{th} sensor. The vectors $\vec{K_\psi}$ and $\vec{K_\phi}$, associated with the angles ψ and ϕ respectively are defined as follows:

$$\vec{K_\psi} = k_0 \cos(\psi)\,\hat{\imath} + k_0 \sin(\psi)\,\hat{\jmath} \tag{2.51}$$

$$\vec{K_\phi} = -k_0 \cos(\phi)\,\hat{\imath} - k_0 \sin(\phi)\,\hat{\jmath} \tag{2.52}$$

with $\hat{\imath}$ and $\hat{\jmath}$ being unit vectors along mutually perpendicular axes and

$$k_0 = \frac{2\pi}{\lambda} \tag{2.53}$$

being the radar wavenumber associated with the radio wavelength, λ, of the transmit antenna. Figure 3 depicts these various vectors as they are related to a four-element square array. Again, note the choice of the 2–4 axis of the array as the reference line for all angles. Of course, for this array with the origin chosen at the centre, the magnitude of $\vec{r_i}$ for all i is a constant (i. e. $|\vec{r_i}| = r$ for all i).

If, as has been conventional for the four-element CODAR, a_i is chosen to be one(1) for all i, then equation (2.50) gives

$$G(\psi,\phi) = \left| \frac{1}{4} \sum_{i=1}^{4} e^{i(\vec{K_\psi} - \vec{K_\phi})\cdot\vec{r_i}} \right|^2 \tag{2.54}$$

Using equations (2.51) and (2.52) along with the obvious algebra, equation (2.54) yields

$$\begin{aligned} G(\psi,\phi) = {} & \cos^2\left\{ \frac{k_0 r}{\sqrt{2}} [\sin(\psi - \tfrac{\pi}{4}) - \sin(\phi - \tfrac{\pi}{4})] \right\} \\ & \cdot \cos^2\left\{ \frac{k_0 r}{\sqrt{2}} [\cos(\psi - \tfrac{\pi}{4}) - \cos(\phi - \tfrac{\pi}{4})] \right\} . \end{aligned} \tag{2.55}$$

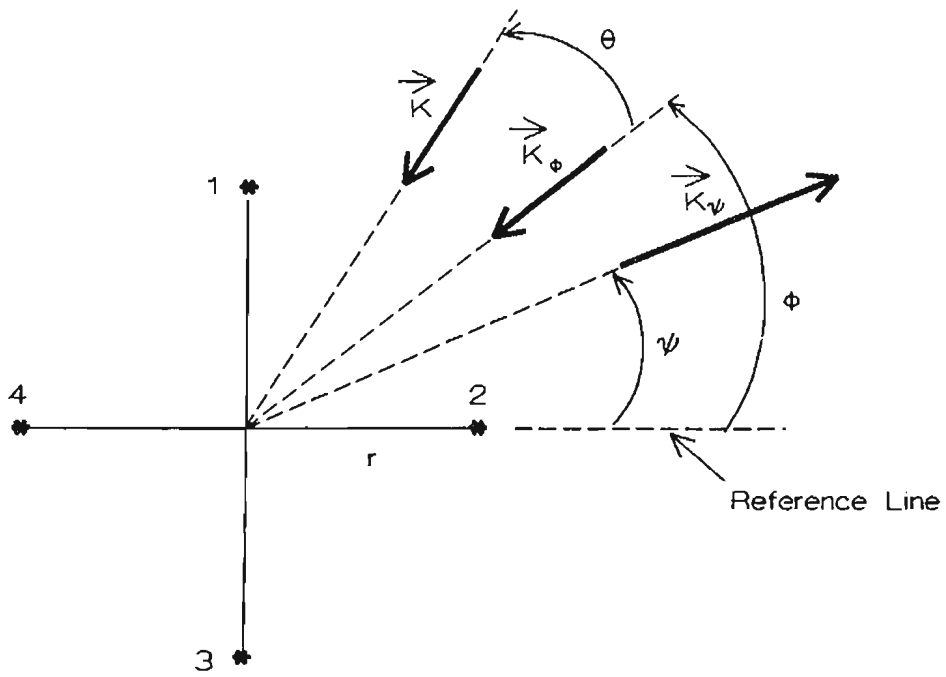

FIGURE 3: Illustration of the various wavevectors associated with the broad beam analysis. The numbered asterisks are the radar elements. The unsubscripted K vector is that of an ocean wave responsible for backscatter.

During the course of the analysis, it is required that $G(\psi,\phi)$ from equation (2.55) be written in its double Fourier series over ψ and ϕ. Here, we state the form of the series and the corresponding Fourier coefficients, while in Appendix A, the derivation of these results is outlined. In general series form, the beam pattern becomes

$$G(\psi,\phi) = \sum_{t,p=0}^{\infty} \left(g_{tpc}\cos(t\psi)\cos(p\phi) + \left(g_{tps}\sin(t\psi)\sin(p\phi)\right)\right) . \tag{2.56}$$

The c and s subscripts have been chosen to represent the cosine and sine subscripts respectively. As is indicated in Appendix A, the coefficients of the cross terms, $\cos(t\psi)\sin(p\phi)$ and $\sin(t\psi)\cos(p\phi)$, are identically zero. In equation (2.56),

$$\begin{aligned} g_{tpc} \;=\; & \epsilon_{tp}\left\{\delta_{tp} + \frac{1}{4}J_t(2\zeta)J_p(2\zeta)\left[\cos\left(\frac{(t-p)\pi}{4}\right)\left(1+(-1)^{t+p}\right)\right.\right. \\ & + \cos\left(\frac{(t+p)\pi}{4}\right)\left((-1)^t+(-1)^p\right) + 4\cos\left(\frac{t\pi}{4}\right)\cos\left(\frac{p\pi}{4}\right)\cos\left(\frac{(t-p)\pi}{2}\right)\Big] \\ & + \frac{1}{8}J_t(2\sqrt{2}\zeta)J_p(2\sqrt{2}\zeta)\left[\left(1+(-1)^t\right)\left(1+(-1)^p\right)\right. \\ & \left.\left. + \cos\left(\frac{(t-p)\pi}{2}\right)\left(1+(-1)^{t+p}\right) + \cos\left(\frac{(t+p)\pi}{2}\right)\left((-1)^t+(-1)^p\right)\right]\right\} \end{aligned} \tag{2.57}$$

and

$$\begin{aligned} g_{tps} \;=\; & \frac{1}{4}J_t(2\zeta)J_p(2\zeta)\left[\cos\left(\frac{(t-p)\pi}{4}\right)\left(1+(-1)^{t+p}\right)\right. \\ & - \cos\left(\frac{(t+p)\pi}{4}\right)\left((-1)^t+(-1)^p\right) + 4\sin\left(\frac{t\pi}{4}\right)\sin\left(\frac{p\pi}{4}\right)\cos\left(\frac{(t-p)\pi}{2}\right)\Big] \\ & + \frac{1}{8}J_t(2\sqrt{2}\zeta)J_p(2\sqrt{2}\zeta)\left[\left(1-(-1)^t\right)\left(1-(-1)^p\right)\right] , \end{aligned} \tag{2.58}$$

where

$$\epsilon_{tp} = \begin{cases} \frac{1}{4}, & t=p=0 \\ \frac{1}{2}, & t=0,\ p\neq 0 \text{ or } t\neq 0,\ p=0 \\ 1, & t,p>0\ , \end{cases}$$

$$\delta_{tp} = \begin{cases} 1, & t=p=0 \\ 0, & \text{otherwise}\ , \end{cases}$$

$$\zeta = \frac{2k_0 r}{\sqrt{2}}\ ,$$

and $J_t(\zeta)$ and $J_t(\zeta)$ are Bessel functions of the first kind.

TABLE 1: The Four-Element Square Array Beam Pattern Coefficients for Array Radius of 2.54 m

t	Cos-Cos Coefficients							Sin-Sin Coefficients						
	p							p						
	0	1	2	3	4	5	6	0	1	2	3	4	5	6
0	.293	.000	.000	.000	-.015	.000	.000	.000	.000	.000	.000	.000	.000	.000
1	.000	.435	.000	.011	.000	.003	.000	.000	.435	.000	-.011	.000	.003	.000
2	.000	.000	.221	.000	.000	.000	.003	.000	.000	.221	.000	.000	.000	-.001
3	.000	.011	.000	.046	.000	-.004	.000	.000	-.011	.000	.046	.000	.004	.000
4	-.015	.000	.000	.000	.011	.000	.000	.000	.000	.000	.000	.000	.000	.000
5	.000	.003	.000	-.004	.000	-.004	.000	.000	.003	.000	.004	.000	.000	.000
6	.000	.000	.003	.000	.000	.000	.000	.000	-.001	.000	.000	.000	.000	.000

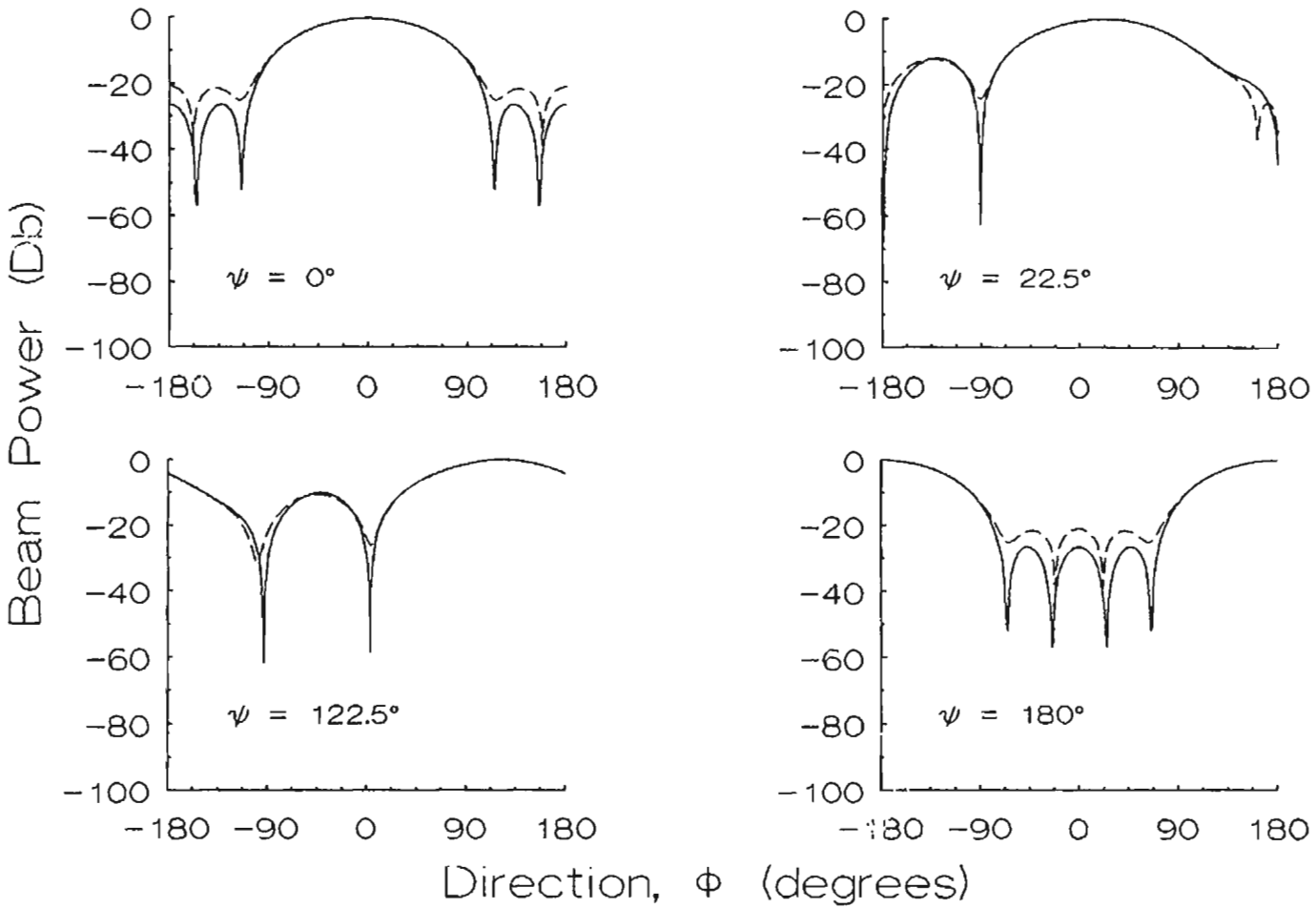

FIGURE 4: Comparison of the 4-element beam pattern (solid line) relative to the maximum power with its truncated Fourier series result (dashed line) for several scan angles, ψ. Array spacing is 2.54 m.

While the series in equation (2.56) does not naturally truncate, it is obvious from the values of g_{tpc} and g_{tps} given in Table 1, that convergence occurs fairly rapidly. This analysis uses values of t and p from 0 to 4 for g_{tpc} and 1 to 3 for g_{tps}. Figure 4 shows the discrepancy between the true $G(\psi, \phi)$ and that obtained from the truncated series for several values of scan angle ψ. The pattern shape is repeated in an *octant-symmetric* fashion (e. g. the shape of the pattern for $\psi = 0°$ and $22.5°$ is the same as for $\psi = 90°$ and $67.5°$ respectively). It is clear from the figure, that for operation from a straight coastline where $-90° \leq \phi \leq 90°$, the truncation is quite valid.

2.3.2 The Ocean Model and its Fourier Coefficients

From the various models of ocean-wave spectra in the literature, we choose the product of a non-directional Pierson-Moskowitz (Moskowitz (1964)) and a cardioid directional factor. Bearing in mind that, as defined following equation (2.12), angle θ is the angle between the scattering wave whose wave vector is $\vec{k}$ and the narrow beam look direction, ϕ (see Figure 3, p. 23), then for the wide beam problem, $\vec{k}$ must make an angle of $(\theta + \phi)$ with the reference line. Thus, in polar form, $\vec{k}$ is given as $(k, \theta + \phi)$. The directional spectrum is then defined by

$$S(\vec{k}) = f(k)\, g(\theta + \phi)\ . \tag{2.59}$$

The Pierson-Moskowitz distribution, $f(k)$, models the typical falloff of saturated-wave energy above a cutoff region defined by wavenumber k_c.

$$f(k) = \frac{0.005 e^{-0.74\left(\frac{k_c}{k}\right)^2}}{k^4}\ . \tag{2.60}$$

The cutoff wavenumber is defined as

$$k_c = \frac{g}{u^2} \tag{2.61}$$

where g is the acceleration due to gravity and u is the wind speed over the region in question. The typical form of the cardioid directional factor (see e. g. Hasselmann et

al. (1980) and Mitsuyasu et al. (1975)) is in general

$$g(\alpha) = \frac{\cos^s\left(\frac{\alpha-\alpha^*}{2}\right)}{\int_{-\pi}^{\pi}\cos^s\left(\frac{\alpha}{2}\right)\,d\alpha} \tag{2.62}$$

where α^* represents the dominant direction of the wavefield. Clearly, here, $\alpha = \theta + \phi$. The quantity s is the spreading factor of the cardioid distribution, and for the purpose of developing simulated radar return in this thesis a typical value of $s = 4$ will be used. Expressed as a Fourier series over angle, truncated to five terms, the directional spectrum is written as

$$S(k,\theta+\phi) = \frac{1}{2\pi}\sum_{n=0}^{2}\left[a_n(k)\cos(n(\theta+\phi)) + b_n(k)\sin(n(\theta+\phi))\right] \tag{2.63}$$

As for any general Fourier series, $b_0(k) = 0$. The other coefficients may be written using the directional coefficients of $g(\theta+\phi)$ provided by Barrick and Lipa (1979b). The results for the first five Fourier coefficients of $S(k,\theta+\phi)$ are:

$$a_0(k) = f(k) \tag{2.64}$$

$$a_1(k) = f(k)\frac{2s}{s+2}\cos(\alpha^*) \tag{2.65}$$

$$a_2(k) = f(k)\frac{2s(s-2)}{(s+2)(s+4)}\cos(2\alpha^*) \tag{2.66}$$

$$b_1(k) = f(k)\frac{2s}{s+2}\sin(\alpha^*) \tag{2.67}$$

$$b_2(k) = f(k)\frac{2s(s-2)}{(s+2)(s+4)}\sin(2\alpha^*)\,. \tag{2.68}$$

When $s = 4$, equations (2.64)–(2.68) become, trivially,

$$a_1(k) = \frac{4f(k)}{3}\cos(\alpha^*) \tag{2.69}$$

$$a_2(k) = \frac{f(k)}{3}\cos(2\alpha^*) \tag{2.70}$$

$$b_1(k) = \frac{4f(k)}{3}\sin(\alpha^*) \tag{2.71}$$

$$b_2(k) = \frac{f(k)}{3}\sin(2\alpha^*)\,. \tag{2.72}$$

For the second scattering wave, whose wave vector is $\vec{k}'$, equation (2.63) is written simply as

$$S(k', \theta' + \phi) = \frac{1}{2\pi} \sum_{l=0}^{2} [a_\ell(k') \cos(\ell(\theta' + \phi)) + b_\ell(k) \sin(\ell(\theta' + \phi))] \ . \tag{2.73}$$

The coefficients a_ℓ and b_ℓ have the same form as those for wavenumber k. Previous investigators (e. g. Lipa and Barrick (1982)) have written θ' to be the same as the Bragg wave direction. While this simplifies the analysis somewhat, it also introduces unnecessary approximations and limits the range of Doppler frequency for which subsequent procedures hold. Here, θ' is therefore kept general.

The normalized ocean spectra, $Z(\vec{K})$ and $Z(\vec{K}')$ defined by equation (2.8) can be written in Fourier series of the form given in equations (2.63) and (2.73). The only difference is that the coefficients will then be

$$a_n(K) = (2k_0)^4 a_n(k) \tag{2.74}$$

and

$$b_n(K) = (2k_0)^4 b_n(k) \tag{2.75}$$

with similar expressions for $a_\ell(K')$ and $b_\ell(K')$.

2.3.3 A Fourier Formulation of the Wide Beam Second-order Cross Section

Writing the second-order wide beam cross section from equation (2.49) and introducing the Fourier expansion for the beam pattern given in equation (2.56) one gets

$$\begin{aligned} \sigma_2(\omega, \psi) \ = \ & \frac{1}{2\gamma} \int_{-\gamma}^{\gamma} \sum_{t,p=0}^{4} [(g_{tpc} \cos(t\psi) \cos(p\phi) \\ & + (g_{tps} \sin(t\psi) \sin(p\phi))] \ \sigma_2(\omega, \phi, d) \, d\phi \ . \end{aligned} \tag{2.76}$$

Here, to simplify the notation, t and p are allowed to vary from 0 to 4 for both g_{tpc} and g_{tps}. However, as previously noted for the four-element square array, $g_{tps} = 0$ for

$t,p = 0$ or 4. Multiplying each term of equation (2.76) by $\frac{\pi}{\pi}$ and interchanging $\int$ and $\sum$ yields

$$\begin{aligned}\sigma_2(\omega,\psi) &= \frac{1}{2\pi}\sum_{t,p=0}^{4}\left\{\cos(t\psi)\int_{-\gamma}^{\gamma}\frac{\pi g_{tpc}\cos(p\phi)}{\gamma}\,\sigma_2(\omega,\phi,d)\,d\phi\right\} \\ &\quad +\frac{1}{2\pi}\sum_{t,p=0}^{4}\left\{\sin(t\psi)\int_{-\gamma}^{\gamma}\frac{\pi g_{tps}\sin(p\phi)}{\gamma}\,\sigma_2(\omega,\phi,d)\,d\phi\right\} \qquad (2.77)\end{aligned}$$

Next, define

$$\left.\begin{aligned}\alpha_t(\omega) &= \frac{\pi}{\gamma}\int_{-\gamma}^{\gamma}\left(\sum_{p=0}^{4} g_{tpc}\cos(p\phi)\right)\sigma_2(\omega,\phi,d)\,d\phi \\ \beta_t(\omega) &= \frac{\pi}{\gamma}\int_{-\gamma}^{\gamma}\left(\sum_{p=0}^{4} g_{tps}\sin(p\phi)\right)\sigma_2(\omega,\phi,d)\,d\phi\end{aligned}\right\} \qquad (2.78)$$

To further compress the notation here and in the remainder of this thesis, consider redefining the range of t to be from -3 to 4. Further, let $g_{tpc} = 0$ for $t < 0$ and $g_{tps} = 0$ for $t > 0$. Then, the pieces of equation (2.78) may be combined into a single coefficient, $b_t(\omega)$, given by

$$b_t(\omega) = \frac{\pi}{\gamma}\int_{-\gamma}^{\gamma}\left\{\sum_{p=0}^{4}\left(g_{tpc}\cos(p\phi) + g_{tps}\sin(p\phi)\right)\right\}\sigma_2(\omega,\phi,d)\,d\phi \qquad (2.79)$$

For later use, we consider normalized coefficients defined by

$$B_t(\eta) = \frac{\gamma b_t(\omega)\omega_B}{\pi}\ . \qquad (2.80)$$

Correspondingly, equation (2.79) normalizes to

$$B_t(\eta) = \int_{-\gamma}^{\gamma}\left(\sum_{p=0}^{4} g_{tpc}\cos(p\phi) + g_{tps}\sin(p\phi)\right)\sigma_2(\eta,\phi,D)\,d\phi\ . \qquad (2.81)$$

Returning, for the present, to unnormalized form, equation (2.79) allows the wide beam cross section of equation (2.77) to be presented as

$$\sigma_2(\omega,\psi) = \frac{1}{2\pi}\sum_{t=-3}^{4} b_t(\omega)\,tf_t(\psi) \qquad (2.82)$$

where

$$tf_t(\psi) = \begin{cases}\cos(t\psi)\ , & t \geq 0 \\ \sin(t\psi)\ , & t < 0\end{cases}\ .$$

Since equation (2.82) is a Fourier representation of $\sigma_2(\omega, \psi)$, we can immediately write

$$b_t(\omega) = \frac{2}{\epsilon_t} \int_{-\pi}^{\pi} \sigma_2(\omega, \psi) t f_t(\psi)\, d\psi \tag{2.83}$$

where

$$\epsilon_t = \begin{cases} 2\,, & t = 0 \\ 1\,, & t \neq 0 \end{cases} .$$

We note that, by simply replacing $\sigma_2(\omega, \psi)$ with $\sigma_1(\omega, \psi)$, the same procedure yields a Fourier formulation of the first-order wide beam cross section. The calculation of the associated coefficients is the subject of Section 2. 4.

The whole subsequent analysis hinges on equations (2.79) and (2.83). While the main body of this thesis deals only with simulated data, Appendix D explains how $\sigma_2(\omega, \psi)$ may be created from real radar data. Once this wide beam cross section is developed, the radar spectral coefficients, $b_t(\omega)$, can be obtained numerically from equation (2.83). Then equation (2.79) or its normalized equivalent (2.81) is *inverted* to yield the Fourier coefficients of the ocean wave spectrum which are an integral part of $\sigma_2(\omega, \phi, d)$ as may be seen from equations (2.12) and (2.63). The details of this inversion are the subject of Chapter 3.

2.4 Calculation of Simulated Normalized Radar Spectral Coefficients

Since the coefficients of the Bragg wave are required for the inversion process, we now present and simplify the expression for the normalized *first-order* radar spectral coefficients. Following this, the *second-order* coefficients given by equation (2.81) are calculated. The whole analysis, apart from the θ-integration within the narrow beam cross section, is completed in closed form.

2.4.1 Simulated First-order Radar Spectral Coefficients

By carrying out a procedure completely analogous to that whereby the normalized second-order radar spectral coefficients were obtained in equation (2.81), the first-order coefficients may be expressed as

$$B_t(\eta) = \int_{-\gamma}^{\gamma} \left(\sum_{p=0}^{4} g_{tpc} \cos(p\phi) + g_{tps} \sin(p\phi) \right) \sigma_1(\eta, \phi)\, d\phi \,. \tag{2.84}$$

It is noteworthy that the depth dependence is ignored here since the first-order return is essentially independent of water depth (see Section 2.1).

Direct substitution of the normalized first-order cross section from equation (2.11) into equation (2.84) yields, upon interchanging $\sum$ and $\int$,

$$\begin{aligned} B_t(\eta) \;=\; 4\pi \sum_{m'=\pm 1} \sum_{p=0}^{4} \int_{-\gamma}^{\gamma} & \left(g_{tpc} \cos(p\phi) + g_{tps} \sin(p\phi) \right) \\ & \cdot Z(-m'\hat{k}_0)\, \delta(\eta - m')\, d\phi \,. \end{aligned} \tag{2.85}$$

Using the Fourier expansion of the ocean model provided by equation (2.63) along with the definitions of $Z(\cdot)$ and the normalized ocean spectral coefficients, $a_n(K)$ and $b_n(K)$, provided in equations (2.8), (2.74) and (2.75) respectively, it is trivial to show that, on changing the coefficient index from n to ℓ,

$$Z(-m'\hat{k}_0) = \frac{1}{2\pi} \sum_{\ell=0}^{2} \left(a_\ell(1) \cos(\ell\phi) + b_\ell(1) \sin(\ell\phi) \right) (-m')^\ell \,. \tag{2.86}$$

It should be noted that in polar form $\hat{k}_0 = (1, \phi)$ where ϕ has the usual meaning. Using equation (2.86) and noting that $\int_{-\gamma}^{\gamma} \cos(\ell\phi)\, \sin(p\phi)\, d\phi = 0$ for all ℓ and p, equation (2.85) takes on the form

$$\begin{aligned} B_t(\eta) \;=\; 2 \sum_{m'=\pm 1} \sum_{\ell=0}^{2} \sum_{p=0}^{4} \int_{-\gamma}^{\gamma} & \left[\left(g_{tpc} a_\ell(1) \cos(\ell\phi) \cos(p\phi) \right. \right. \\ & \left. \left. + g_{tps} b_\ell(1) \sin(\ell\phi) \sin(p\phi) \right] (-m')^\ell \delta(\eta - m')\, d\phi \,. \end{aligned} \tag{2.87}$$

From any suitable mathematics tables (e. g. Prudnikov et al. (1986)) along with an

application of L'Hopital's rule, the ϕ-integration may be written

$$\left.\begin{array}{ll} (1) & \int_{-\gamma}^{\gamma} \cos(\ell\phi)\cos(p\phi)\,d\phi = i_{\ell p_1} + i_{\ell p_2} \\ & \text{where} \quad i_{\ell p_1} = \begin{cases} \frac{\sin((p+\ell)\gamma)}{(p+\ell)} & , p+\ell \neq 0 \\ \gamma & , p+\ell = 0 \end{cases} \\ & \text{and} \quad i_{\ell p_2} = \begin{cases} \frac{\sin((p-\ell)\gamma)}{(p-\ell)} & , p-\ell \neq 0 \\ \gamma & , p-\ell = 0 \end{cases} \\ (2) & \int_{-\gamma}^{\gamma} \sin(\ell\phi)\sin(p\phi)\,d\phi = i_{\ell p_2} - i_{\ell p_1}\ . \end{array}\right\} \quad (2.88)$$

Then,

$$B_t(\eta) = 2 \sum_{m'=\pm 1} \sum_{\ell=0}^{2} \sum_{p=0}^{4} (a_\ell(1) g_{tpc} (i_{\ell p_1} + i_{\ell p_2}) + b_\ell(1) g_{tps} (i_{\ell p_2} - i_{\ell p_1})) \cdot (-m')^\ell \delta(\eta - m')\ . \quad (2.89)$$

The delta-function in equation (2.89) shows the first-order spectral coefficients to be ideally impulse functions occurring at the normalized Bragg frequencies, $\eta_B = \pm 1$. As indicated in section 2.1, these peaks, in nature, are broadened by such influences as system effects (e.g. finite sampling time) and fluctuating ocean currents. To illustrate , Figure 5, to which other references will be made throughout this section, provides a real four-element CODAR spectrum produced in June, 1989 during an experiment designed by the author. To *simulate* the first order, we convolve the first-order spectral coefficients of equation (2.89) with a Gaussian function of the form

$$W(\eta) = \frac{e^{\frac{-\pi\eta^2}{\tau^2}}}{|\tau|} \quad (2.90)$$

where τ is the normalized width of the window $W(\eta)$ (i.e. $\tau = \omega_B \cdot T$, where T is unnormalized width). The rationale for using this function is that, as discussed by Bracewell (1978), it facilitates extraction of information from functions with impulsive behaviour. The procedure yields *smeared* coefficients, $B_{t_c}(\eta)$ of the form

$$\begin{aligned} B_{t_c}(\eta) &= \sum_{m'=\pm 1} E_c \int_{-\infty}^{\infty} \delta(\eta' - m') W(\eta - \eta')\,d\eta' \\ &= \sum_{m'=\pm 1} E_c W(\eta - m') \end{aligned} \quad (2.91)$$

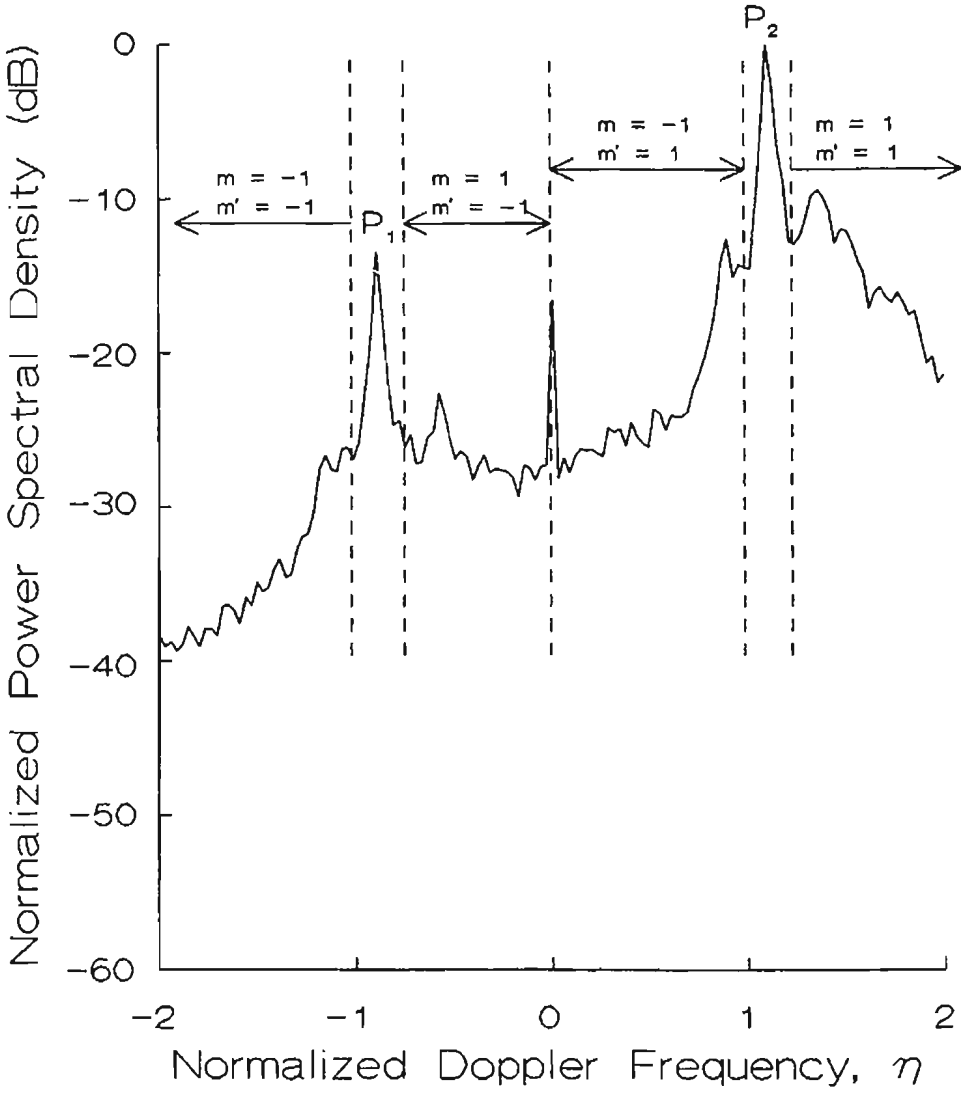

FIGURE 5: A 40-sample averaged CODAR power spectrum obtained on June 14, 1989 for the 45-minute period commencing at 12:38 AM. The spectral density is normalized with respect to its largest value. P_1 and P_2 represent the broadened first-order spectral peaks. The second-order continuum is in the arrowed portions of the spectrum while the values of m and m' represent the possible directions of wavevectors giving rise to the particular portions of the second-order return as referred to in the text.

where E_c includes all the terms on the right side of equation (2.89) except the delta-function. Any convenient value of τ may be used to produce these simulated coefficients. Lipa and Barrick (1986) have effectively used $\tau = 0.05$ in presenting simulated crossed-loops spectral coefficients. Also, the total frequency spread, say $\Delta\eta$, around the normalized Bragg frequencies for use in $W(\eta - m')$ must be examined in view of where nulls between the first- and second-order regions of the radar spectrum occur. For any sea state of interest (see Section 3.1), the simulation programs have shown that $\Delta\eta = 0.24$ will include the region of any significant first-order energy. These values of τ and $\Delta\eta$ will be used throughout the simulations in this thesis.

Rather than plotting the convolved first-order coefficients for various modelled sea states separately, simulated second-order coefficients will be developed so that both may be illustrated together (see Section 2.4.3).

The whole purpose of the procedure outlined in this section is that it might be later shown how a typical, broadened, first-order radar spectrum can be analyzed to give the coefficients of the Bragg wave (see Appendix B). Of course, real first-order radar spectral coefficients can be obtained from equation (2.83) with $\sigma_2(\omega, \psi)$ replaced by $\sigma_1(\omega, \psi)$. The procedure to obtain $\sigma_1(\omega, \psi)$ from real data is the same as presented in Appendix D.

2.4.2 Simulated Second-Order Radar Spectral Coefficients

The form of the simulated second-order coefficients developed will be such as to facilitate the inversion approach in the next chapter. It should be noted that the second-order coefficients, unlike the first-order, already represent a continuum (see Figure 5) and, here, no convolution is carried out. Another reason why the window of the previous section is not applied beyond the first-order peaks is that the already extensive computational time might be kept to a minimum. If the window was applied, it would not affect the ultimate inversion process.

From equations (2.27), (2.34) and (2.81) the normalized second-order radar spectral coefficients become

$$B_t(\eta) = 2^4\pi \sum_{m,m'=\pm1} \sum_{p=0}^{4} \int_{-\theta_0}^{\theta_0} \int_{-\gamma}^{\gamma} [g_{tpc}\cos(p\phi) + g_{tps}\sin(p\phi)] \cdot Z(m\vec{K})Z(m'\vec{K}')\,|\Gamma_N|^2\, y^3 \left|\frac{\partial y}{\partial h}\right|_\theta |_{y=y^*} d\phi\, d\theta \quad (2.92)$$

Using equations (2.63) and (2.73)–(2.75) and the fact that $m, m' = \pm 1$, normalized ocean spectra may be written, using the first five terms of a Fourier series, as

$$\left.\begin{aligned} Z(m\vec{K}) &= \frac{1}{2\pi}\sum_{n=0}^{2} m^n \left(a_n(K)\cos\left(n(\theta+\phi)\right) + b_n(K)\sin\left(n(\theta+\phi)\right)\right) \\ \text{and} \\ Z(m'\vec{K}') &= \frac{1}{2\pi}\sum_{\ell=0}^{2} m'^{\ell} \left(a_\ell(K')\cos\left(\ell(\theta'+\phi)\right) + b_\ell(K')\sin\left(\ell(\theta'+\phi)\right)\right) \end{aligned}\right\} \quad (2.93)$$

Let
$$T(\vec{K},\vec{K}') = Z(m\vec{K}) \cdot Z(m'\vec{K}') \quad (2.94)$$

On expanding the sines and cosines in equation (2.93)

$$\begin{aligned} T(\vec{K},\vec{K}') = \frac{1}{4\pi^2}\sum_{n=0}^{2}\sum_{\ell=0}^{2} m^n m'^{\ell} \{ & a_n(K)a_\ell(K')\left[\cos(n\theta)\cos(\ell\theta')\cos(n\phi)\cos(\ell\phi)\right. \\ & -\cos(n\theta)\sin(\ell\theta')\cos(n\phi)\sin(\ell\phi) - \sin(n\theta)\cos(\ell\theta')\sin(n\phi)\cos(\ell\phi) \\ & \left.+\sin(n\theta)\sin(\ell\theta')\sin(n\phi)\sin(\ell\phi)\right] \\ & +a_n(K)b_\ell(K')\left[\cos(n\theta)\sin(\ell\theta')\cos(n\phi)\cos(\ell\phi)\right. \\ & +\cos(n\theta)\cos(\ell\theta')\cos(n\phi)\sin(\ell\phi) - \sin(n\theta)\sin(\ell\theta')\sin(n\phi)\cos(\ell\phi) \\ & \left.-\sin(n\theta)\cos(\ell\theta')\sin(n\phi)\sin(\ell\phi)\right] \\ & +b_n(K)a_\ell(K')\left[\sin(n\theta)\cos(\ell\theta')\cos(n\phi)\cos(\ell\phi)\right. \\ & -\sin(n\theta)\sin(\ell\theta')\cos(n\phi)\sin(\ell\phi) + \cos(n\theta)\cos(\ell\theta')\sin(n\phi)\cos(\ell\phi) \\ & \left.-\cos(n\theta)\sin(\ell\theta')\sin(n\phi)\sin(\ell\phi)\right] \\ & +b_n(K)b_\ell(K')\left[\sin(n\theta)\sin(\ell\theta')\cos(n\phi)\cos(\ell\phi)\right. \\ & +\sin(n\theta)\cos(\ell\theta')\cos(n\phi)\sin(\ell\phi) + \cos(n\theta)\sin(\ell\theta')\sin(n\phi)\cos(\ell\phi) \\ & \left.+\cos(n\theta)\cos(\ell\theta')\sin(n\phi)\sin(\ell\phi)\right]\} \ . \end{aligned} \quad (2.95)$$

Before substituting $T(\vec{K},\vec{K}')$ into equation (2.92) we note the following aids to simplification:

(1) from equation (2.30) it is straightforward to show that $\sin(\theta')$ is an odd function of θ; i. e.

$$\sin(\theta')\,|_{\theta} = -\sin(\theta')\,|_{-\theta}$$

and $\cos(\theta')$ is an even function of θ; i. e.

$$\cos(\theta')\,|_{\theta} = \cos(\theta')\,|_{-\theta}\ ;$$

(2) using (1), it is easy to see from equations (2.14), (2.43) and (2.45) that Γ_N is an even function of θ ;

and

(3) $\frac{\partial y}{\partial h}\,|_{\theta}$, given in equation (2.33), is an even function of θ.

Considering facts (1), (2), and (3) above, it is obvious that any terms of $T(\vec{K},\vec{K}')$ containing the products $\cos(n\theta)\sin(\ell\theta')$ or $\sin(n\theta)\cos(\ell\theta')$ will integrate to zero in equation (2.92). Thus, we define a new function, $T_1(\vec{K},\vec{K}')$ which contains only those terms of $T(\vec{K},\vec{K}')$ capable of producing non-zero results in the evaluation of the θ-integral of $B_i(\eta)$:

$$\begin{aligned}
T_1(\vec{K},\vec{K}') \;=\; & \frac{1}{4\pi^2}\sum_{n=0}^{2}\sum_{\ell=0}^{2} m^n m'^{\ell}\,\{a_n(K)a_\ell(K') \\
& [\cos(n\theta)\cos(\ell\theta')\cos(n\phi)\cos(\ell\phi) + \sin(n\theta)\sin(\ell\theta')\sin(n\phi)\sin(\ell\phi)] \\
& + a_n(K)b_\ell(K')\,[\cos(n\theta)\cos(\ell\theta')\cos(n\phi)\sin(\ell\phi) \\
& \qquad - \sin(n\theta)\sin(\ell\theta')\sin(n\phi)\cos(\ell\phi)] \\
& + b_n(K)a_\ell(K')\,[\cos(n\theta)\cos(\ell\theta')\sin(n\phi)\cos(\ell\phi) \\
& \qquad - \sin(n\theta)\sin(\ell\theta')\cos(n\phi)\sin(\ell\phi)] \\
& + b_n(K)b_\ell(K')\,[+\cos(n\theta)\cos(\ell\theta')\sin(n\phi)\sin(\ell\phi) \\
& \qquad + \sin(n\theta)\sin(\ell\theta')\cos(n\phi)\cos(\ell\phi)]\}
\end{aligned} \tag{2.96}$$

Similar reductions are possible for the ϕ-integration of equation (2.92) because

the angle reference line is chosen to make the ϕ integration limits from $-\gamma$ to γ. If the expression for $T_1(\vec{K},\vec{K}')$ in equation (2.96) were substituted into equation (2.92), the beam pattern part of the integrand (i. e. $[g_{tpc}\cos(p\phi)+g_{tps}\sin(p\phi)]$) would, upon multiplication by the former, produce terms containing $\cos(p\phi)\cos(n\phi)\sin(\ell\phi)$, $\cos(p\phi)\sin(n\phi)\cos(\ell\phi)$, $\sin(p\phi)\cos(n\phi)\cos(\ell\phi)$, and $\sin(p\phi)\sin(n\phi)\sin(\ell\phi)$. These odd functions of ϕ obviously integrate to zero. Thus, carrying out the suggested substitution will yield an integrand containing only eight terms to be integrated over ϕ rather than sixteen terms present if the reference line were not chosen through the centre of the ocean annulus being viewed (see Figure 2, p. 21). In fact, these eight terms really consist of four pairs of integrations of the form

$$s_{n\ell p_1} = \int_{-\gamma}^{\gamma}\cos(n\phi)\cos(\ell\phi)\cos(p\phi)\,d\phi \tag{2.97}$$

$$s_{n\ell p_4} = \int_{-\gamma}^{\gamma}\cos(n\phi)\sin(\ell\phi)\sin(p\phi)\,d\phi \tag{2.98}$$

$$s_{n\ell p_6} = \int_{-\gamma}^{\gamma}\sin(n\phi)\sin(\ell\phi)\cos(p\phi)\,d\phi \tag{2.99}$$

$$s_{n\ell p_7} = \int_{-\gamma}^{\gamma}\sin(n\phi)\cos(\ell\phi)\sin(p\phi)\,d\phi \tag{2.100}$$

The missing terms, $s_{n\ell p_2}$, $s_{n\ell p_3}$, $s_{n\ell p_5}$, and $s_{n\ell p_8}$, are those which integrate to zero over the natural course of the algebra.

To facilitate the presentation of the integral values in equations (2.97)–(2.100) we define the following:

$$\left.\begin{aligned} t_1 &= n+\ell+p \\ t_2 &= \ell+p-n \\ t_3 &= n+p-\ell \\ t_4 &= n+\ell-p \end{aligned}\right\} \tag{2.101}$$

and

$$d_j = \begin{cases} \frac{\sin(t_j\gamma)}{t_j} & , t_j \neq 0 \\ \gamma & , \ t_j = 0 \end{cases} \tag{2.102}$$

where $j = 1,\ldots,4$. Then from Prudnikov et al. (1986) and using l'Hopital's rule,

$$s_{n\ell p_1} = \frac{1}{2}\left[d_1+d_2+d_3+d_4\right] \tag{2.103}$$

$$s_{n\ell p_4} = \frac{1}{2}\left[d_3+d_4-d_1-d_2\right] \tag{2.104}$$

$$s_{n\ell p_6} = \frac{1}{2}\left[d_2 + d_3 - d_1 - d_4\right] \tag{2.105}$$

$$s_{n\ell p_7} = \frac{1}{2}\left[d_2 + d_4 - d_1 - d_3\right] \tag{2.106}$$

Rewriting equation (2.92) using equations (2.93), (2.94), and (2.96) and the discussion following the latter, the normalized radar coefficients take on the form

$$\begin{aligned} B_t(\eta) = \frac{8}{\pi} \sum_{m,m'=\pm 1} \sum_{n=0}^{2} \sum_{\ell=0}^{2} \sum_{p=0}^{4} \int_0^{\theta_0} |\Gamma_N|^2 \left|\frac{\partial y}{\partial h}\right|_\theta |_{y=y^*} y^3 m^n m'^\ell \cdot \\ \left\{a_n(K)\left[\cos(n\theta)\cos(\ell\theta')C_{1_{an\ell pt}} + \sin(n\theta)\sin(\ell\theta')C_{2_{an\ell pt}}\right] + \right. \\ \left. b_n(K)\left[\cos(n\theta)\cos(\ell\theta')C_{1_{bn\ell pt}} + \sin(n\theta)\sin(\ell\theta')C_{2_{bn\ell pt}}\right]\right\} d\theta \end{aligned} \tag{2.107}$$

where

$$\left.\begin{aligned} C_{1_{an\ell pt}} &= g_{tpc}a_\ell(K')s_{n\ell p_1} + g_{tps}b_\ell(K')s_{n\ell p_4} \\ C_{2_{an\ell pt}} &= g_{tpc}a_\ell(K')s_{n\ell p_6} - g_{tps}b_\ell(K')s_{n\ell p_7} \\ C_{1_{bn\ell pt}} &= g_{tps}a_\ell(K')s_{n\ell p_7} + g_{tpc}b_\ell(K')s_{n\ell p_6} \\ C_{2_{bn\ell pt}} &= -g_{tps}a_\ell(K')s_{n\ell p_4} + g_{tpc}b_\ell(K')s_{n\ell p_1} \end{aligned}\right\} \tag{2.108}$$

In equation (2.107), the θ-integral limits have been changed to 0, θ_0 from -θ_0, θ_0 because the integrand is an even function of θ. The integral limits are easily shown to be $\pm\pi$ for $|\eta| \leq \sqrt{2}$ and $\pm\left[\pi - \cos^{-1}(\frac{2}{\eta^2})\right]$ for $|\eta| > \sqrt{2}$. Also shown by Lipa and Barrick (1982) for the narrow beam radar is that the four possible combinations of m and m' represent four different regions of the Doppler radar spectrum. Since the wide beam cross section is simply the integration of the product of the beam pattern with the narrow beam cross section, the same θ-limits and m, m' characteristics hold here. Figure 5, p. 34, shows the regions of a real spectrum from a four-element square array (CODAR) which correspond to the various values of m and m'. Also, as explained by Lipa and Barrick (1986) equation (2.107) is valid for

$$h < \frac{1}{k_0} \tag{2.109}$$

where h is the *rms* waveheight and k_0 is, as before, the radar wavenumber. If h exceeds this limit, the second-order radar spectrum begins to saturate and the ocean wave height obtained on inverting equation (2.107) will be underestimated. Subject

to other limitations as discussed in the inversion presentation of Chapter 3, lowering the transmit frequency could overcome this problem.

2.4.3 Illustration of Radar Spectral Coefficients

Figures 6–8 show simulated normalized CODAR spectral coefficients for straight shore operation, dominant wave directions of 0, 45, and 90 degrees and a wind speed of $u = 10m/s$ corresponding to a 0.092 normalized cutoff wavenumber. An operational frequency of 25.4 MHz is assumed. The broadened first-order peaks are evident at values of $\eta = \pm 1$. The peaks in the spectrum at $|\eta| = \sqrt{2}$ and $|\eta| = 2^{\frac{3}{4}}$, referred to in Sections 2.2.1 and 2.2.4 respectively, can also be clearly distinguished. The apparent singularities in the spectrum as $\eta \rightarrow 0$ from either side are results of the breakdown in the theoretical formulation of the cross sections in these regions. In the region very close to $\eta = 0$, the ocean waves producing the backscatter are really capillary waves while the theory is devised for gravity waves (Barrick (1972b)). It should be noted that, in practice, all available wave information is extracted well out of this problem region (see Section 3.1). While these coefficients have been calculated for straight shoreline operation, the program of Appendix C can be used for any size ocean sector. If the sector size is reduced by land masses such as headlands, the results may have to take into consideration the interaction of the signal with these obstructions. However, Shearman et al. (1982) have presented results which suggest that, in spite of irregular coastlines, the parts of the antenna pattern in the open-sea direction essentially remain intact.

Figure 9 shows how changing water depth affects the $t = 0$ coefficient for dominant wave direction of 0° and wind speed of 10 m/s. The general effect of increasing energy with decreasing depth is similar for all values of t as well as for different values of dominant direction and sea state. For this reason and because of the author's limited computer space the other coefficients are not shown.

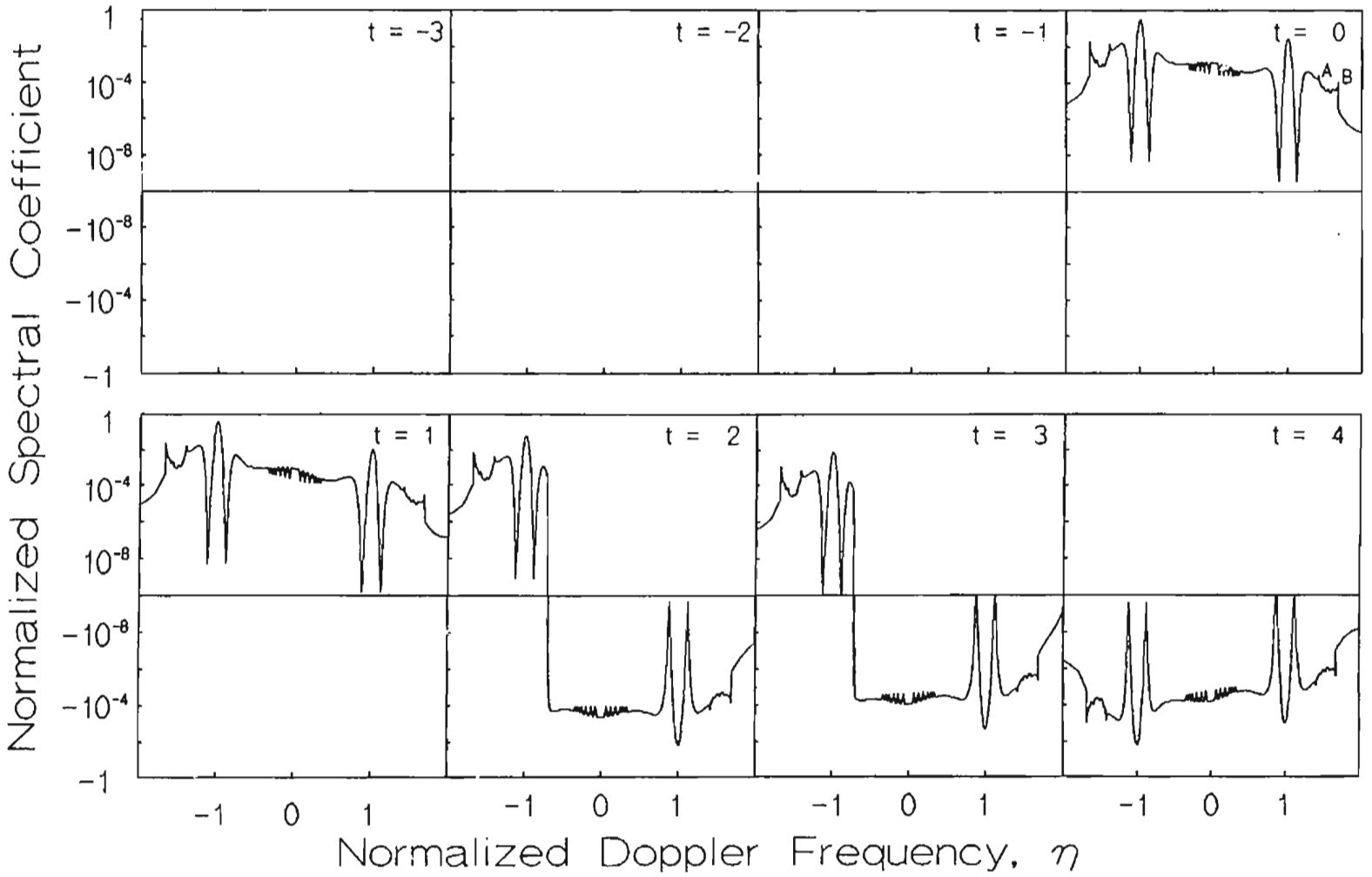

FIGURE 6: Simulated radar spectral coefficients for windspeed of 10 m/s and water depth of 100 m. Points A and B are illustrative of the singularities referred to in the text. Dominant wavefield direction is 0°.

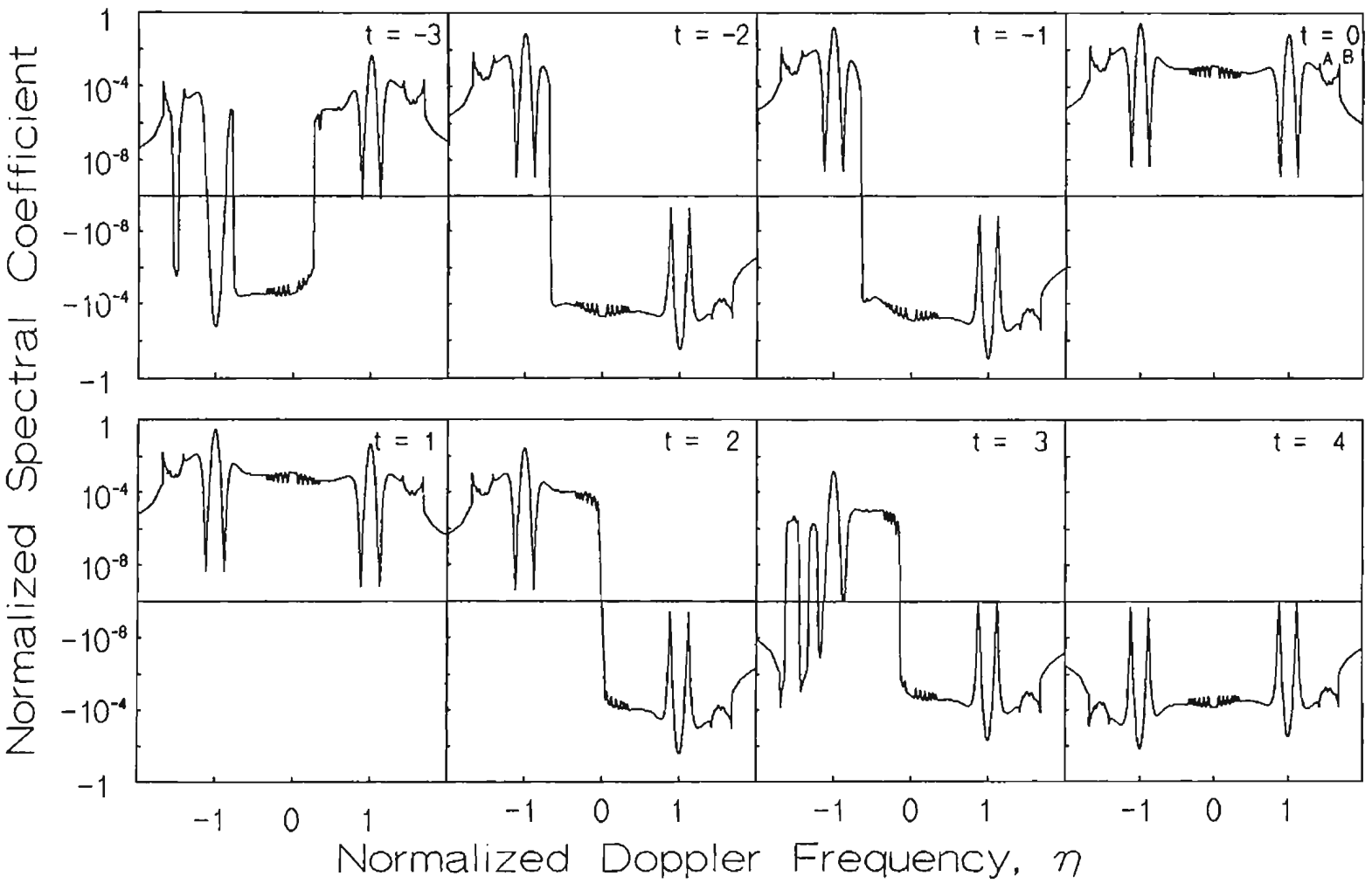

FIGURE 7: Simulated radar spectral coefficients for windspeed of 10 m/s and water depth of 100 m. Points A and B are illustrative of the singularities referred to in the text. Dominant wavefield direction is 45°.

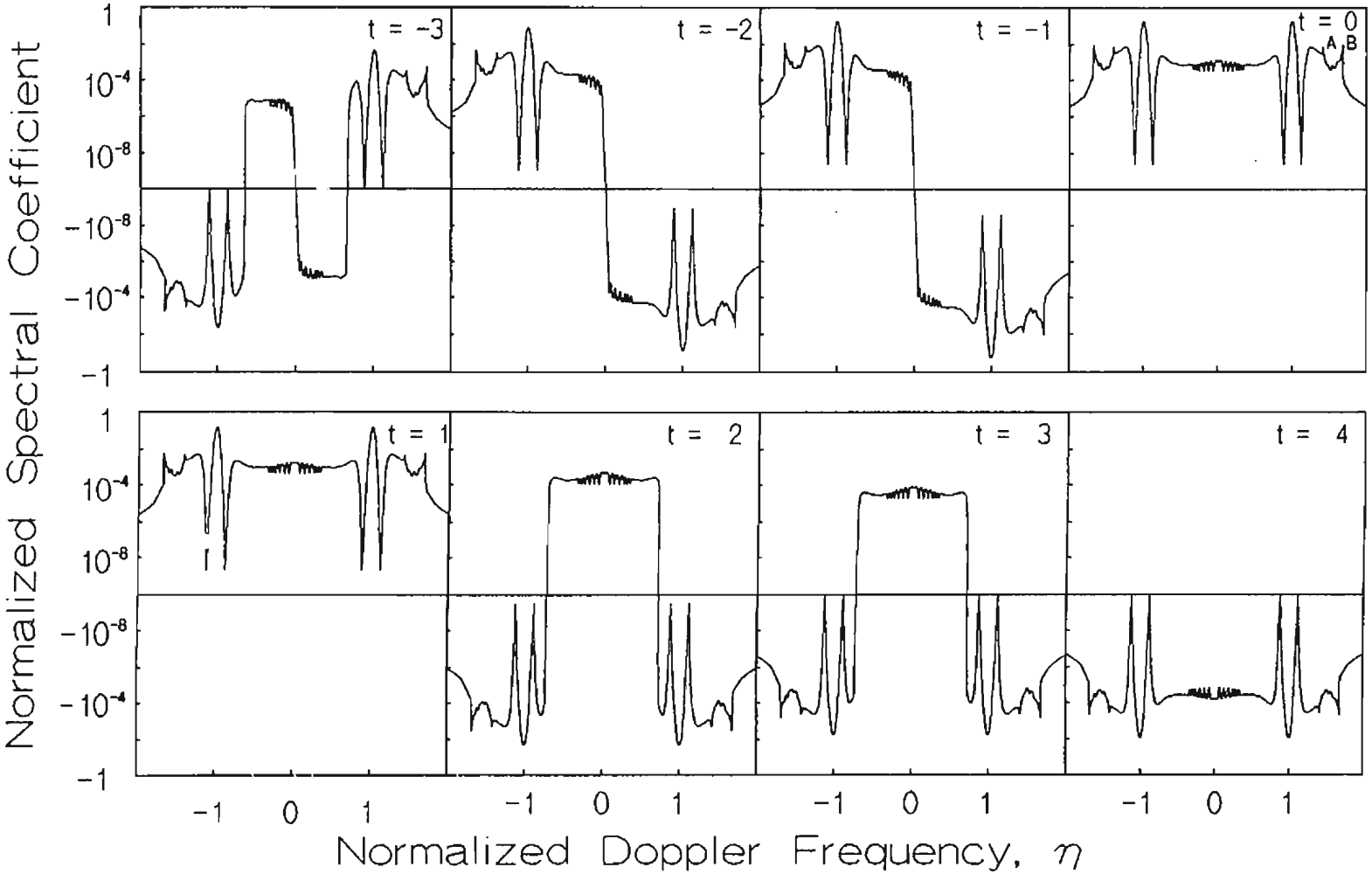

FIGURE 8: Simulated radar spectral coefficients for windspeed of 10 m/s and water depth of 100 m. Points A and B are illustrative of the singularities referred to in the text. Dominant wavefield direction is 90°.

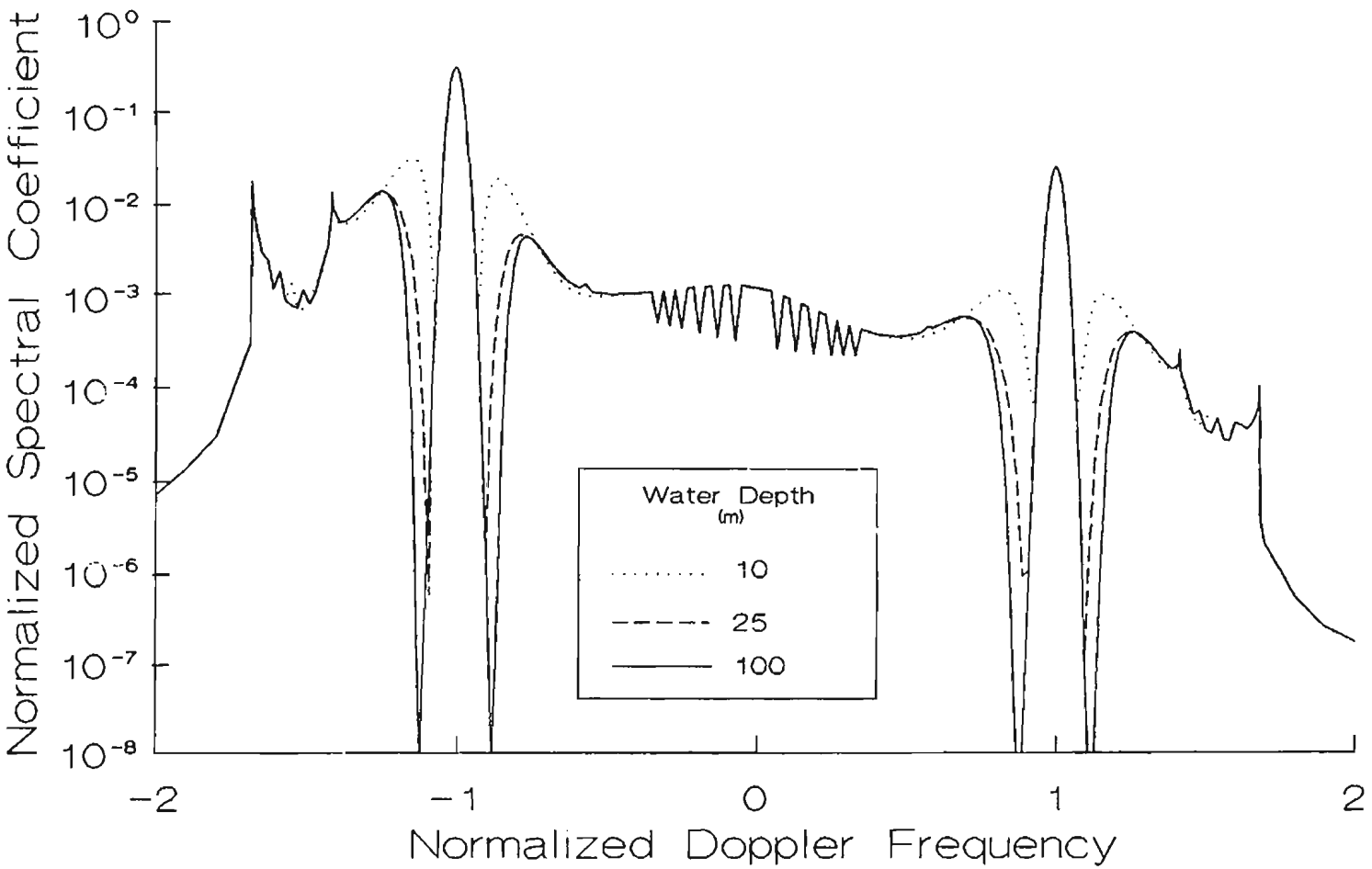

FIGURE 9: Simulated zero-order spectral coefficients showing the effect of water depth on the radar return. The dominant direction of the wavefield with respect to the reference is 0 degrees. Wind speed is 10 m/s.

Figure 10 illustrates the effect on the CODAR spectrum of increasing sea state with depth held fixed. Again, only the coefficient $B_0(\eta)$ is shown and then only for dominant direction of 45°. As before, plotting the other coefficients will not add new information. This simulation was executed by allowing wind speed to increase, thus decreasing the cutoff wavenumber, and increasing the *rms* waveheight according to equations (2.60), (2.64), (2.74) and (3.22) .

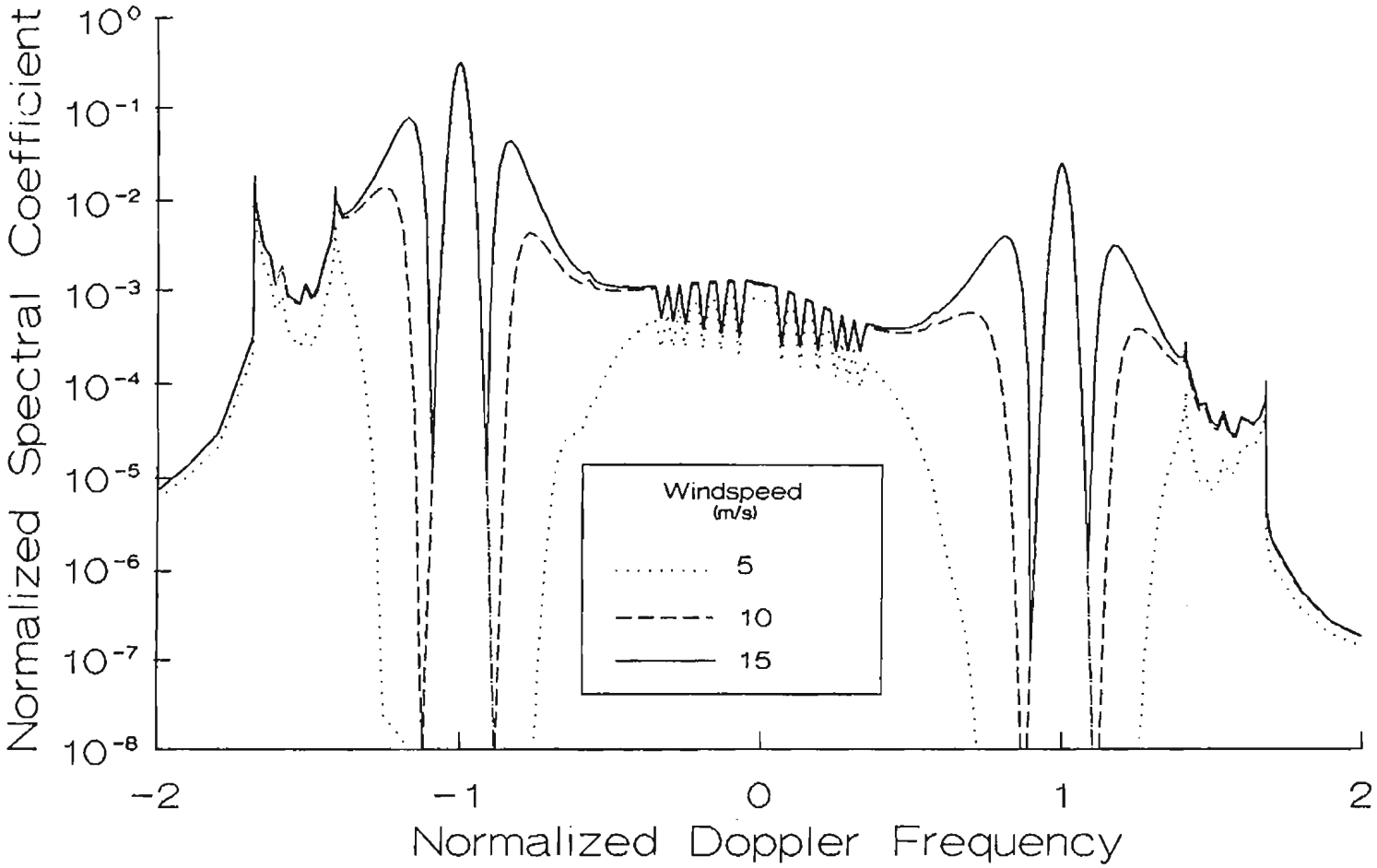

FIGURE 10: Simulated zero-order spectral coefficients showing the effect of increasing seastate on the radar return. The dominant direction of the wavefield with respect to the reference is 0 degrees. Water depth is 100 m.

Chapter 3

The Integral Inversion

The integral inversion of equation (2.107) to provide the normalized Fourier coefficients, $a_n(K)$ and $b_n(K)$, of the ocean wave spectrum is now considered. The limitations of the particular techniques used and the regions of the radar and ocean spectra to which they apply, are discussed. Since we are assuming that there are no ocean currents affecting the radar return, no consideration is given to removing the Doppler frequency bias which would ordinarily be caused by such. Lipa and Barrick (1986), however, show how the cross section equations may be altered to include ocean current effects for crossed-loops radar data. That analysis could also be used, along with the techniques discussed in the previous chapter, for the four-element case.

3.1 The Linearization Scheme

When examined in view of the C's defined by equation (2.108), it is obvious that the integrand in the radar spectral coefficients of equation (2.107) is nonlinear. That is, the integrand contains factors such as $a_n(K)a_\ell(K')$, $a_n(K)b_\ell(K')$, etc. all of which are the product of two unknown, but related, quantities. Before the integral equation can be *inverted* to yield the quantities of interest, namely $a_n(K)$ and $b_n(K)$, it must be linearized.

First, in the spirit of Lipa and Barrick (1982), it is assumed that the waves with wave vector $\vec{K}'$ lie in the saturated region of the ocean wave spectrum along with the

Bragg wave. Further, it is assumed that the directional distribution of all $\vec{K}'$ vectors is the same as that of the Bragg wave. The linearization implements a Phillips equilibrium spectrum (Phillips (1977)) given by

$$f_{\mathrm{P}} = \begin{cases} \frac{0.005}{K'^4} , & K' \geq K_c = \frac{g}{2k_0 u^2} \\ 0 , & K' < K_c . \end{cases} \tag{3.1}$$

The assumption (after Lipa and Barrick (1982)) then invoked for the Fourier coefficients of the scatterer whose wavenumber is K' is that these are related to the Bragg wave of normalized wavenumber K_B by

$$a_\ell(K') = \frac{a_\ell(K_B)}{K'^4} \tag{3.2}$$

and

$$b_\ell(K') = \frac{b_\ell(K_B)}{K'^4} . \tag{3.3}$$

Clearly, $K_B = 1$ (see equations (2.4) and (2.7)). The coefficients $a_\ell(K_B)$ and $b_\ell(K_B)$ are obtained from the first-order radar return (see Appendix B).

Rather than taking the direction of the $\vec{K}'$ scatterer to be the same as that of the Bragg wave as was suggested by Lipa and Barrick, we maintain the general direction of this wave vector as θ'. While this adds only slight complication to the analysis, it does reduce the approximation in the linearization process, as θ' deviates up to $\approx 10^\circ$ from the values of either 0° or 180° which are the possible directions of the Bragg wave. Barrick (1977a) indicates that the approximation introduced by equations (3.2)–(3.3) is valid for $k_0 h > 0.15$ where h is, as before, *rms* waveheight. For an operational frequency of 25.4 MHz, this corresponds to a minimum h of $\approx$ 30 cm or, equivalently, sustained wind speed of $\approx$ 8 m/s over the ocean region under examination. As alluded to in Section 2.1, this linearization approach clearly eliminates the need for knowledge of system and path gains and losses, provided these are essentially the same for both the first- and second-order radar cross sections of the ocean surface.

Using equations (3.2)–(3.3), equation (2.107) for the normalized second-order four-element CODAR coefficients is written in linearized form as

$$
\begin{aligned}
B_t(\eta) \;=\; & \frac{8}{\pi} \sum_{m,m'=\pm 1} \sum_{n=0}^{2} \sum_{\ell=0}^{2} \sum_{p=0}^{4} \int_0^{\theta_0} |\Gamma_N|^2 \left| \frac{\partial y}{\partial h} \right|_\theta |_{y=y^*} \left(\frac{y^3}{K_4'} \right) m^n m'^{\ell} \cdot \\
& \Big\{ a_n(K) \left[\cos(n\theta) \cos(\ell\theta') C_{1_{an\ell pt}} + \sin(n\theta) \sin(\ell\theta') C_{2_{an\ell pt}} \right] \; + \\
& b_n(K) \left[\cos(n\theta) \cos(\ell\theta') C_{1_{bn\ell pt}} + \sin(n\theta) \sin(\ell\theta') C_{2_{bn\ell pt}} \right] \Big\} \, d\theta \qquad (3.4)
\end{aligned}
$$

where the C's of equation (2.108) are redefined as

$$
\left.
\begin{aligned}
C_{1_{an\ell pt}} &= g_{tpc} a_\ell(K_B) s_{n\ell p_1} + g_{tps} b_\ell(K_B) s_{n\ell p_4} \\
C_{2_{an\ell pt}} &= g_{tpc} a_\ell(K_B) s_{n\ell p_6} - g_{tps} b_\ell(K_B) s_{n\ell p_7} \\
C_{1_{bn\ell pt}} &= g_{tps} a_\ell(K_B) s_{n\ell p_7} + g_{tpc} b_\ell(K_B) s_{n\ell p_6} \\
C_{2_{bn\ell pt}} &= -g_{tps} a_\ell(K_B) s_{n\ell p_4} + g_{tpc} b_\ell(K_B) s_{n\ell p_1}
\end{aligned}
\right\} \qquad (3.5)
$$

with $K_B = 1$.

In light of the preceding linearization assumptions and the constraint imposed on the *rms* waveheight by equation (2.109), equation (3.4) can be expected to apply during sea states for which 0.30 m $< h <$ 1.9 m. As mentioned in Section 2.4.2, h may be extended beyond this limit by operating at a lower frequency. It must, however, be remembered that reducing the frequency is constrained by the assumptions made in equations (3.2)–(3.3). That is, it must always be considered whether all the $\vec{K}'$ vectors of interest still correspond to waves in the saturated region of the ocean wave spectrum.

Howell (1990), using a similar linearization for the second-order narrow beam cross section, has achieved very good inversion results for the above mentioned sea states. Further, he has found that essentially all useful ocean spectral information is found from regions of the radar spectrum for which $||\eta| - 1| < 0.4$. Thus, in reality, a relatively small range of Doppler frequency need be examined. Again, since the wide beam cross section is simply the integration of the product of the beam pattern and the narrow beam cross section, the same range of Doppler will be examined here. Furthermore, since, here, the direction of $\vec{K}'$ is not restricted, it is to be expected that our linearization should be even more robust than that given in the above references.

3.2 Discretization of the Second-order Equation

We recall from Section 2.3.3 that the radar spectral coefficients, $B_t(\eta)$, given in normalized form can, in practice, be developed from the raw radar data. It has been explained that here, however, only simulated coefficients are examined. Whether one discusses real or simulated coefficients, the process of inverting equation (3.4) to obtain the normalized ocean spectral coefficients, $a_n(K)$ and $b_n(K)$, remains the same. In this section, a discrete matrix system is created from the integral equation. Inversion of this system leads to the desired ocean spectral information.

To facilitate the presentation, we define the following:

$$\begin{aligned}\alpha_{n\ell pt}(\theta,\eta) &= \frac{8}{\pi}|\Gamma_N|^2\left|\frac{\partial y}{\partial h}\right|_\theta|_{y=y^*}\left(\frac{y^3}{K_4'}\right)m^n m'^\ell \\ &\quad\cdot\left(\cos(n\theta)\cos(\ell\theta')C_{1_{an\ell pt}}+\sin(n\theta)\sin(\ell\theta')C_{2_{an\ell pt}}\right)\ . \qquad (3.6)\end{aligned}$$

$$\begin{aligned}\beta_{n\ell pt}(\theta,\eta) &= \frac{8}{\pi}|\Gamma_N|^2\left|\frac{\partial y}{\partial h}\right|_\theta|_{y=y^*}\left(\frac{y^3}{K_4'}\right)m^n m'^\ell \\ &\quad\cdot\left(\cos(n\theta)\cos(\ell\theta')C_{1_{bn\ell pt}}+\sin(n\theta)\sin(\ell\theta')C_{2_{bn\ell pt}}\right)\ . \qquad (3.7)\end{aligned}$$

From Section 2.4.2 it is evident that, for each value of η, that value determines which *one* of the four possible combinations of m and m' give non-zero results for the second-order integration. Then, using equations (3.6)–(3.7), the normalized radar spectral coefficients of equation (3.4) may be written as

$$\begin{aligned}B_t(\eta) &= \sum_{n=0}^{2}\sum_{\ell=0}^{2}\sum_{p=0}^{4}\int_0^{\theta_0}\alpha_{n\ell pt}(\theta,\eta)\,a_n(K)\,d\theta \\ &\quad+\sum_{n=0}^{2}\sum_{\ell=0}^{2}\sum_{p=0}^{4}\int_0^{\theta_0}\beta_{n\ell pt}(\theta,\eta)\,b_n(K)\,d\theta \\ &= \sum_{\ell=0}^{2}\sum_{p=0}^{4}\int_0^{\theta_0}\alpha_{0\ell pt}(\theta,\eta)\,a_0(K)\,d\theta \\ &\quad+\sum_{\ell=0}^{2}\sum_{p=0}^{4}\int_0^{\theta_0}\alpha_{1\ell pt}(\theta,\eta)\,a_1(K)\,d\theta \\ &\quad+\cdots \\ &\quad+\sum_{\ell=0}^{2}\sum_{p=0}^{4}\int_0^{\theta_0}\beta_{2\ell pt}(\theta,\eta)\,b_2(K)\,d\theta\ . \qquad (3.8)\end{aligned}$$

In this formulation of $B_t(\eta)$, it must be observed that, for fixed η, K changes with each value of θ. This is clear from the solution to the delta-function constraint in Section 2.2.3. Thus, if the integral equation (3.8) is to be discretized, some assumption must be made as to ranges of wavenumbers over which the ocean spectral coefficients $a_0(K), \ldots, b_2(K)$ are considered constant. The author has found, numerically, that the problem of inverting the matrix equation to be formed from equation (3.8) becomes more stable if these ranges of wavenumber are decreased for η's closer to the Bragg frequencies. This is accomplished by using a technique formulated by Howell (1990) based on a description of the η contours in $K - \theta$ space provided by Lipa and Barrick (1982). From the latter, it may be deduced using the delta-function constraint that the smallest ocean wave frequency of interest occurs at the smallest value of $||\eta| - 1|$ under consideration with $L = mm' = -1$ and $\theta = 180°$. The largest frequency appears at the biggest value of $||\eta| - 1|$ with $L = 1$ and $\theta = 180°$. Howell divided this total ocean wave frequency range into a convenient number of sub-ranges depending on the desired resolution. Appendix C allows for alteration of these ranges. Using the dispersion relation of equation (2.2) the equal length sub-ranges or *bands* of frequency were converted into wavenumber *bands*. Due to the non-linearity of the dispersion relation, the latter are not of equal size and, as desired, are smaller for smaller frequencies.

Let i wavenumber bands be demarcated by $K_1, K_2, \ldots, K_j, K_{j+1}, \ldots, K_i, K_{i+1}$. Any wavenumber K_j such that $1 \leq j < i+1$ shall be considered to belong to the j^{th} band. That is, the j^{th} band may be represented as $[K_j, K_{j+1})$ which is an interval closed on the lower end but open on the upper. Next, we let the wavenumber K_{m_j} defined by

$$K_{m_j} = \frac{K_j + K_{j+1}}{2}$$

be representative of the entire j^{th} band. Then, equation (3.8) is to be inverted for $a_0(K_{m_j}), \ldots, b_2(K_{m_j})$. To illustrate the discretization process, consider, initially,

only the first term on the right-hand-side of equation (3.8) to be evaluated at some particular normalized Doppler frequency, say $\eta = \eta_p$. For this frequency, that term becomes

$$\begin{aligned}\sum_{\ell=0}^{2}\sum_{p=0}^{4}\int_{0}^{\theta_0}\alpha_{0\ell pt}(\theta,\eta_p)\,a_0(K)\,d\theta &= \left[\sum_{\ell=0}^{2}\sum_{p=0}^{4}\int_{0}^{\theta_1}\alpha_{0\ell pt}(\theta,\eta_p)\,d\theta\right]\,a_0(K_{m_1}) \\ &\quad + \cdots + \left[\sum_{\ell=0}^{2}\sum_{p=0}^{4}\int_{\theta_{i-1}}^{\theta_i}\alpha_{0\ell pt}(\theta,\eta_p)\,d\theta\right]\,a_0(K_{m_i}) \\ &= \Psi_{a_0 1t}a_0(K_{m_1}) + \cdots + \Psi_{a_0 it}a_0(K_{m_i}) \qquad (3.9)\end{aligned}$$

where the definitions of $\Psi_{a_0 1t},\ldots,\Psi_{a_n it}$ are obvious. In this illustration, a_0 is considered, so $n = 0$. Also, the upper limit on each integral corresponds to the direction of the largest wavenumber in the band to which that integration applies. Thus, for example, $\theta_i = \theta_0$, is associated with the last wavenumber of the i^{th} band. No η will require the use of all i bands. The Ψ's for unused bands for a particular Doppler frequency will simply have the value zero.

Now, the other four terms on the right-hand-side of equation (3.8) can be expressed after the fashion of equation (3.9). That is, at Doppler frequency point η_p, the entire normalized coefficient $B_t(\eta_p)$ becomes

$$\begin{aligned}B_t(\eta_p) &= [\Psi_{a_0 1t}a_0(K_{m_1}) + \cdots + \Psi_{a_0 it}a_0(K_{m_i})]_{\eta_p} \\ &\quad + [\Psi_{a_1 1t}a_1(K_{m_1}) + \cdots + \Psi_{a_1 it}a_1(K_{m_i})]_{\eta_p} \\ &\quad + \cdots \\ &\quad + [\Psi_{b_2 1t}b_2(K_{m_1}) + \cdots + \Psi_{b_2 it}b_2(K_{m_i})]_{\eta_p} \qquad (3.10)\end{aligned}$$

In matrix notation, this becomes

$$B_t(\eta_p) = \left[\left[\begin{array}{ccc} \Psi_{a_0 1t} & \cdots & \Psi_{b_2 1t} \end{array} \right] \cdots \left[\begin{array}{ccc} \Psi_{a_0 it} & \cdots & \Psi_{b_2 it} \end{array} \right] \right]_{\eta_p} \left[\begin{array}{c} \left[\begin{array}{c} a_0(K_{m_1}) \\ \vdots \\ b_2(K_{m_1}) \end{array} \right] \\ \vdots \\ \left[\begin{array}{c} a_0(K_{m_j}) \\ \vdots \\ b_2(K_{m_j}) \end{array} \right] \\ \vdots \\ \left[\begin{array}{c} a_0(K_{m_i}) \\ \vdots \\ b_2(K_{m_i}) \end{array} \right] \end{array} \right] . \tag{3.11}$$

Now, for each value of η, there are eight B_t's corresponding to $t = -3, \ldots, 4$. Noting that for each of the i wavenumber bands there are five ocean coefficients, we define the following $(8 \times 5i)$ matrix $\underline{\underline{A}}_p$ as

$$\underline{\underline{A}}_p = \left[\begin{array}{ccc} \left[\begin{array}{ccc} \Psi_{a_0 1(-3)} & \cdots & \Psi_{b_2 1(-3)} \end{array} \right] & \cdots & \left[\begin{array}{ccc} \Psi_{a_0 i(-3)} & \cdots & \Psi_{b_2 i(-3)} \end{array} \right] \\ \vdots & & \vdots \\ \left[\begin{array}{ccc} \Psi_{a_0 14} & \cdots & \Psi_{b_2 14} \end{array} \right] & \cdots & \left[\begin{array}{ccc} \Psi_{a_0 i4} & \cdots & \Psi_{b_2 i4} \end{array} \right] \end{array} \right]_{\eta_p} . \tag{3.12}$$

Secondly, consider defining $\underline{B}_p$ to be the (8×1) column vector of *radar* spectral coefficients corresponding to Doppler frequency η_p by

$$\underline{B}_p = \left[\begin{array}{c} B_{-3}(\eta_p) \\ \vdots \\ B_4(\eta_p) \end{array} \right] . \tag{3.13}$$

Lastly, we denote the $(5i \times 1)$column vector of *ocean* spectral coefficients appearing on the far right of equation (3.11) to be $\underline{X}$. From equations (3.12) and (3.13) and the last definition, the complete matrix form of equation (3.11) may be represented as

$$\underline{\underline{A}}_p \underline{X} = \underline{B}_p . \tag{3.14}$$

Equation (3.14) represents information on only particular normalized frequency. For every other frequency of interest, an equation of the latter form may be written.

If there are ξ values of η, then the total system may be represented by

$$\begin{bmatrix} \underline{\underline{A}}_1 \\ \vdots \\ \underline{\underline{A}}_p \\ \vdots \\ \underline{\underline{A}}_\xi \end{bmatrix} \cdot \underline{X} = \begin{bmatrix} \underline{B}_1 \\ \vdots \\ \underline{B}_p \\ \vdots \\ \underline{B}_\xi \end{bmatrix} \tag{3.15}$$

or simply

$$\underline{\underline{A}} \cdot \underline{X} = \underline{B} \,. \tag{3.16}$$

Since the elements of $\underline{\underline{A}}$ are themselves $(8 \times 5i)$ matrices, $\underline{\underline{A}}$ may be considered to be an $(8\xi \times 5i)$ matrix. Similarly, $\underline{B}$ is an $(8\xi \times 1)$ column vector. Recalling, in summary, that ξ is the number of values of η and i is the number of wave number bands, we see that equation (3.16) is a discrete version of the second-order four-element square array cross section of the ocean surface given by equation (3.4).

3.3 Solution of the Matrix Equation

Before proceeding to solve equation (3.16), certain characteristics of that system should be examined. Firstly, the system is a discretized form of a Fredholm-type integral equation of the *first kind.* As indicated by Phillips (1962) and Twomey (1963), the inversion problem is usually *ill-posed.* That is, small changes in the $\underline{B}$ values, due, for example, to noise, can often lead to large distortion in the solution vector, $\underline{X}$. Further degradation occurs here because the integral equation (3.4) is itself an approximation due to the linearization scheme used to obtain it. For these reasons, matrix $\underline{\underline{A}}$ in equation (3.16) will, in general, be singular, and an exact solution is not possible. Indeed, in all the calculations of $\underline{\underline{A}}$ done for this present work, this matrix has turned out to be rank-deficient. Although the present analysis using simulated data does not include noise, it is desired that the inversion process be made robust enough to be adapted to measured data.

For the sea states referred to in Section (3.1), Howell (1990) has solved a system

similar to that in equation (3.16) using measured narrow beam data. The regions of the radar spectrum significantly affecting the inversion process were from 10–20 dB above the noise floor. His technique, involving a singular value decomposition (SVD) of the matrix $\underline{\underline{A}}$, has produced results for ocean spectra which correlated well with other sensors.

Among others, Stewart (1973) provides the theory of the SVD of a matrix. Here, we simply outline how it is applied to the system of equation (3.16). The basic premise is that, for any real $(m \times n)$ matrix $\underline{\underline{A}}$, there are orthogonal matrices $\underline{\underline{U}}$ and $\underline{\underline{V}}$, of dimensions $(m \times m)$ and $(n \times n)$ respectively, such that

$$\underline{\underline{U}}^T \underline{\underline{A}}\, \underline{\underline{V}} = \begin{bmatrix} \Sigma & \cdots & 0 \\ \vdots & \ddots & \vdots \\ 0 & \cdots & 0 \end{bmatrix}, \tag{3.17}$$

where $\sum$ is a diagonal matrix whose non-zero elements are $\mu_1, \mu_2, \ldots, \mu_r$ with $\mu_1 \geq \mu_2 \geq \ldots \geq \mu_r > 0$. The matrix $\underline{\underline{U}}^T$ is the transpose of $\underline{\underline{U}}$. Equation (3.17) represents the singular value decomposition of the matrix $\underline{\underline{A}}$.

The *pseudo-inverse* of $\underline{\underline{A}}$, sometimes referred to as the generalized inverse (see Strang (1976)), is defined by

$$\underline{\underline{A}}^+ = \underline{\underline{V}} \begin{bmatrix} \Sigma^{-1} & \cdots & 0 \\ \vdots & \ddots & \vdots \\ 0 & \cdots & 0 \end{bmatrix} \underline{\underline{U}}^T . \tag{3.18}$$

If in equation (3.16) $\underline{\underline{A}}$ is singular, one cannot say that $\underline{X} = \underline{\underline{A}}^{-1} \underline{B}$. Rather, using the pseudo-inverse, we write

$$\underline{X}_r = \underline{\underline{A}}^+ \underline{B} \tag{3.19}$$

where, as shown by Strang (1976), $\underline{X}_r$ is the *optimal* linear least squares solution to the initial system $\underline{\underline{A}}\, \underline{X} = \underline{B}$. A routine developed by Dongarra et al. (1979) to produce the SVD of a matrix is incorporated into the inversion program of Appendix C. To help stabilize the present routine, the author has found that it is better to create matrix $\underline{\underline{A}}$ by placing rows associated with increasingly large values of $||\eta| - 1|$

adjacent to each other. If this is not done, the zero-elements referred to in Section 3.2 will be spread sporadically throughout the matrix rather than being *grouped*, and the inversion results will be less smooth.

Once the SVD of matrix $\underline{\underline{A}}$ is calculated, it becomes clear that some of the singular values, $\mu_1, \ldots, \mu_r$, are extremely small. It has been found for this analysis that the singular value list must be truncated or the smallest values will overpower the inversion algorithm. The decision of how many of these values should be retained for the subsequent calculation of $\underline{\underline{X}}_r$ is discussed in the next sections.

3.4 Calculation of Ocean Spectra from Simulated Radar Data

Before illustrating inversion results obtained using the software given in Appendix C, a few comments regarding the general nature and limitations of these procedures and outcomes are in order.

Firstly, the FORTRAN code presented herein uses single-precision calculations almost exclusively. One of the reasons for this is that the creation and storage of matrix $\underline{\underline{A}}$, whose dimensions are usually about (448×160), require a large amount of computer workspace which would be essentially twice as big for double-precision. It has been found that the SVD routine performs better when $\underline{\underline{A}}$ is submitted to it as a double-precision matrix, even though the latter is created using single-precision variables. In light of this it is expected that minimizing round-off errors, by initially creating $\underline{\underline{A}}$ with double-precision variables, would add to the stability of the subsequent inversion. Of course, for a dedicated system precision would not be a constraining factor.

Secondly, as previously mentioned, if those singular values of $\underline{\underline{A}}$ which are relatively very small are not deleted before $\underline{\underline{A}}^+$ is calculated, the inversion becomes unstable. There is generally a range of such values over which inversion results are

nearly constant. The selection of this range is done by comparing ocean spectra obtained from the inversion process with those calculated directly from a model. While the inversion itself is done only for simulated data to begin with, Howell (1990) has found that the number of singular values retained for good results using real data have the same ranges as for corresponding modelled data. Particular details on this aspect of the algorithm follow.

3.4.1 Illustrations of Typical Ocean Spectra

Figures 11–12 show examples of ocean spectra obtained from data simulated as shown in Section 2.4 for various sea states and a water depth of 100 m. Figure 13 depicts the typical behaviour of the singular values associated with the inversion process. It has been found, numerically, that for sea states to which the analysis applies (see Section 3.1), the appropriate choice of singular values falls in the range of about 120–138 regardless of the dominant wavefield direction. This range is seen in the singular value plots to occur just preceding an appreciable increase in the absolute value of the slopes. Thus, of the typical 160 columns of matrix $\underline{\underline{A}}$ one can expect that only about 75–85% of these are actually linearly independent.

The oscillations which are apparent to the right of the spectral peaks may, at least partially, be accounted for by the fact that the linearization assumption of Section 3.1 is not as good for the smaller values of K' (and thus for larger values of K). Also, the wavenumber bands discussed in Section 3.2 become wider for larger values of K, so that the resolution for the right-hand tails of the spectra produced by the inversion process is reduced. Finally, because $\underline{\underline{A}}$ is large, it is to be expected that round-off errors in the SVD process may lead to some instability in the final result.

To improve the inversion results, the ranges of Doppler frequency, η, which should be implemented for particular sea states are adjusted to ensure that the largest radar spectral values are always included. As sea state increases, this necessitates that the

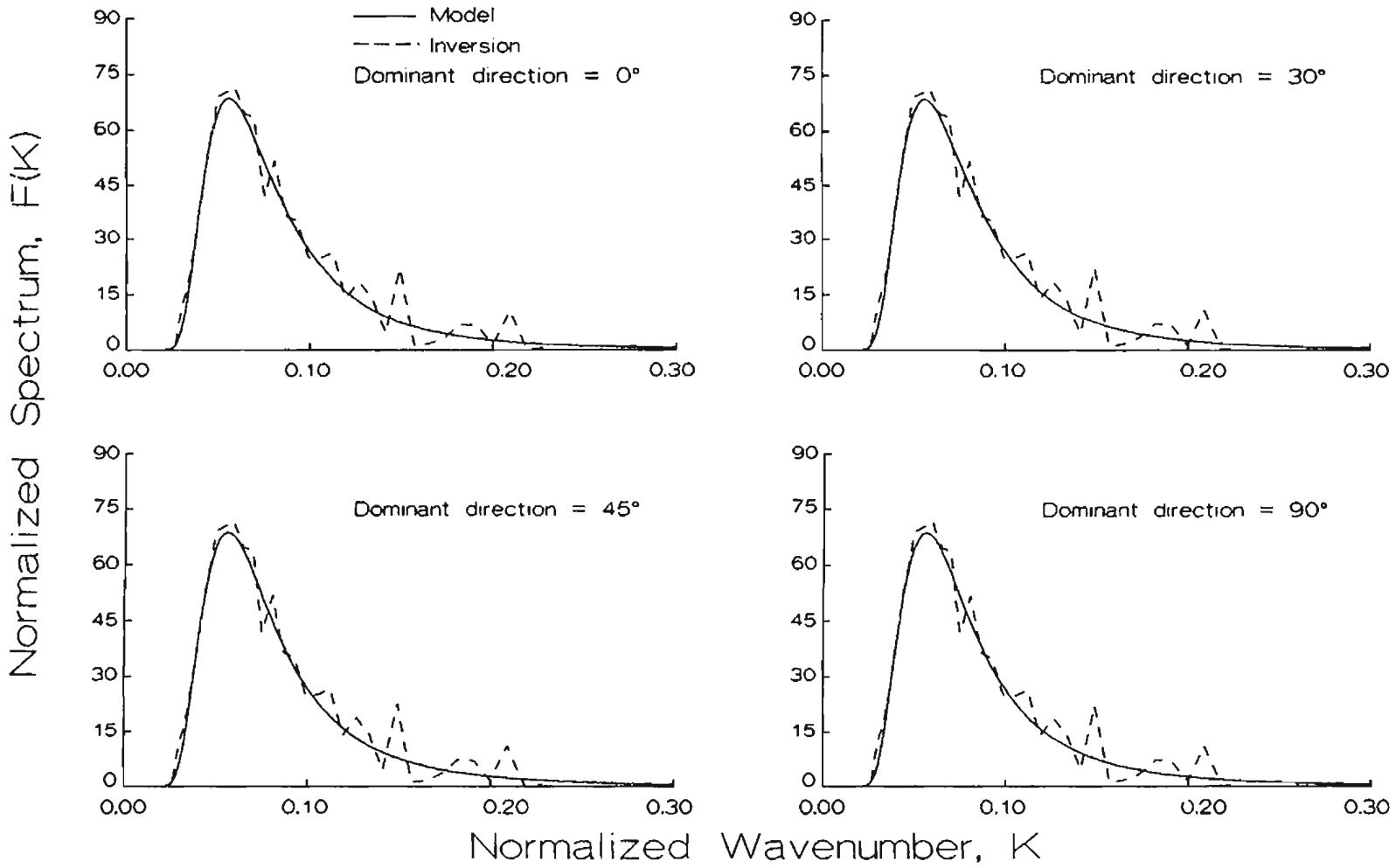

FIGURE 11: Comparison of spectra from inversion with Pierson–Moskowitz model for four dominant wavefield directions. The windspeed is 10 m/s corresponding to normalized cutoff wavenumber of 0.092.

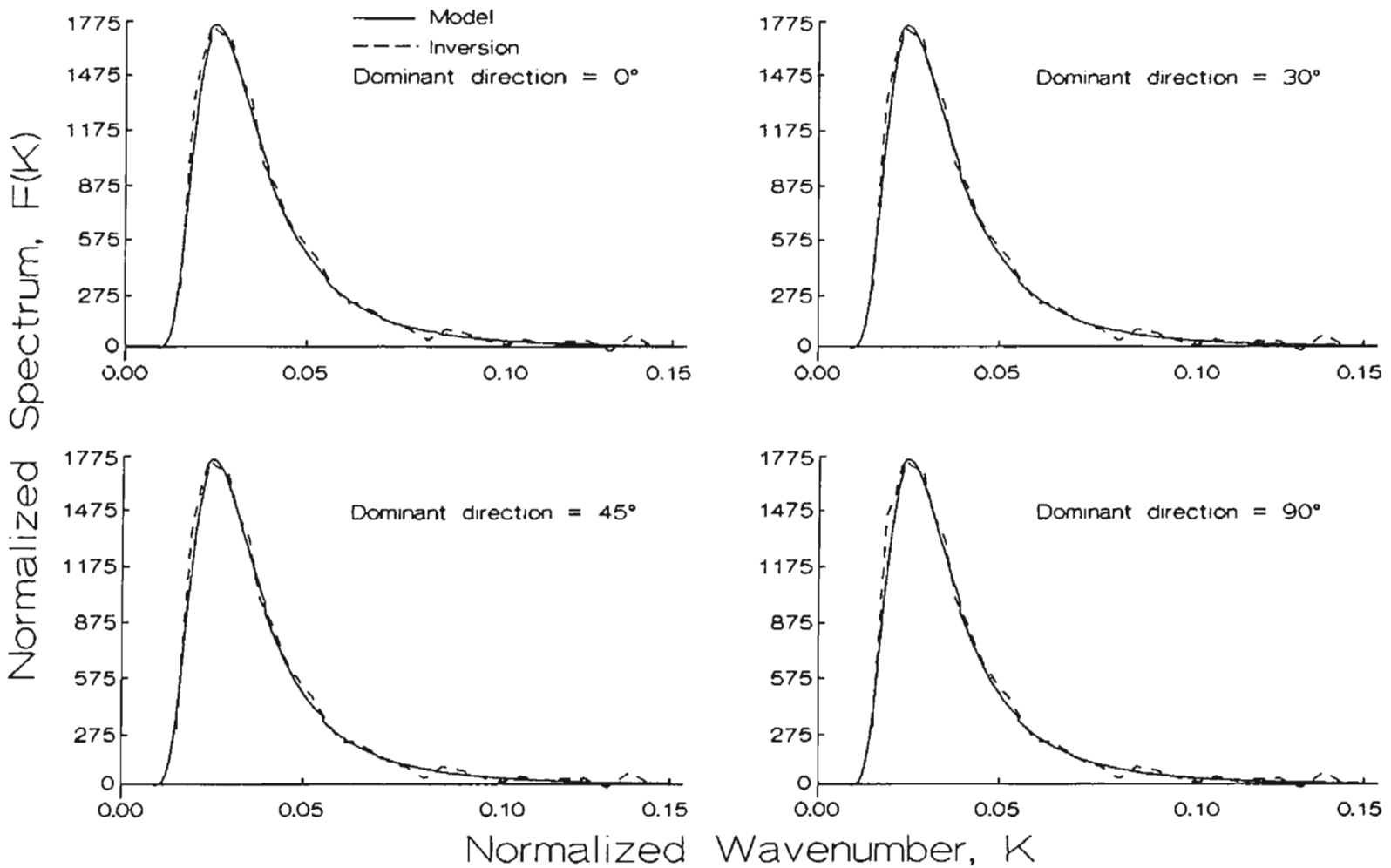

FIGURE 12: Comparison of spectra from inversion with Pierson–Moskowitz model for four dominant wavefield directions. The windspeed is 15 m/s corresponding to normalized cutoff wavenumber of 0.041.

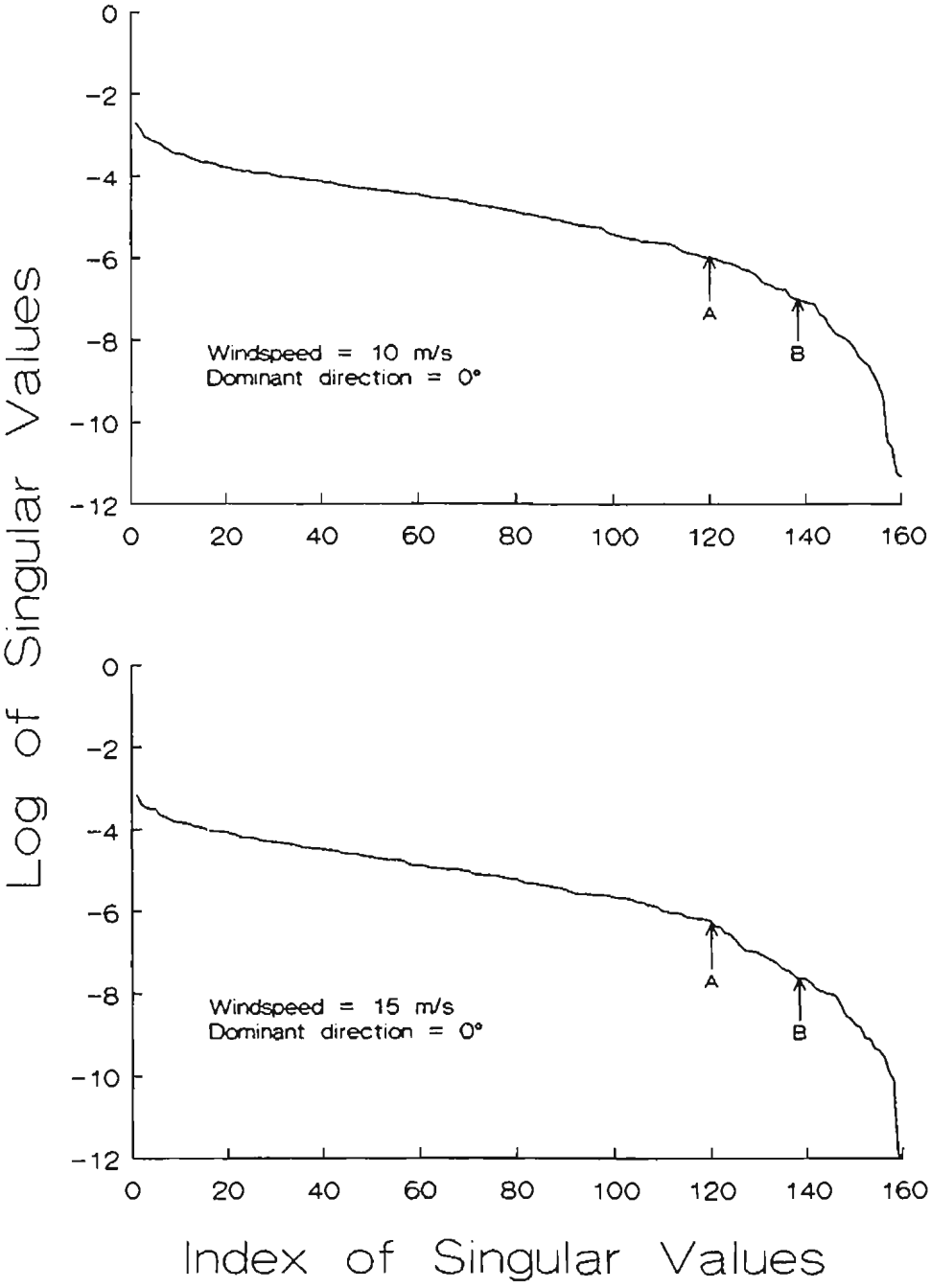

FIGURE 13: Behaviour of the singular values used in the inversion algorithm for two cases of windspeed and dominant wavefield direction. The interval between arrows A and B gave the best results.

radar spectrum be analyzed starting at ever decreasing values of $||\eta| - 1|$. By the same token, as sea state increases, the *total* range of η, which must be included to give good inversion results, may be decreased to yield better resolution in the ocean spectrum. By comparing Figures 11 and 12, it becomes evident that the oscillations associated with the larger wavenumbers are smaller for higher sea states.

3.4.2 Normalized RMS Waveheight

By defining normalized *rms* waveheight as

$$H = 2k_0 h \tag{3.20}$$

where h is the *rms* waveheight, one may write from Lipa and Barrick (1986) that

$$H^2 = \int_0^{\infty} \int_{-\pi}^{\pi} K Z(\vec{K})\, dK\, d(\theta + \phi) \tag{3.21}$$

where, again, $\vec{K} = (K, \theta + \phi)$. Using the first five Fourier coefficients of $Z(\vec{K})$ from equation (2.93), equation (3.21) simplifies to

$$H^2 = \int_0^{\infty} K a_0(K)\, dK\ . \tag{3.22}$$

Table 2 gives values of H calculated directly from a Pierson-Moskowitz ocean wave model with those extracted from simulated radar spectral coefficients through the inversion process outlined in Section (3.3). The waveheights obtained in the latter case use the zero-order coefficients of the K_m's (i. e. $a_0(K_{m_j})$) defined in Section 3.2. Equation (3.22) is then approximated in the following manner:

$$\begin{aligned} H^2 \;\approx\; & \int_{K_1}^{K_2} K a_0(K_{m_1})\, dK + \cdots \int_{K_j}^{K_{j+1}} K a_0(K_{m_j})\, dK \\ & + \cdots + \int_{K_i}^{K_{i+1}} K a_0(K_{m_i})\, dK \\ =\; & \frac{K_2^2 - K_1^2}{2} a_0(K_{m_1}) + \cdots + \frac{K_{i+1}^2 - K_i^2}{2} a_0(K_{m_i})\ . \end{aligned} \tag{3.23}$$

TABLE 2: Normalized Waveheights for Various Wavefield Conditions

Windspeed (m/s)	Dominant Wavefield Direction (degrees)	Model Normalized rms Waveheight	Inversion Normalized rms Waveheight	% Difference in Normalized rms Waveheight
10	0	0.612	0.626	2.29
10	30	0.612	0.614	0.33
10	45	0.612	0.628	2.61
10	90	0.612	0.628	2.61
15	0	1.422	1.408	0.99
15	30	1.422	1.407	1.06
15	45	1.422	1.408	0.99
15	90	1.422	1.409	0.91

3.4.3 Dominant Direction of the Ocean Wavefield

From the expressions for the Fourier coefficients of the directional ocean wavefield given by equations (2.65)–(2.68) it is easy to see that the dominant direction, α^*, is given by

$$\alpha^* = \tan^{-1}\left(\frac{b_1(K)}{a_1(K)}\right) \tag{3.24}$$

or

$$\alpha^* = \tan^{-1}\left(\frac{b_2(K)}{a_2(K)}\right) . \tag{3.25}$$

In the simulations provided here, α^* is recovered without significant errors for dominant directions of $0°$ and $90°$. For other directions, the results are quite good except in the tails of the spectra where oscillatory features produce some spurious angles. The details of this are clearly seen in Figures 14–15. These figures also indicate the portions of the spectra from which meaningful values of α^* could be obtained. While not shown here, similar success was achieved for negative values of α^*.

3.4.4 Recovery of the Spread Parameter

From equations (2.65)–(2.68) it is readily determined, by squaring and adding the appropriate expressions, that the spread parameter, s, is written in terms of the ocean spectral coefficients as

$$s = \frac{2\sqrt{a_1^2(K) + b_1^2(K)}}{2a_0 - \sqrt{a_1^2(K) + b_1^2(K)}} \tag{3.26}$$

or

$$s = \frac{a_0 + 3\sqrt{a_2^2(K) + b_2^2(K)} + \sqrt{4a_0^2 + 28a_0\sqrt{a_2^2(K) + b_2^2(K)} + (a_2^2(K) + b_2^2(K))}}{2a_0 - \sqrt{a_2^2(K) + b_2^2(K)}} . \tag{3.27}$$

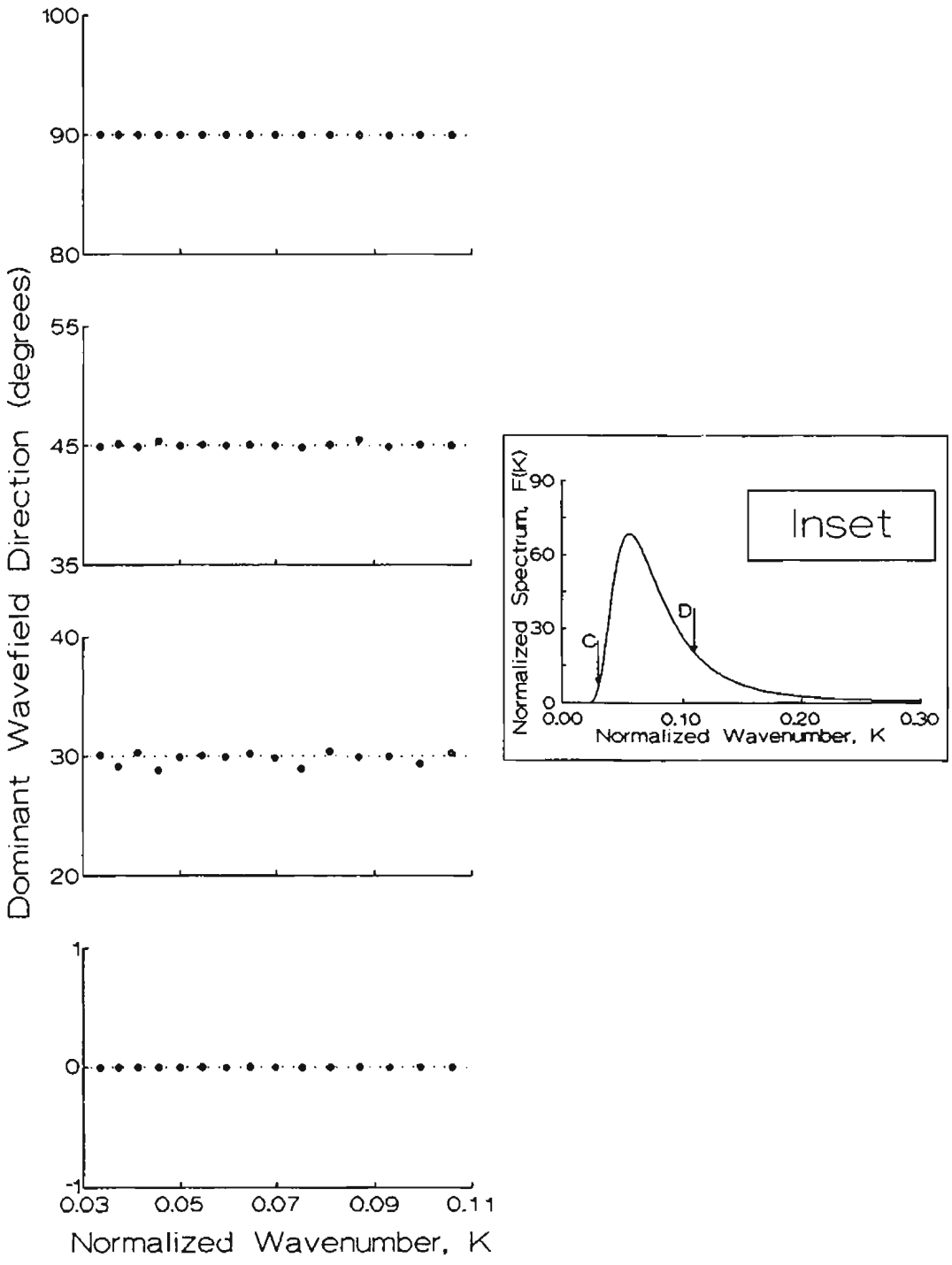

FIGURE 14: Dominant directions for windspeed of 10 m/s. Arrows C and D of the inset indicate the range of ocean wavenumbers for which the dominant directions could be recovered.

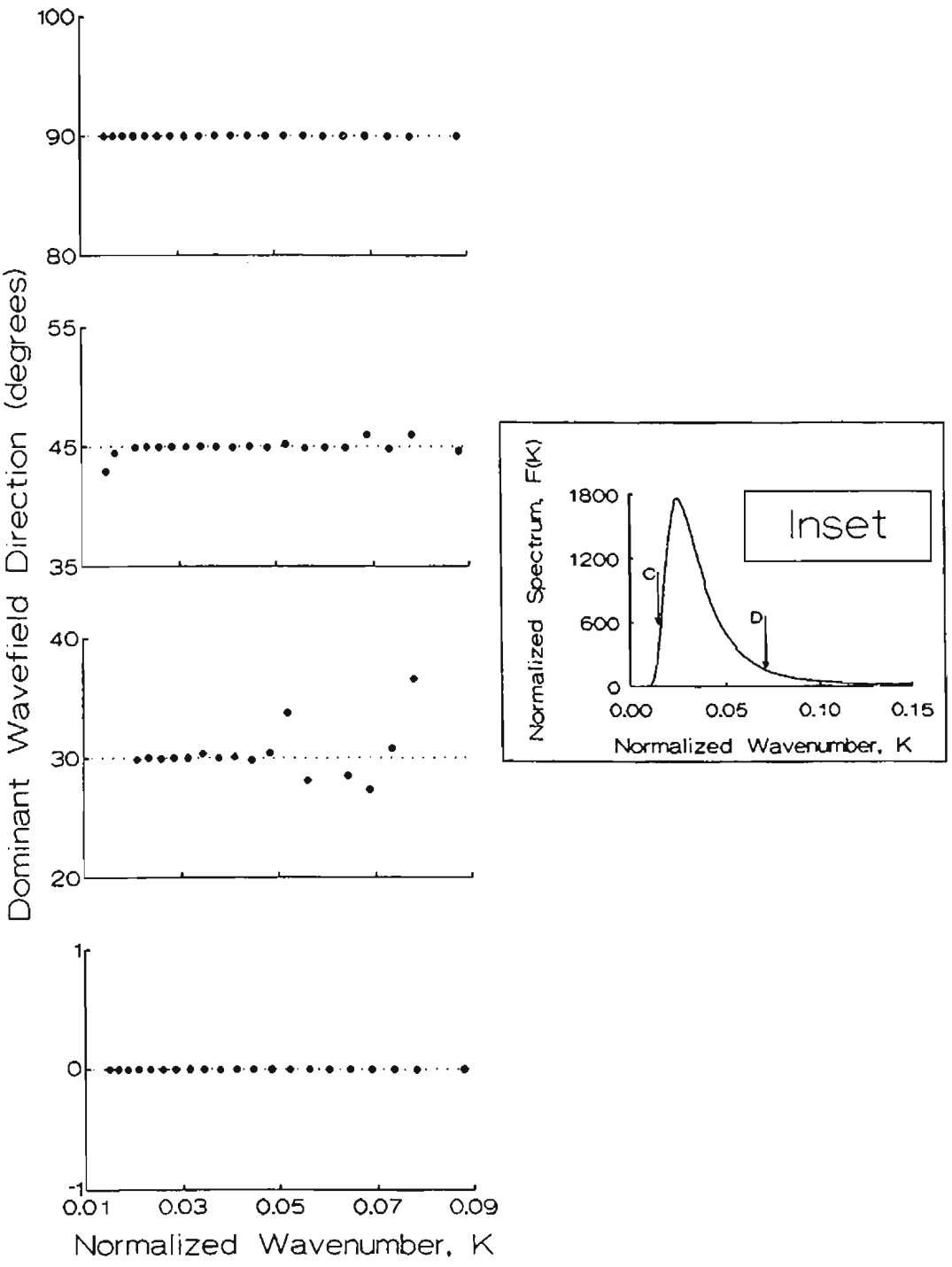

FIGURE 15: Dominant directions for windspeed of 15 m/s. Arrows C and D of the inset indicate the range of ocean wavenumbers for which the dominant directions could be recovered.

Figures 16–17 show values of s recovered through the above equations for sea states corresponding to those of Figures 11–12. Recovery of the spread parameter is best for the wave vectors associated with the most energetic waves. However, in the tails of the spectra where oscillatory behaviour is more pronounced, spurious values of s occur.

In creating simulated data for use in the inversion process, $s = 4$ was used throughout. It is to be expected that in many experimental situations the value of this spread parameter may vary across the ocean spectrum. In these latter cases, s may still be obtained from equations (3.26)–(3.27).

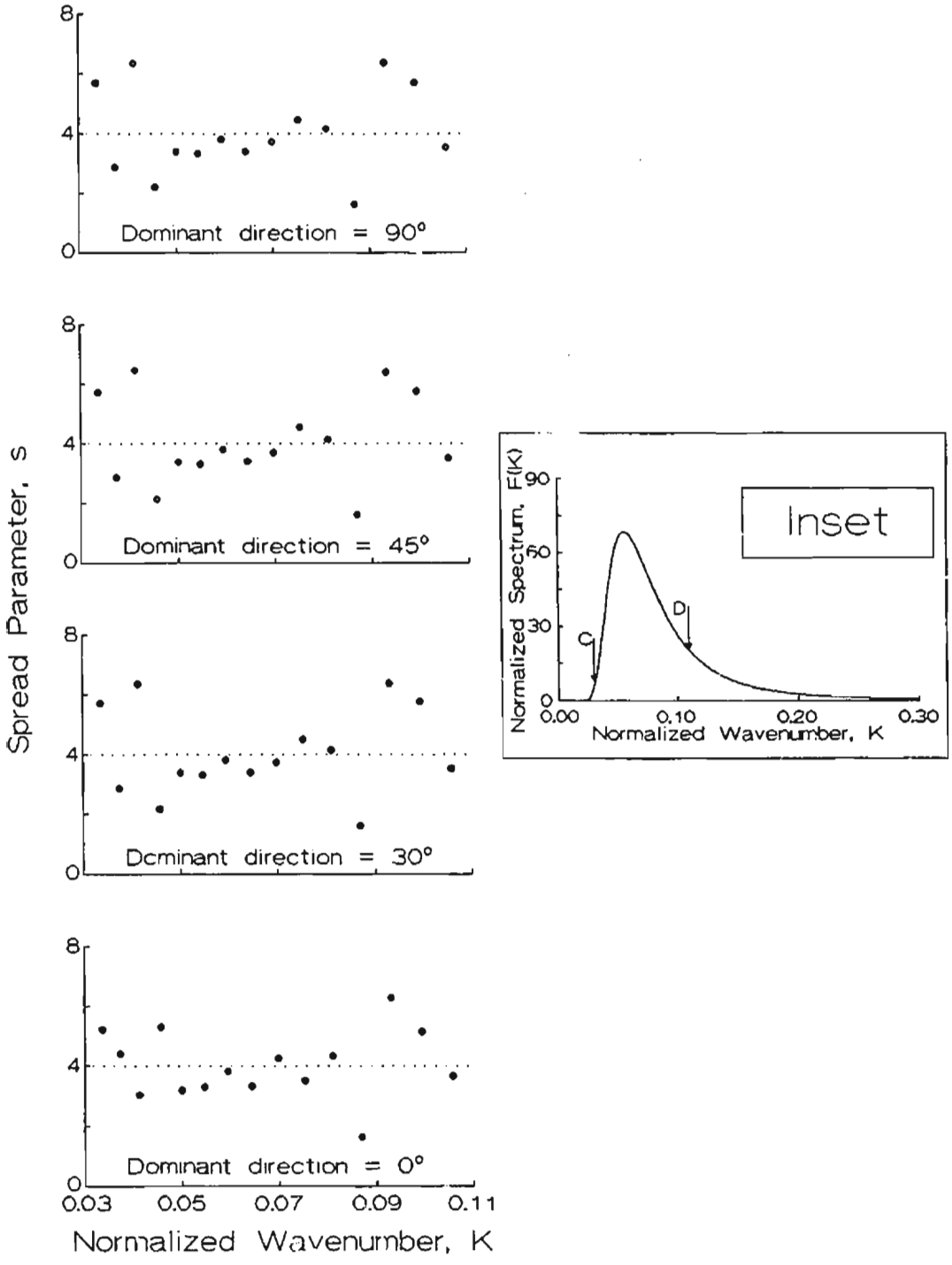

FIGURE 16: The spread parameter for windspeed of 10 m/s. Arrows C and D of the inset indicate the range of ocean wavenumbers for which the spread parameter could be recovered. The true value is s = 4.

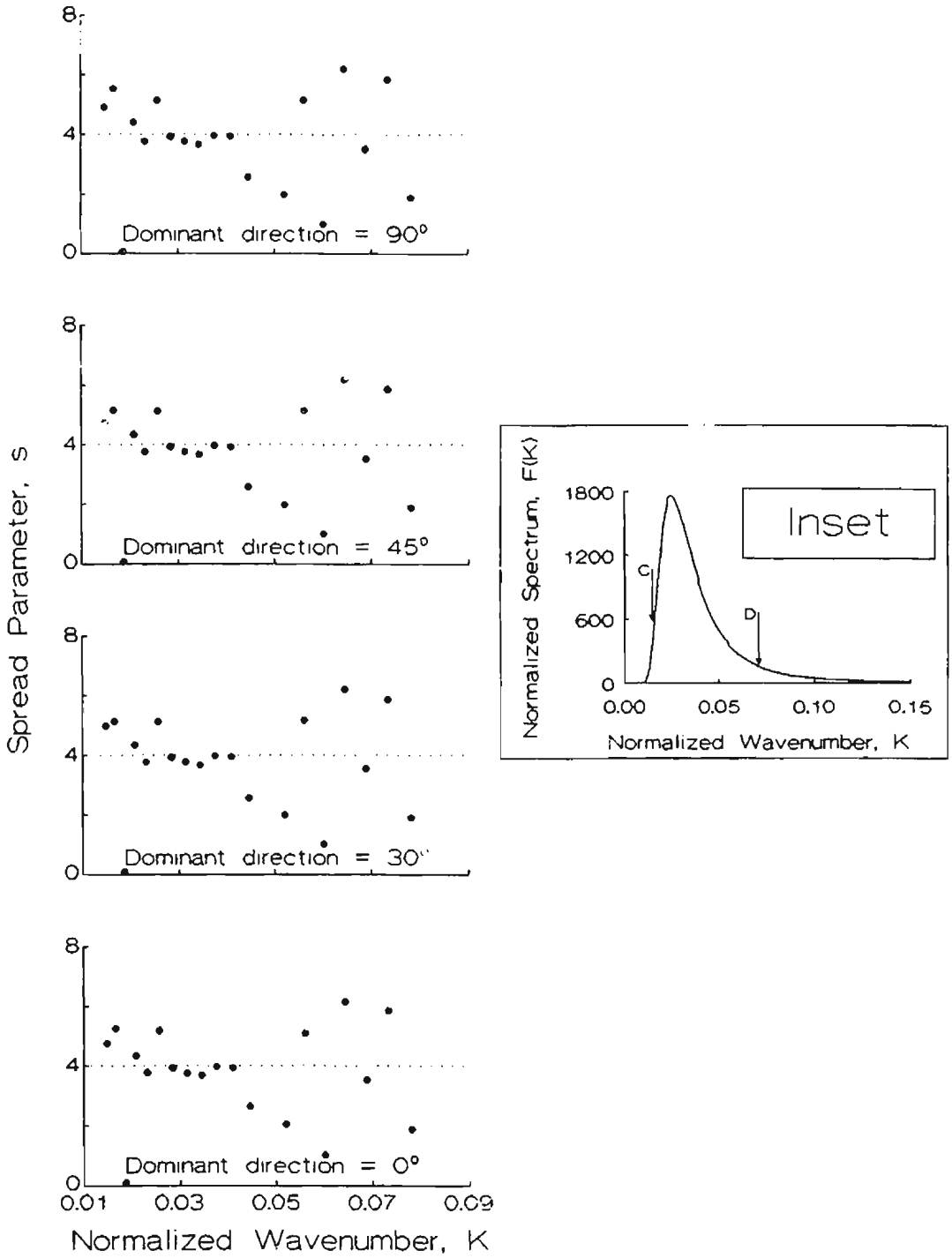

FIGURE 17: The spread parameter for windspeed of 15 m/s. Arrows C and D of the inset indicate the range of ocean wavenumbers for which the spread parameter could be recovered. The true value is s = 4.

Chapter 4

Conclusions

4.1 General Summary

The development of a procedure which could be used to extract directional waveheight spectra from HF ocean backscatter received by a four-element square array has been carried out. The technique is based on a method in which the wide beam radar cross section is expressed as an angular Fourier series having eight coefficients. In a manner similar to that which Barrick and Lipa (1979b) used for the crossed-loops/monopole radar, it has been shown how these radar spectral coefficients may be obtained from raw data and, further, how they may be related to the narrow beam radar cross section.

For use in the analysis, a closed form expression in terms of Bessel functions was developed for the Fourier coefficients of the four-element array beam pattern. Subsequently, these coefficients along with those for a Pierson-Moskowitz ocean spectral model with a cardioid directional factor were entered into the broad beam cross section equations. Then, the integrations over broad beam return angle, required to produce the radar spectral coefficients, were carried out in closed form. Using modelled ocean spectra, four-element radar coefficients were calculated for a variety of oceanic conditions. It was assumed that the radar operated at 25.4 MHz from a straight shoreline, although the analysis would work equally well for other ocean views. The only stipulation in the physical positioning of the the radar was that the

line joining elements 2 and 4 be pointed along the centre of the ocean sector. This constraint simplified much of the detail involved in carrying out the integrations.

The process of inverting the radar coefficient equations to recover ocean spectral parameters involved a linearization scheme similar to that suggested by Lipa and Barrick (1982). For this purpose, the characteristics of the short ocean waves involved in the backscatter process were assumed to be related to the Bragg wave through a Phillips equilibrium spectrum. The technique presented here, however, has the advantage of not constraining these waves to lie in the direction of the Bragg wave.

Following the linearization of the integral equations for the second-order radar spectral coefficients, this system was reduced to matrix form. To facilitate the process, it was assumed that the ocean spectral coefficients were constant over narrow ranges of wavenumber, these ranges increasing in size for larger wavenumbers. Having formed the matrix system, the inversion was carried out using a singular value decomposition (SVD) approach. The latter provided the optimal linear least-squares solution to the problem of recovering ocean spectral coefficients from the simulated radar coefficients. Using the ocean information thus obtained, rms waveheight was calculated to, at worst, within 2.61% of values obtained directly from the models. Directional information in the form of dominant direction and the spread factor of the wavefield were also derived from simulated radar coefficients. The dominant direction was reproduced without significant error for the cases of 0° and 90°. For other directions, this parameter was recovered with similar success except for wavenumbers in the tails of the spectra, produced by inversion, where oscillatory features were observed. While the spread factor, s, proved to be the most difficult to recover, results were still quite good in the portions of the spectra containing the bulk of the spectral energy.

While the analysis was not carried out for real data, it was noted that for sea states with *rms* waveheight between about 0.3 m and 1.9 m, the regions of typical

measured four-element square array spectra which must be inverted lie 10–20 dB above the noise floor. One may therefore expect that the method given here for simulated data should yield reasonable results for measured data. Such being the case, this radar would become useful for not only current mapping but also for the determination of ocean spectral characteristics.

4.2 Suggestions for Future Work

The analysis of the four-element square array cross sections of the ocean surface examined in this thesis suggests several directions for future research. The first might involve adding noise to the simulated data to see how this affects the stability of the inversion algorithm. The shifting and smearing of the radar spectrum due to currents superimposed on the wavefield should also be examined. Next, radar equations could be developed for regions of varying ocean depth within the range cells.

Other approaches to the presentation of the system of integral equations in matrix form and the subsequent solution of these equations should be tried. For example, a matrix system could be formed and solved for the four Doppler sidebands of the radar spectrum separately. This would lead to a reduction of the size of the matrix on which the SVD must be carried out and could lead to more stability in the inversion process. Of course, if one assumes that the four sidebands give independent information of the ocean spectrum, some of the detail will be lost using this procedure. Then, too, inversion of the matrix system using an iterative least squares approach might be considered.

In the future, the cross section equations developed by other investigators should also be integrated into the wide beam equations. Comparisons may then be made as to which of the theories is more suited to the inversion problem.

The ultimate effect of using fewer Fourier coefficients of the beam pattern in the wide beam cross sections is another subject for future investigations. Limiting the

number of these coefficients will reduce the size of the matrix system.

As well, for certain sea states, all four Doppler sidebands may not be significant in the inversion process. Whenever this is the case, omitting the insignificant sidebands will also reduce the size of the matrix system, and thus add further stabilization to the inversion technique.

The ultimate goal would, of course, be to calculate the cross section values for the four-element square array from real data as outlined in Appendix D. Subsequently, these would be used in the algorithms developed here to determine directional ocean-wave spectra for regions up to 30 km from the position of the array.

Bibliography

[1] Barrick, D. E. (1971), Theory of HF and VHF propagation across the rough sea, 1, The effective surface impedance for slightly rough highly conducting medium at grazing incidence, *Radio Science*, vol. 6, No. 5, pp 517-526.

[2] Barrick, D. E. (1971), Theory of HF and VHF propagation across the rough sea, 2, Application to HF and VHF propagation above the sea, *Radio Science*, vol. 6, No. 5, pp 527–533.

[3] Barrick, D. E. (1972), First-order theory and analysis of MF/HF/VHF scatter from the sea, *IEEE Trans. Antennas and Propag.*, vol. AP-20, No. 1, pp 2–10.

[4] Barrick, D. E. (1972b), Remote sensing of sea state by radar, in *Remote Sensing of the Troposphere*, V. E. Derr (Ed.), U.S. Government Printing Office, Washington, DC, chapter 12, pp 1–46.

[5] Barrick, D. E., and J. B. Snider (1977), The statistics of HF sea-echo Doppler spectra, *IEEE Trans. Antennas Propag.*, vol. AP-25, No. 1, pp 19–28.

[6] Barrick, D. E. (1977a), Extraction of wave parameters from measured HF radar sea-echo Doppler spectra, *Radio Science*, vol. 12, No. 3, pp 415–424.

[7] Barrick, D. E. (1977b), The ocean waveheight nondirectional spectrum from inversion of the HF sea-echo Doppler Spectrum, *Remote Sens. Environ.*, vol. 6, pp 201–227.

[8] Barrick, D. E., and B. J. Lipa (1979a), Ocean surface features observed by HF coastal ground-wave radars: a progress review, in *Ocean Wave Climate*, M. D. Earle and A. Malahoff (eds.), Plenum, New York, pp 129–152.

[9] Barrick, D. E., and B. J. Lipa (1979b), A compact transportable HF radar system for directional coastal wave field measurements, in *Ocean Wave Climate*, M. D. Earle and A. Malahoff (eds.), Plenum, New York, pp 153–201.

[10] Barrick, D. E. (1986), The second-order shallow-water hydrodynamic coupling coefficient in interpretation of HF radar sea echo, *IEEE Journal of Oceanic Engineering*, vol. OE-11, No. 2, pp 310–315.

[11] Bracewell, R. N. (1978), *The Fourier Transform and its Applications*, New York: McGraw-Hill, Inc.

[12] Capon, J., et al. (1967), Multidimensional maximum-likelihood processing of a large seismic array, *Proc. IEEE*, vol. 55, pp 192-211.

[13] Capon, J. (1969), High-resolution frequency-wavenumber spectrum analysis, *Proc. IEEE*, vol. 57, No. 8, pp 1408–1418.

[14] Crombie, D. D. (1955), Doppler Spectrum of Sea Echo at 13.56 Mc./s., *Nature*, vol. 175, pp 681–682.

[15] Dongarra, J. J., et al. (1979), *LINPACK Users' Guide*, SIAM, Philadelphia.

[16] Hasselmann, K. (1971), Determination of ocean wave spectra from Doppler radio return from the sea surface, *Nature Physical Science*, vol. 229, pp 16–17.

[17] Hasselmann, D. E., et al. (1980), Directional wave spectra observed during JONSWAP 1973, *J. Phys. Oceanog.*,vol. 10, pp 1264–1280.

[18] Howell, R. (1990), An Algorithm for the Extraction of Ocean Wave Spectra from Narrow Beam HF Radar Backscatter, *M. Eng. Thesis*, Memorial University of Newfoundland, St. John's, Canada, in preparation.

[19] James, M. L., et al. (1977), *Applied Numerical Methods for Digital Computation with FORTRAN and CSMP*, New York: Harper & Row, Publishers, Inc.

[20] Kinsman, B. (1984), *Wind Waves*, New York: Dover Publications, Inc.

[21] Kufner, A., and J. Kadlec (1971), *Fourier Series*, Prague: Academia Publishing House of the Czechoslovak Academy of Sciences.

[22] Lipa, B. J. (1977), Derivation of directional ocean-wave spectra by integral inversion of second-order radar echoes, *Radio Science*, vol. 12, No. 3, pp 425–434.

[23] Lipa, B. J. (1978), Inversion of second-order radar echoes from the sea, *Journal of Geophysical Research*, vol. 83, No. C2, pp 959–962.

[24] Lipa, B. J., et al. (1981), HF radar measurements of long ocean waves, *Journal of Geophysical Research*, vol. 86, No. C5, pp 4089–4102.

[25] Lipa, B. J., and D. E. Barrick (1982), Analysis methods for narrow- beam high-frequency radar sea echo,*Technical Report ERL 420-WPL 56*, NOAA, Boulder, Colorado.

[26] Lipa, B. J., and D. E. Barrick (1983), Least-squares methods for the extraction of surface currents from CODAR crossed-loop data: Application at ARSLOE, *IEEE Journal of Oceanic Engineering*, vol. OE-8, No. 4, pp 226–253.

[27] Lipa, B. J., and D. E. Barrick (1986), Extraction of sea state from HF radar sea echo: Mathematical theory and modeling, *Radio Science*, vol. 21, No. 1, pp 81–100.

[28] Mitsuyasu, H., et al. (1975), Observations of the directional spectrum of ocean waves using a clover leaf buoy, *J. Phys. Oceanogr.*, vol. 5, pp 750–760.

[29] Moiseiwitsch, B. L. (1977), *Integral Equations*, New York: Longman Inc.

[30] Moskowitz, L. (1964), Estimates of the power spectrums of fully developed seas for wind speeds of 20 to 40 knots, *Journal of Geophysical Research*, vol. 69, pp 5161–5179.

[31] Phillips, D. L. (1962), A technique for the numerical solution of certain integral equations of the first kind, *Journal of the Association for Computing Machinery*, vol. 9, pp 84–97.

[32] Phillips, O. M. (1977), *The Dynamics of the Upper Ocean*, Cambridge, England: Cambridge University Press.

[33] Prudnikov, A. P., et al. (1986), *Integrals and Series*, New York: Gordon and Breach Science Publishers.

[34] Rice, S. O. (1950), Reflection of electromagnetic waves from a slightly rough surface, in *Theory of Electromagnetic Waves*, ed. M. Kline, New York: Interscience, pp. 351–378.

[35] Rosich, R. K., and J. R. Wait (1977), A general perturbation solution for reflection from two-dimensional surfaces, *Radio Science*, vol. 12, No. 5, pp 719–729.

[36] Shearman, E. D. R., et al. (1982), Experimental studies of the performance of an MF/HF ground-wave radar on a coastal site of irregular contour, *IEE RADAR-82 Conf. Publn.*, pp 107–109.

[37] Shearman, E. D. R., et al. (1982b), HF ground-wave radar for sea-state and swell measurement; theoretical studies, experiments and proposals, *IEE RADAR-82 Conf. Publn.*, pp 101–106.

[38] Shearman, E. D. R., (1983), Radio science and oceanography, *Radio Science*, vol. 18, No. 3, pp 299–320.

[39] Srivastiva, S. K. (1984), Scattering of High Frequency Electromagnetic Waves from an Ocean Surface: An Alternative Approach Incorporating a Dipole Source, *Ph.D. Thesis*, Memorial University of Newfoundland, St. John's, Canada.

[40] Stewart, G. W. (1973), *Computer Science and Applied Mathematics*, New York: Academic Press, Inc.

[41] Strang, G. (1976), *Linear Algebra and its Applications*, New York: Academic Press, Inc.

[42] Strutt, J. W. (Lord Rayleigh) (1896), *The Theory of Sound*, vol. 2, New York: Macmillan.

[43] Twomey, S. (1963), On the numerical solutions of Fredholm integral equations of the first kind by the inversion of the linear system produced by quadrature, *Journal of the Association for Computing Machinery*, vol. 10, pp 97–101.

[44] Wait, J. R. (1971), Perturbation analysis for the reflection from two-dimensional periodic sea waves, *Radio Science*, vol. 6, No. 3, pp 387–391.

[45] Walsh, J. (1980b), On the theory of electromagnetic propagation across a rough surface and calculations in the VHF region, *OEIC Report*, No. N00242, Memorial University of Newfoundland, St. John's, Canada.

[46] Walsh, J., and R. Howell (1990), Model development for evaluation studies of ground wave radar, *Technical Report W7714-8-5655101-55*, prepared for the Canadian Dept. of National Defence, Dept. of Supply and Services.

[47] Weber, B. L., and D. E. Barrick (1977), On the nonlinear theory for gravity waves on the ocean's surface, part 1: derivations, *Journal of Physical Oceanography*, vol. 7, pp 3–10.

[48] Wyatt, L. R., et al. (1985), Remote sensing letters, *Int. Journal of Remote Sensing*, vol. 6, No. 1, pp 275–282.

[49] Wyatt, L. R., et al. (1986), HF radar measurements of ocean wave parameters during NURWEC, *IEEE Journal of Oceanic Engineering*, vol. OE-11, No. 2, pp 219–234.

[50] Wyatt, L. R. (1986a), The measurement of the ocean wave directional spectrum from HF radar Doppler spectra, *Radio Science*, vol. 21, No. 3, pp 473–485.

Appendix A

Calculation of the Beam Pattern Coefficients

The beam pattern of the four-element square array is given by

$$\begin{aligned} G(\psi,\phi) &= \cos^2\left\{\frac{\zeta}{2}[\sin(\psi-\frac{\pi}{4})-\sin(\phi-\frac{\pi}{4})]\right\} \\ &\quad\cdot\cos^2\left\{\frac{\zeta}{2}[\cos(\psi-\frac{\pi}{4})-\cos(\phi-\frac{\pi}{4})]\right\} . \end{aligned} \tag{A.1}$$

where $\zeta = \frac{2k_0 r}{\sqrt{2}}$, with k_0 being the radar wavenumber and r the distance of each array sensor from the geometrical centre of the array.

The general form for the double Fourier expansion of such a function is (see, for example, Kufner and Kadlec (1971))

$$\begin{aligned} G(\psi,\phi) &= \sum_{t,p=0}^{\infty}[g_{tpc}\cos(t\psi)\cos(p\phi)+g_{tpcs}\cos(t\psi)\sin(p\phi) \\ &\quad+(g_{tpsc}\sin(t\psi)\cos(p\phi)+(g_{tps}\sin(t\psi)\sin(p\phi)] , \end{aligned} \tag{A.2}$$

where

$$g_{tpc} = \frac{\epsilon_{tp}}{\pi^2}\int_{-\pi}^{\pi}\int_{-\pi}^{\pi} G(\psi,\phi)\cos(t\psi)\cos(p\phi)\,d\psi\,d\phi , \tag{A.3}$$

$$g_{tpcs} = \frac{\epsilon_{tp}}{\pi^2}\int_{-\pi}^{\pi}\int_{-\pi}^{\pi} G(\psi,\phi)\cos(t\psi)\sin(p\phi)\,d\psi\,d\phi , \tag{A.4}$$

$$g_{tpsc} = \frac{\epsilon_{tp}}{\pi^2}\int_{-\pi}^{\pi}\int_{-\pi}^{\pi} G(\psi,\phi)\sin(t\psi)\cos(p\phi)\,d\psi\,d\phi , \tag{A.5}$$

$$g_{tps} = \frac{\epsilon_{tp}}{\pi^2}\int_{-\pi}^{\pi}\int_{-\pi}^{\pi} G(\psi,\phi)\sin(t\psi)\sin(p\phi)\,d\psi\,d\phi , \tag{A.6}$$

with $t, p = 0, 1, 2, \cdots$ and

$$\epsilon_{tp} = \begin{cases} \frac{1}{4}, & t = p = 0 \\ \frac{1}{2}, & t = 0,\ p \neq 0 \text{ or } t \neq 0,\ p = 0 \\ 1, & t, p > 0 \,. \end{cases}$$

It is tedious, but straightforward to show that g_{tpcs} and g_{tpsc} are identically zero. We omit the details here. For the purpose of illustration, we shall outline the calculation of g_{tpc} and note that g_{tps} follows similarly. The large amount of algebraic detail associated with this process is omitted.

To aid the presentation, we make the following definitions:

$$f_1(\psi, \phi) = \zeta[\sin(\psi - \frac{\pi}{4}) - \sin(\phi - \frac{\pi}{4})] \tag{A.7}$$

and

$$f_2(\psi, \phi) = \zeta[\cos(\psi - \frac{\pi}{4}) - \cos(\phi - \frac{\pi}{4})] \,. \tag{A.8}$$

Rewriting equation (A.3) using equations (A.1), (A.7), and (A.8), one gets

$$g_{tpc} = \frac{\epsilon_{tp}}{\pi^2} \int_{-\pi}^{\pi} \int_{-\pi}^{\pi} \cos^2\left(f_1(\psi, \phi)\right) \cdot \cos^2\left(f_2(\psi, \phi)\right) \cos(t\psi) \cos(p\phi)\, d\psi\, d\phi \,. \tag{A.9}$$

Expanding the integrand using the half-angle cosine formula, equation (A.9) becomes

$$\begin{aligned} g_{tpc} \;=\; & \frac{\epsilon_{tp}}{\pi^2} \int_{-\pi}^{\pi} \int_{-\pi}^{\pi} \{1 + \cos\left(2f_1(\psi, \phi)\right) + \cos\left(2f_2(\psi, \phi)\right) \\ & + \cos\left(2f_1(\psi, \phi)\right) \cos\left(2f_2(\psi, \phi)\right)\} \cos(t\psi) \cos(p\phi)\, d\psi\, d\phi \,. \end{aligned} \tag{A.10}$$

Next, each part of the sum in the integrand is examined separately. Clearly,

$$\int_{-\pi}^{\pi} \int_{-\pi}^{\pi} 1 \cdot \cos(t\psi) \cos(p\phi)\, d\psi\, d\phi = \begin{cases} 0, & t \text{ or } p \neq 0 \\ 4\pi^2, & t = p = 0 \end{cases} \,. \tag{A.11}$$

Then, consider

$$\int_{-\pi}^{\pi} \int_{-\pi}^{\pi} \cos\left(2f_1(\psi, \phi)\right) \cos(t\psi) \cos(p\phi)\, d\psi\, d\phi \,.$$

Without showing the details, we note that the sine and cosine functions contained in $f_1(\psi, \phi)$ are expanded using the sum and difference formulae for trigonometric

functions. This gives, from Prudnikov et al. (1986),

$$\int_{-\pi}^{\pi}\int_{-\pi}^{\pi}\cos\left(2f_1(\psi,\phi)\cos(t\psi)\cos(p\phi)\right)\,d\psi\,d\phi$$
$$= \pi J_t(2\zeta)\left\{\cos\left(\frac{t\pi}{4}\right)\cos\left(\frac{p\pi}{4}\right)\left[1+(-1)^p\right]\pi J_p(2\zeta)\left[1+(-1)^t\right]\right.$$
$$\left.-2(-1)^t\sin\left(\frac{t\pi}{4}\right)\sin\left(\frac{p\pi}{4}\right)\left[1-(-1)^p\right]\pi J_p(2\zeta)\right\} \quad \text{(A.12)}$$

where the J's are Bessel functions of the first kind.

The third part of the integrand of equation (A.10) similarly integrates as

$$\int_{-\pi}^{\pi}\int_{-\pi}^{\pi}\cos\left(2f_2(\psi,\phi)\cos(t\psi)\cos(p\phi)\right)\,d\psi\,d\phi$$
$$= 2\pi J_t(2\zeta)\cos\left(\frac{t\pi}{4}\right)\left\{2\pi\cos\left(\frac{t\pi}{2}\right)\cos\left(\frac{p\pi}{4}\right)\cos\left(\frac{p\pi}{2}\right)J_p(2\zeta)\right.$$
$$\left.+\ 2\pi\sin\left(\frac{t\pi}{2}\right)\sin\left(\frac{p\pi}{4}\right)\sin\left(\frac{p\pi}{2}\right)J_p(2\zeta)\right\}\ . \quad \text{(A.13)}$$

Lastly,

$$\int_{-\pi}^{\pi}\int_{-\pi}^{\pi}\cos\left(2f_1(\psi,\phi)\right)\cos\left(2f_2(\psi,\phi)\right)\cos(t\psi)\cos(p\phi)\,d\psi\,d\phi$$
$$= \left(\cos\left(\frac{t\pi}{2}\right)+1\right)\left[1+(-1)^t\right]\pi J_t(2\sqrt{2}\zeta)$$
$$\cdot\left\{\left(\cos\left(\frac{p\pi}{2}\right)+1\right)\left[1+(-1)^p\right]\left(\frac{\pi}{4}\right)J_p(2\sqrt{2}\zeta)\right\}$$
$$+2\left(\sin\left(\frac{t\pi}{2}\right)+1\right)\left[1-(-1)^t\right]\pi J_t(2\sqrt{2}\zeta)$$
$$\cdot\left\{\sin\left(\frac{p\pi}{2}\right)\left[1-(-1)^p\right]\left(\frac{\pi}{4}\right)J_p(2\sqrt{2}\zeta)\right\}$$
$$+\left(\cos\left(\frac{t\pi}{2}\right)-1\right)\left[1+(-1)^t\right]\pi J_t(2\sqrt{2}\zeta)$$
$$\cdot\left\{\left(\cos\left(\frac{p\pi}{2}\right)-1\right)\left[1+(-1)^p\right]\left(\frac{\pi}{4}\right)J_p(2\sqrt{2}\zeta)\right\}\ . \quad \text{(A.14)}$$

Combining the results of equations (A.11) and (A.12)–(A.14) and carrying out the obvious simplifications, the coefficient expressed by equation (A.3) is written as

$$g_{tpc} = \epsilon_{tp}\left\{\delta_{tp}+\frac{1}{4}J_t(2\zeta)J_p(2\zeta)\left[\cos\left(\frac{(+t-p)\pi}{4}\right)\left(1+(-1)^{t+p}\right)\right.\right.$$
$$+\cos\left(\frac{(t+p)\pi}{4}\right)\left((-1)^t+(-1)^p\right)+4\cos\left(\frac{t\pi}{4}\right)\cos\left(\frac{p\pi}{4}\right)\cos\left(\frac{(t-p)\pi}{2}\right)\Big]$$
$$+\frac{1}{8}J_t(2\sqrt{2}\zeta)J_p(2\sqrt{2}\zeta)\left[\left(1+(-1)^t\right)\left(1+(-1)^p\right)\right.$$
$$\left.\left.+\cos\left(\frac{(t-p)\pi}{2}\right)\left(1+(-1)^{t+p}\right)+\cos\left(\frac{(t+p)\pi}{2}\right)\left((-1)^t+(-1)^p\right)\right]\right\} \quad \text{(A.15)}$$

A similar analysis for the g_{tps} coefficient results in

$$\begin{aligned} g_{tps} &= \frac{1}{4}J_t(2\zeta)J_p(2\zeta)\left[\cos\left(\frac{(t-p)\pi}{4}\right)\left(1+(-1)^{t+p}\right)\right. \\ &\quad \left.-\cos\left(\frac{(t+p)\pi}{4}\right)\left((-1)^t+(-1)^p\right)+4\sin\left(\frac{t\pi}{4}\right)\sin\left(\frac{p\pi}{4}\right)\cos\left(\frac{(t-p)\pi}{2}\right)\right] \\ &\quad +\frac{1}{8}J_t(2\sqrt{2}\zeta)J_p(2\sqrt{2}\zeta)\left[\left(1-(-1)^t\right)\left(1-(-1)^p\right)\right] . \end{aligned} \tag{A.16}$$

The ϵ_{tp} need not appear in g_{tps} because the only non-zero values of this coefficient occur when both t and p are greater than zero, in which case $\epsilon_{tp} = 1$.

The complete surfaces of $G(\psi, \phi)$, its Fourier approximation, and the difference between the two are given in Figure 18.

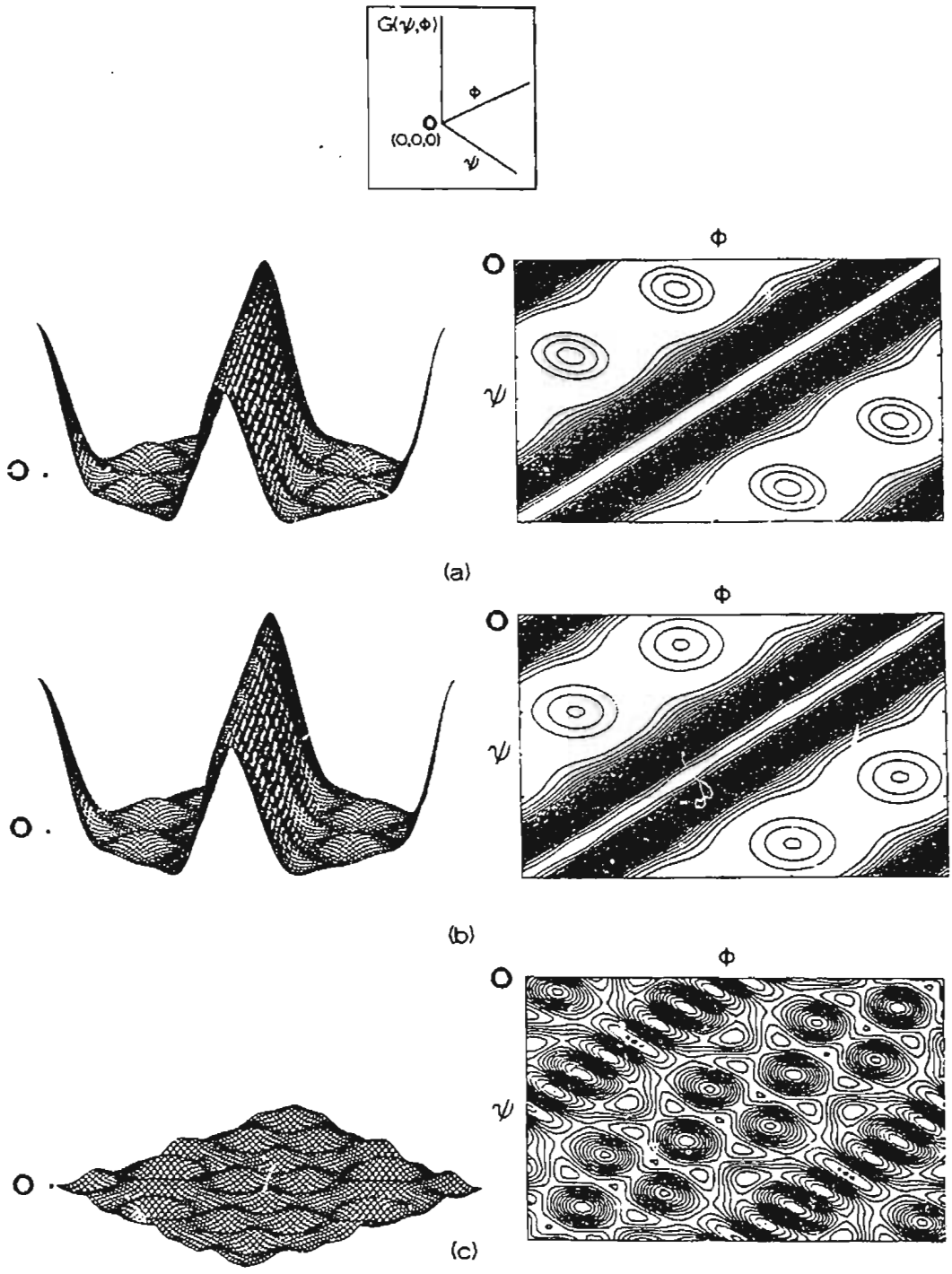

FIGURE 18: Plot of beam pattern with $\psi-\Phi$ plotted in the horizontal plane: (a) the exact function, $G(\psi,\Phi)$ and its contour; (b) the Fourier approximation of $G(\psi,\Phi)$ and its contour; (c) difference between (a) and (b) -- maximum difference 1.53%. Angles vary $0-2\pi$.

Appendix B

Inversion of the First-Order Return

Since, in reality, the first-order spectral peaks will be broadened somewhat, the spectral coefficients found from equation (2 83) with σ_2 replaced by σ_1 will represent a continuum. Let these *measured*, smeared, coefficients be represented by $B_{t_c}(\eta)$. The coefficients of the Bragg wave are then estimated by equating the integral (over normalized frequency in the first-order region) of the broadened coefficients to that of the idealized coefficients. If ϵ' represents the width of the spectral peak about the normalized Bragg frequency, η_B, then we write

$$\int_{\pm\eta_B-\frac{\epsilon'}{2}}^{\pm\eta_B+\frac{\epsilon'}{2}} B_t(\eta)\,d\eta = \int_{\pm\eta_B-\frac{\epsilon'}{2}}^{\pm\eta_B+\frac{\epsilon'}{2}} B_{t_c}(\eta)\,d\eta \tag{B.1}$$

where $B_t(\eta)$ is the expression for the idealized Bragg coefficients of equation (2.87). The coefficients $B_{t_c}(\eta)$, which were simulated in the thesis by equation (2.91), may be determined numerically from real data after the manner outlined in Appendix D. Substituting the $B_t(\eta)$ result of equation (2.87) into equation (B.1) gives

$$\begin{aligned} 2 \sum_{m'=\pm 1} \sum_{\ell=0}^{2} \sum_{p=0}^{4} \int_{-\gamma}^{\gamma} \int_{\pm\eta_B-\frac{\epsilon'}{2}}^{\pm\eta_B+\frac{\epsilon'}{2}} & [g_{tpc} a_\ell(1) \cos(\ell\phi)\cos(p\phi) \\ & + g_{tps} b_\ell(1) \sin(\ell\phi)\sin(p\phi)]\,(-m')^\ell \delta(\eta - m')\,d\eta\,d\phi \\ = 2 \sum_{m'=\pm 1} \sum_{\ell=0}^{2} \sum_{p=0}^{4} \int_{-\gamma}^{\gamma} & (-m')^\ell [g_{tpc} a_\ell(1)\cos(\ell\phi)\cos(p\phi) \\ + g_{tps} b_\ell(1) \sin(\ell\phi)\sin(p\phi)]\,d\phi &= \int_{\pm\eta_B-\frac{\epsilon'}{2}}^{\pm\eta_B+\frac{\epsilon'}{2}} B_{t_c}(\eta)\,d\eta\,. \end{aligned} \tag{B.2}$$

We note that g_{tpc} and g_{tps} are not functions of ϕ. Further, by definition (see Section 2.3.3), $g_{tpc} = 0$ for $t < 0$ while $g_{tps} = 0$ for $t \geq 0$. We also recall, as is indicated by the presence of the delta-function, that $\eta > 0$ is associated with $m' = +1$ and $\eta < 0$ contributes only when $m' = -1$. Integrating over ϕ and summing over ℓ and p, equation (B.2) easily reduces to a matrix system of the form

$$\underline{\underline{A}}_B \underline{X}_B = \underline{B}_B \,. \tag{B.3}$$

Here,

$$\underline{X}_B = \begin{bmatrix} a_0(1) \\ \vdots \\ b_2(1) \end{bmatrix},$$

$$\underline{B}_B = \begin{bmatrix} \int_{-\eta_B - \frac{\zeta'}{2}}^{-\eta_B + \frac{\zeta'}{2}} B_{-3_c}(\eta)\, d\eta \\ \vdots \\ \int_{-\eta_B - \frac{\zeta'}{2}}^{-\eta_B + \frac{\zeta'}{2}} B_{4_c}(\eta)\, d\eta \\ \vdots \\ \int_{+\eta_B - \frac{\zeta'}{2}}^{+\eta_B + \frac{\zeta'}{2}} B_{-3_c}(\eta)\, d\eta \\ \vdots \\ \int_{+\eta_B - \frac{\zeta'}{2}}^{+\eta_B + \frac{\zeta'}{2}} B_{4_c}(\eta)\, d\eta \end{bmatrix},$$

and

$$\underline{\underline{A}}_B = \begin{bmatrix} A_{a_0,-1,-3} & A_{a_1,-1,-3} & \cdots & A_{b_2,-1,-3} \\ \vdots & \vdots & \vdots & \vdots \\ A_{a_0,1,4} & A_{a_1,1,4} & \cdots & A_{b_2,1,4} \end{bmatrix}.$$

The last two subcripts on the elements of matrix $\underline{\underline{A}}_B$ are the values of m' and t respectively. These elements themselves are a direct result of completing the integration and summation of equation (B.2). It is understood that the elements of $\underline{X}_B$ are the five Fourier coefficients of the Bragg wave. As for the second-order matrix equation, the matrix $\underline{\underline{A}}_B$ of equation (B.3) will ,in general, be singular. By using a singular value decomposition approach, we define the optimal linear least squares solution as

$$\underline{X}_{B_r} = \underline{\underline{A}}_B^{+} \underline{B}_B \tag{B.4}$$

where $\underline{\underline{A}}_B^+$ is the pseudo-inverse of $\underline{\underline{A}}_B$.

In the simulations conducted for this thesis, the first-order spectral coefficients were recovered with negligible error using the above technique.

Appendix C

FORTRAN Code for the Inversion of the Second-order Backscatter

The FORTRAN code contained here presents the major routine used in inverting the second-order radar return to give simulated ocean spectral coefficients. Other smaller programs which provide input into the inversion process contain most of the same subroutines as found here and for this reason they appear only as comments at the appropriate places. To help with the formatting, non-code statements are started and ended with a line of asterisks.

```
**********************************************
**PROGRAM TO CREATE AND INVERT THE MATRIX*****
**WHICH MULTIPLIES THE SOLUTION VECTOR OF*****
**OCEAN SPECTRAL COEFFICIENTS.  USING MATRIX**
**OPERATIONS, THE SOLUTION IS THEN DETERMINED*
**FOR SIMULATED DATA**************************
**********************************************
**********************************************
**DECLARE VARIABLES AND NECESSARY WORKSPACE***
**FOR CALLS FROM THE VAX LIBRARY**************
**********************************************
COMMON/WORKSP/RWKSP
REAL RWKSP(164000)
REAL ETA,PI,K0,H,ETABIG
REAL CANLPT2(0:2,0:2,0:4,-4:4),CBNLPT1(0:2,0:2,0:4,-4:4)
REAL CANLPT1(0:2,0:2,0:4,-4:4),CBNLPT2(0:2,0:2,0:4,-4:4)
INTEGER ETACOUNT,I,J,L,IRANK,IPATH,NRA,NCA,LDA,LDU,LDV,NB
PARAMETER(NRA=448,NCA=160,LDA=NRA,LDU=NRA,LDV=NCA)
REAL MATRIX(448,160),SUM,D,DEPTH,K1,K2
REAL*8 UA(LDU,NRA),V(LDV,NCA),S(NCA),A(NRA,NCA),TOL
REAL U,ALPHASTAR,PHI,BAND(40)
REAL AINV(LDV,LDU),BTCA(NRA),ANS(NCA)
**********************************************
**CREATE COMPUTER WORKSPACE AND INITIALIZE****
**THE MATRIX TO BE SUBSEQUENTLY INVERTED******
**********************************************
```

```
CALL IWKIN(164000)
DO I=1,448
   DO J=1,160
     MATRIX(I,J) = 0.
   END DO
END DO
*********************************************
**'DATA' CONTAINS DEPTH, WIND SPEED, DOMINANT*
**DIRECTION, ANGLE INTEGRATION LIMIT, AND*****
**THE NUMBER OF WAVENUMBER BANDS.  'CNLPT'****
**CREATES A PARTIAL INTEGRATION TABLE*********
**INVOLVING VALUES NOT AFFECTED BY THE THETA**
**INTEGRAL************************************
*********************************************
CALL DATA(DEPTH,U,ALPHASTAR,PHI,NB)
CALL CNLPT(CANLPT1,CANLPT2,CBNLPT1,CBNLPT2,U,ALPHASTAR,PHI)
*********************************************
**'BAND.DAT' HAS WAVENUMBER BANDS CONSTRUCTED*
**FROM THE DISPERSION RELATION FOR WATER******
**WAVES IN A SIMPLE EXTERNAL ROUTINE**********
*********************************************
OPEN(UNIT=10,NAME='BAND.DAT',TYPE='OLD')
DO I = 1,NB+1
   READ(10,*) BAND(I)
END DO
*********************************************
**MAKE IDENTIFIABLE EXTREMES TO THE SERIES****
```

```
**OF WAVENUMBER BANDS************************
*********************************************
BAND(1) = 0.
AND(NB+1) = 1.
*********************************************
**INITIALIZE RADAR WAVENUMBER, NORMALIZE******
**DEPTH, AND INTRODUCE RADIANS-DEGREES********
**CONVERSION FACTOR***************************
*********************************************
PI=ACOS(-1.)
K0=2*PI/(3.E3/25.4E6)
D = DEPTH*2*K0
H = PI/180.
*********************************************
**THE FOLLOWING CALLS CREATE THE 'A' MATRIX***
**OF THE TEXT*********************************
*********************************************
ETACOUNT = 7
DO ETA = .83,.64,-.0145
  CALL MAIN(ETA,DEPTH,U,ALPHASTAR,PHI,MATRIX,CANLPT1,
&   CANLPT2,CBNLPT1,CBNLPT2,PI,K0,D,H,ETACOUNT,BAND)
  ETACOUNT = ETACOUNT + 16
  ETABIG = 2.-ETA
  CALL MAIN(ETABIG,DEPTH,U,ALPHASTAR,PHI,MATRIX,CANLPT1,
&   CANLPT2,CBNLPT1,CBNLPT2,PI,K0,D,H,ETACOUNT,BAND)
  ETACOUNT = ETACOUNT + 16
END DO
```

```
**********************************************
**CONVERT MATRIX A TO DOUBLE PRECISION********
**********************************************
DO I=1,NRA
  DO J=1,NCA
    A(I,J)=MATRIX(I,J)
  END DO
END DO
**********************************************
**CALL SINGULAR VALUE DECOMPOSITION ROUTINE***
**FROM VAX (IMSL) LIBRARY TO GET**************
**PSEUDO-INVERSE AND THE RANK OF MATRIX 'A'***
**BASED ON THE GIVEN TOLERANCE (TOL)**********
**FOR THE SINGULAR VALUES*********************
**********************************************
IPATH = 11
TOL = .0000001
CALL DLSVRR(NRA,NCA,A,LDA,IPATH,TOL,IRANK,S,UA,LDU,V,LDV)
OPEN(UNIT=95,NAME='SVDSEC.DAT',TYPE='NEW')
WRITE(95,*) 'RANK OF MATRIX =',IRANK
DO I = 1,NCA
WRITE(95,*) S(I)
END DO
CLOSE(95)
**********************************************
**THE USER MAY ALTER THE NUMBER OF SINGULAR***
**VALUES TO GIVE THE BEST INVERSION RESULTS***
```

```
      **BY ALTERING IRANK AS IN THE FOLLOWING LINE.*
      **WITH LARGER AMOUNTS OF COMPUTER TIME********
      **AVAILABLE, THIS COULD BE MADE INTO A DO******
      **LOOP SO THAT SEVERAL POSSIBLITIES COULD BE**
      **EXAMINED SIMULTANEOUSLY**********************
      ********************************************
      IRANK=130
      ********************************************
      **GET THE PSEUDO-INVERSE OF 'A'***************
      ********************************************
      DO 400 I = 1,LDV
         DO 410 L = 1,LDU
            SUM = 0.
            DO 430 J = 1,NRA
               IF(J.GT.IRANK) THEN
                  GOTO 420
               ELSE
                  SUM=SUM+V(I,J)*(1./S(J))*UA(L,J)
               END IF
  430       CONTINUE
  420       AINV(I,L) = SUM    ! INVERSE MATRIX ELEMENTS
  410    CONTINUE
  400 CONTINUE
      ********************************************
      **WE NOW REPRODUCE THE SPECTRAL COEFFICIENTS**
      **OF THE OCEAN WAVES. 'BTMATRIX.DAT' CONTAINS*
      **THE SIMULATED DATA CREATED USING A ROUTINE**
```

```
      **VERY SIMILAR TO SUBROUTINE 'MAIN' BUT WITH**
      **THE OCEAN SPECTRAL COEFFICIENTS APPEARING***
      **IN THE THETA INTEGRAL**********************
      ********************************************
      OPEN(UNIT=15,NAME='BTMATRIX.DAT',TYPE='OLD')
      DO I = 1,NRA
         READ(15,*) BTCA(I)
      END DO
      CLOSE(15)
      DO 510 L = 1,NCA
         SUM = 0.
         DO 520 J = 1,NRA
            SUM = SUM + AINV(L,J) * BTCA(J)
520      CONTINUE
         ANS(L) = SUM
510   CONTINUE
      ********************************************
      **WRITE OUT THE COMPUTED WAVE COEFFICIENTS****
      **WHICH ARE IN ARRAY 'ANS'********************
      ********************************************
      OPEN(UNIT=53,NAME='ANS090.DAT',TYPE='NEW')
      DO I = 1,NCA
         WRITE(53,*) ANS(I)
      END DO
      CLOSE(53)
      STOP
      END
```

```
*********************************************
*********************************************

*********************************************
**SUBROUTINE 'MAIN' CREATES THE MATRIX WHICH**
**MUST BE INVERTED BEFORE THE OCEAN SPECTRAL**
**COEFFICIENTS CAN BE CALCULATED**************
*********************************************
      SUBROUTINE MAIN(ETA,DEPTH,U,ALPHASTAR,PHI,MATRIX,CANLPT1,
     &            CANLPT2,CBNLPT1,CBNLPT2,PI,K0,D,H,ETACOUNT,BAND)
*********************************************
**DECLARE VARIABLES***************************
*********************************************
      IMPLICIT NONE
      REAL A,ETA,M1,M2,PI,K0,L,EL,HY,GAMSQR,DN,H
      REAL U,ALPHASTAR,COFSUMA,COFSUMAN,COFSUMB,COFSUMBN
      REAL*8 FINAL,D,DEPTH,K1,K2,ANGLE,P1,P2,KERNAL1,THETA1,JAC
      REAL*8 MAXMAX,MINMIN,DELTAK,KERN,KERNNEG
      REAL CANLPT2(0:2,0:2,0:4,-4:4),CBNLPT1(0:2,0:2,0:4,-4:4)
      REAL CANLPT1(0:2,0:2,0:4,-4:4),CBNLPT2(0:2,0:2,0:4,-4:4)
      REAL PHI,ANGFACT1,ANGFACT2,MATRIX(448,160),BAND(40)
      REAL SUM,INTGNDA,INTGNDB,SUMA(3),SUMANEG(3),SUMB(2)
      REAL SUMBNEG(2),INTMATRIX(5,125),INTMATRIXNEG(5,125)
      INTEGER N,L1,P,T,COUNT,TT5,NEWCOUNT,ETACOUNT,KCOUNT,EC,MC
      INTEGER MCMIN,MCMAX,J,KSCOUNT,KBCOUNT,II,JJ,KFLAG,I
      LOGICAL DONE
      IF(ETA.GT.1.) THEN
```

```
         M1=1.
         M2=1.
      ELSE
         M1=-1.
         M2=1.
      END IF
      L= M1*M2
      ****************************************
      **THE FOLLOWING DO LOOP CALCULATES ALL EIGHT**
      **RADAR SPECTRAL COEFFICIENTS*****************
      ****************************************
      DO 710 TT5 = -3,4
        EC = ETACOUNT + TT5*2
        ANGLE = 0.
        CALL WAVNUM(D,K0,K2,ANGLE,K1,ETA,M1,M2)
        DONE = .FALSE.
        II = 0
        DO WHILE( .NOT. DONE)
          II = II+1
          IF(K1.GE.BAND(II).AND.K1.LT.BAND(II+1)) DONE=.TRUE.
        END DO
        KFLAG = II
500     COUNT = 1
        KCOUNT = KFLAG
        DO WHILE ((KFLAG.EQ.KCOUNT).AND.(ANGLE.LE.180.))
390       CALL COPCOF(D,K0,K2,ANGLE,K1,ETA,L,EL,HY,GAMSQR,THETA1)
          CALL JACMOD(D,K0,K2,ANGLE,K1,JAC,L)
```

```
      KERNAL1 = GAMSQR*JAC*(K1**1.5)*(1/(K2**4.))*(8./PI)
      DO 450 N=0,2
        SUMA(N+1) = 0.
        SUMANEG(N+1) = 0.
        IF(N.EQ.0)GOTO 400
        SUMB(N) = 0.
        SUMBNEG(N) = 0.
400     DO 430 L1=0,2
          ANGFACT1 = COSD(N*ANGLE) * COSD(L1*THETA1)
          ANGFACT2 = SIND(N*ANGLE) * SIND(L1*THETA1)
          KERN = (M1**N)*(M2**L1)*KERNAL1
          KERNNEG = ((-M1)**N)*((-M2)**L1)*KERNAL1
          DO 425 P=0,4
            INTGNDA = CANLPT1(N,L1,P,TT5)*ANGFACT1 +
     &                CANLPT2(N,L1,P,TT5)*ANGFACT2
            SUMA(N+1) = SUMA(N+1)+INTGNDA*KERN
            SUMANEG(N+1) = SUMANEG(N+1)+INTGNDA*KERNNEG
            IF(N.EQ.0.) GOTO 425
            INTGNDB=CBNLPT1(N,L1,P,TT5)*ANGFACT1+
     &      CBNLPT2(N,L1,P,TT5)*ANGFACT2
            SUMB(N) = SUMB(N)+INTGNDB*KERN
            SUMBNEG(N) = SUMBNEG(N)+INTGNDB*KERNNEG
425       END DO
430     END DO
        INTMATRIX(N+1,COUNT) = SUMA(N+1)
        INTMATRIXNEG(N+1,COUNT) = SUMANEG(N+1)
        IF(N.EQ.0)GO TO 450
```

```
            INTMATRIX(N+3,COUNT) = SUMB(N)
            INTMATRIXNEG(N+3,COUNT) = SUMBNEG(N)
450         END DO
            COUNT = COUNT + 1
            ANGLE=ANGLE+1.
            CALL WAVNUM(D,K0,K2,ANGLE,K1,ETA,M1,M2)
            DONE = .FALSE.
            JJ = 0
            DO WHILE( .NOT. DONE)
              JJ = JJ+1
              IF(K1.GE.BAND(JJ).AND.K1.LT.BAND(JJ+1)) DONE=.TRUE.
            END DO
            KFLAG = JJ
          END DO
          DO 705 N = 0,2
            MC = (KCOUNT - 1)*5 +(N+1)
            COFSUMA = 0.
            COFSUMAN = 0.
            IF(N.EQ.0)GO TO 480
            COFSUMB = 0.
            COFSUMBN = 0.
480         DO 700 J = 2,COUNT-2
              COFSUMA = INTMATRIX(N+1,J) + COFSUMA
              COFSUMAN = INTMATRIXNEG(N+1,J)+COFSUMAN
              IF(N.EQ.0) GOTO 700
              COFSUMB = INTMATRIX(N+3,J)+COFSUMB
              COFSUMBN = INTMATRIXNEG(N+3,J)+COFSUMBN
```

```
700       END DO
          MATRIX(EC,MC)=H/2.*(INTMATRIX(N+1,1)+
     &    INTMATRIX(N+1,COUNT-1)+2.*COFSUMA)
          MATRIX(EC+1,MC)=H/2.*(INTMATRIXNEG(N+1,1)+
     &    INTMATRIXNEG(N+1,COUNT-1)+2.*COFSUMAN)
          IF(N.EQ.0)GOTO 705
          MATRIX(EC,MC+2)=H/2.*(INTMATRIX(N+3,1)+
     &    INTMATRIX(N+3,COUNT-1)+2.*COFSUMB)
          MATRIX(EC+1,MC+2)=H/2.*(INTMATRIXNEG(N+3,1)+
     &    INTMATRIXNEG(N+3,COUNT-1)+2.*COFSUMBN)
705     END DO
        IF(ANGLE.GT.180.) GOTO 710
        GOTO 500
710   END DO
      RETURN
      END
      ***********************************************
      ***********************************************

      ***********************************************
      **THE FOLLOWING SUBROUTINE GIVES THE**********
      **SOLUTION TO THE DELTA FUNCTION CONSTRAINT***
      **WHICH DETERMINES THE VALUE OF K1 TO BE******
      **PASSED TO THE COUPLING COEFFICIENT**********
      **ROUTINE (COPCOF).  ALSO PASSED IS L.********
      **THE NEWTON-RAPHSON METHOD IS USED***********
      ***********************************************
```

```
      SUBROUTINE WAVNUM(D,K0,K2,ANGLE,K1,ETA,M1,M2)
      ********************************************
      **DECLARE VARIABLES***************************
      ********************************************
      IMPLICIT NONE
      REAL Y,GY,DERIVG, A,B,C,ETA
      REAL M1,M2,PI,K0,X,Z,Z1,T
      REAL TINY,X1,X2,X3,X5,X6,X7,X8
      REAL*8 K1,K2,ANGLE,P,D,Y1
      ********************************************
      **AS AN INITIAL GUESS WE USE THE FOLLOWING****
      **VALUE OF 'TINY'.  THIS VALUE HAS PROVIDED***
      **THE NECESSARY CONVERGENCE FOR ALL VALUES****
      **OF NORMALIZED FREQUENCY*********************
      ********************************************
      TINY = 0.001
      K1=(ABS(1.-ABS(ETA)))**2
      Y=SQRT(K1)
      T=Y
10    IF(Y.LT.0)THEN
         T=-Y
      ELSE
         T=Y
      END IF
      X=(TANH(D*T**2))**0.5
      X1=(TANH(D))**.5
      IF ((D*T**2).GT.20.) THEN
```

```
  X2=0.
ELSE
  X2=(T**2)*D*(1./COSH(D*T**2)**2)
END IF
X3=X*X1
K2=(T**4 +2.*(T**2)*COSD(ANGLE)+1.)**.5
X5=(T**4 +2.*(T**2)*COSD(ANGLE)+1.)**.25
IF (Y.GT.0) THEN
  X6=((T**3.)+(T*COSD(ANGLE)))
ELSE
  X6=-((T**3.)+(T*COSD(ANGLE)))
END IF
X7=SQRT(TANH(D*K2))
IF ((D*K2).GT.80.)THEN
  X8=0.
ELSE
  X8=(1./COSH(D*K2))**2.
END IF
*********************************************
**'GY' IS THE FUNCTION 'ETA - H(Y,THETA,D)'***
**OF THE TEXT**********************************
*********************************************
GY=ETA-(M1*Y*X/X1)-(M2*X5*X7/X1)
*********************************************
**'DERIVG' IS THE DERIVATIVE OF GY************
*********************************************
DERIVG=-(M1*X/X1)-(M1*X2/X3)-(M2*X6*X7/(X1*X5**3))
```

```
     &          -(M2*X6*X8/(X5*X7*X1))
        Y1=Y-(GY/DERIVG)
        IF (ABS(Y1-Y).LT.TINY) THEN
          GOTO 50
        ELSE
          Y=Y1
          GOTO 10
        END IF
50      CONTINUE
        K1 = Y1**2
        RETURN
        END
        ***********************************************
        ***********************************************

        ***********************************************
        **THIS SUBROUTINE CALCULATES THE COUPLING*****
        **COEFFICIENT AND THE SQUARE OF ITS MODULUS***
        ***********************************************
        SUBROUTINE COPCOF(D,K0,K2,ANGLE,K1,ETA,L,EL,HY,
     &                    GAMSQR,THETA1)
        ***********************************************
        **DECLARE VARIABLES**************************
        ***********************************************
        IMPLICIT NONE
        REAL ETA,B,C,DN,E,F,G,H,I,J1,J2,J3,L,M,N,O,REL(291)
        REAL DEPTH(291),POS,EL,P,Q,R,S,S2,T1,T2
```

```
REAL ABSGAM,GAMSQR,K,KO,DE,PI,S3,S4,S5,I1,HY
REAL AL
REAL*8 DEP,ANGLE,THETA,THETA1,THETA2,ALPHA,K1,K2
REAL*8 SQRMAX,Z,Z2,D,ARG
COMPLEX*8 GAMEM,GAMHY,GAM
THETA = ANGLE
DEP=D
**********************************************
**THETA,THETA1,THETA2 ARE ANGLES BETWEEN K1***
**AND KO, K2 AND KO, AND K1 &K2 RESPECTIVELY**
**********************************************
ARG=(-1.+K1**2+K2**2)/(2.*K1*K2)
IF(ABS(ARG).LT..005)THEN
  ARG = 0.
ELSE
  IF(ARG.GT.1.)THEN
ARG = 1.
  ELSE
    IF(ARG.LT.-1.)THEN
      ARG = -1.
    END IF
  END IF
END IF
ALPHA=DACOSD(ARG)
THETA2=180.-ALPHA
IF((THETA.GE.0.).AND.(THETA.LE.180.)) THEN
  THETA1=180.+THETA-ALPHA
```

```
ELSE
  THETA1 = -180.+ALPHA+THETA
END IF
C=K1*DCOSD(THETA)
DN=K2*DCOSD(THETA1)
E=K1*K2*DCOSD(THETA2)
G=C*DN
H=2*E
IF(E.GE.0)THEN
  F=SQRT(E)
**********************************************
**THE NUMERICAL VALUES IN THE NEXT TWO STEPS**
**ACCOUNT FOR THE NORMALIZED IMPEDANCE********
**********************************************
  I=F-0.0055
  B=0.006
  Z=(G-H)*I/(2*(I**2+B**2))
  Z2=(H-G)*B/(2*(I**2+B**2))
**********************************************
**'GAMEM' IS THE ELECTROMAGNETIC COUPLING ****
**COEFFICIENT*********************************
**********************************************
  GAMEM=DCMPLX(Z,Z2)
ELSE
  POS = ABS(E)
  F = SQRT(POS)
  I1 = F + .006
```

```
      AL = .0055
      Z = (H-G)*AL/(AL**2 + I1**2)
      Z2 = (H-G)*I1/(AL**2 + I1**2)
      GAMEM = DCMPLX(.5*Z,.5*Z2)
    END IF
    EL = CABS(GAMEM)
    ***********************************************
    **J1 AND J2 ARE DEEP WATER EQUIVALENTS OF K1**
    **AND K2.  WE NOW GET THE HYDRODYNAMIC********
    **PORTION OF COUPLING COEFFICIENT(GAMHY)******
    ***********************************************
    J1=K1*TANH(K1*DEP)
    J2=K2*TANH(K2*DEP)
    J3=SQRT(J1*J2)
    IF ((K1*DEP).GT.25.) THEN
      M=0
    ELSE
      M=(1/DSINH(K1*DEP))**2.
    END IF
    IF ((K2*DEP).GT.25.) THEN
      N=0
    ELSE
      N=(1/DSINH(K2*DEP))**2.
    END IF
    O=TANH(DEP)
    P=ETA**2
    R=1-P
```

```
Q=(1+P)/R
S=J1+J2
S2=L*(J1*J2-E)
S3=(S2*Q)/SQRT(J1*J2)
S4=SQRT(J1)+L*SQRT(J2)
S5=((J1**1.5)*M+L*(J2**1.5)*N)/(O*R)
T1= S+S3-S4*S5
T2= T1*(-.5)
GAMHY=DCMPLX(0.,T2)
HY = CABS(GAMHY)
*********************************************
**TOTAL COEFFICIENT (GAM) IS ELECTROMAGNETIC**
***+ HYDRODYNAMIC PARTS************************
*********************************************
GAM = GAMEM + GAMHY
ABSGAM = CABS(GAM)
GAMSQR = ABSGAM**2
RETURN
END
*********************************************
*********************************************

*********************************************
**HERE THE PARTIAL DERIVATIVE EXPRESSION******
**OCCURRING IN THE SECOND-ORDER INTEGRAND*****
**IS CALCULATED*******************************
*********************************************
```

```
SUBROUTINE JACMOD(D,K0,K2,ANGLE,K1,JAC,L)
**********************************************
**DECLARE VARIABLES*****************************
**********************************************
IMPLICIT NONE
REAL*8 Y,D,THETA,L,E1,E2,E3,E4,E5,E6,K2,K1,JAC
REAL*8 JAC1,ANGLE
REAL K0,U
Y=K1**.5
**********************************************
**MODULARIZE THE DERIVATIVE EXPRESSION********
**(I.E. JAC)***********************************
**********************************************
E1 = (TANH(D))**.5
E2 = (TANH((Y**2.)*D))**.5
IF(((Y**2.)*D).LT.25.) THEN
  E3 = (Y**2.)*D*(1/COSH((Y**2.)*D))**2.
ELSE
  E3 = 0.
END IF
E4 = L*((Y**3.)+(Y*COSD(ANGLE)))/(K2**1.5)
E5 = (TANH(K2*D))**.5
IF((K2*D).LT.25.) THEN
  E6 = K2*D*(1/COSH(K2*D))**2.
ELSE
  E6 = 0.
END IF
```

```
      JAC1 = E1/(E2 +(E3/E2) + E4*(E5 + (E6/E5)))
      JAC = ABS(JAC1)
      RETURN
      END
*********************************************
*********************************************

*********************************************
**THE FOLLOWING ROUTINE CONSISTS OF MODULES***
**REQUIRED TO EVALUATE THE 'CANLPT'S' AND*****
**'CBNLPT'S' OF THE MAIN EQUATION. THESE******
**MODULES ARE: (1) SNLP MODULE****************
***************(2) BEMCOF MODULE**************
***************(3) BRAGG.DAT******************
*********************************************
      SUBROUTINE CNLPT(CANLPT1,CANLPT2,CBNLPT1,CBNLPT2,
     &            U,ALPHASTAR,PHI)
*********************************************
**DECLARE VARIABLES***************************
*********************************************
      IMPLICIT NONE
      REAL SNLP, PHI,BEMCOF,GTPC(0:4,0:4),GTPS(0:4,0:4)
      REAL SNLP1(0:2,0:2,0:4),SNLP4(0:2,0:2,0:4)
      REAL SNLP6(0:2,0:2,0:4),SNLP7(0:2,0:2,0:4)
      REAL BRAGGCOF,AK1(0:2),BK1(0:2),CANLPT1(0:2,0:2,0:4,-4:4)
      REAL CANLPT2(0:2,0:2,0:4,-4:4),CBNLPT1(0:2,0:2,0:4,-4:4)
      REAL CBNLPT2(0:2,0:2,0:4,-4:4),U,ALPHASTAR
```

```
INTEGER N,L1,P,T,T5,I
CALL SNLP(SNLP1,SNLP4,SNLP6,SNLP7, PHI)
CALL BEMCOF(GTPC,GTPS)
*********************************************
**WE ARE NOW IN POSITION TO FIND THE**********
**CANLPT'S & CBNLPT'S.  BRAGG.DAT CONTAINS****
**THE SPECTRAL COEFFICIENTS OF THE BRAGG******
**WAVE OBTAINED FROM THE FIRST-ORDER PORTION**
**OF THE RADAR SPECTRUM.  THE ROUTINE WHICH***
**GIVES THESE, IS THE SAME IN APPROACH AS*****
**THAT PRESENTED HERE FOR SECOND-ORDER WITH***
**THE LESS COMPLEX FIRST-ORDER CROSS-SECTION**
**REPLACING THE SECOND-ORDER.*****************
*********************************************
OPEN(UNIT=54,NAME='BRAGG.DAT',TYPE='OLD')
DO I = 0,2
  READ(54,*) AK1(I)
END DO
DO I = 0,2
  IF(I.EQ.0)THEN
    BK1(I)=0.
  ELSE
    READ(54,*) BK1(I)
  END IF
END DO
CLOSE(54)
DO N = 0,2
```

```
      DO L1 = 0,2
        DO P = 0,4
          DO T = -4,4
            IF(T.LT.0)THEN
              T5 =-T
              CANLPT1(N,L1,P,T) =  (GTPS(T5,P)*BK1(L1)*
     &                              SNLP4(N,L1,P))
              CANLPT2(N,L1,P,T) = -(GTPS(T5,P)*BK1(L1)*
     &                              SNLP7(N,L1,P))
              CBNLPT1(N,L1,P,T) = (GTPS(T5,P)*AK1(L1)*
     &                             SNLP7(N,L1,P))
              CBNLPT2(N,L1,P,T) = -(GTPS(T5,P)*AK1(L1)*
     &                              SNLP4(N,L1,P))
            ELSE
              CANLPT1(N,L1,P,T) = (GTPC(T,P)*AK1(L1)*
     &                             SNLP1(N,L1,P))
              CANLPT2(N,L1,P,T) = (GTPC(T,P)*AK1(L1)*
     &                             SNLP6(N,L1,P))
              CBNLPT1(N,L1,P,T) = (GTPC(T,P)*BK1(L1)*
     &                             SNLP6(N,L1,P))
              CBNLPT2(N,L1,P,T) = (GTPC(T,P)*BK1(L1)*
     &                             SNLP1(N,L1,P))
            END IF
          END DO
        END DO
      END DO
    END DO
```

```
RETURN
END
**********************************************
**********************************************

**********************************************
**SUBROUTINE TO CALCULATE THE PHI INTEGRAL****
**COMPONENTS*********************************
**********************************************
SUBROUTINE SNLP(SNLP1,SNLP4,SNLP6,SNLP7, PHI)
**********************************************
**DECLARE VARIABLES**************************
**********************************************
IMPLICIT NONE
REAL A,B,C,D,T1,T2,T3,T4, PHI
REAL SNLP1(0:2,0:2,0:4),SNLP4(0:2,0:2,0:4)
REAL SNLP6(0:2,0:2,0:4),SNLP7(0:2,0:2,0:4)
INTEGER N,L1,P
DO 10 N = 0.,2.,1.
  DO 20 L1 = 0.,2.,1.
    DO 30 P = 0.,4.,1.
      T1=N+L1+P
      T2=L1+P-N
      T3=N+P-L1
      T4=N+L1-P
      IF(T1.EQ.0) THEN
        A =  PHI*ACOS(-1.)/180.
```

```
            ELSE
              A = (SIND(T1* PHI))/T1
            END IF
            IF(T2.EQ.0) THEN
              B =  PHI*ACOS(-1.)/180.
            ELSE
              B = (SIND(T2* PHI))/T2
            END IF
            IF(T3.EQ.0) THEN
              C =  PHI*ACOS(-1.)/180.
            ELSE
              C = (SIND(T3* PHI))/T3
            END IF
            IF(T4.EQ.0) THEN
              D =  PHI*ACOS(-1.)/180.
            ELSE
              D = (SIND(T4* PHI))/T4
            END IF
            SNLP1(N,L1,P) = .5*(A+B+C+D)
            SNLP4(N,L1,P) = .5*(-A-B+C+D)
            SNLP6(N,L1,P) = .5*(-A+B+C-D)
            SNLP7(N,L1,P) = .5*(-A+B-C+D)
30        CONTINUE
20      CONTINUE
10    CONTINUE
      RETURN
      END
```

```
**********************************************
**********************************************

**********************************************
**THIS ROUTINE SUPPLIES THE FOURIER***********
**COEFFICIENTS OF THE BEAM PATTERN.  THE******
**FILES OPENED BELOW CONTAIN THE FOURIER******
**COEFFICIENTS OF THE 4-ELEMENT CODAR*********
**WHICH ARE CALCULATED EXTERNAL TO THIS*******
**PROGRAM ACCORDING TO THE FORMULAE DERIVED***
**IN THE TEXT*********************************
**********************************************
SUBROUTINE BEMCOF(GTPC,GTPS)
**********************************************
**DECLARE VARIABLES****************************
**********************************************
IMPLICIT NONE
REAL GTPC(0:4,0:4),GTPS(0:4,0:4)
INTEGER T,P,T1,P1
OPEN(UNIT=10,NAME='COSCOS.OUT',TYPE='OLD')
OPEN(UNIT=15,NAME='SINSIN.OUT',TYPE='OLD')
DO T = -4,5
  IF(T.LE.0) THEN
    READ(15,*) (GTPS(T+4,P),P=0,4)
  ELSE
    IF(T.GT.0) THEN
      READ(10,*) (GTPC(T-1,P),P=0,4)
```

```
    END IF
  END IF
END DO
CLOSE(10)
CLOSE(15)
RETURN
END
************************************************
************************************************

************************************************
**THE FOLLOWING IS A DATA ROUTINE CONTAINING**
**THE INPUT PARAMETERS REQUIRED BY THE********
**PARENT PROGRAM******************************
************************************************
SUBROUTINE DATA(DEPTH,U,ALPHASTAR,PHI,NB)
IMPLICIT NONE
REAL U,ALPHASTAR,PHI
REAL*8 DEPTH
INTEGER NB
OPEN(UNIT=100,NAME='DATAFILE.DAT',TYPE='OLD')
READ(100,*) DEPTH,U,ALPHASTAR,PHI,NB
CLOSE(100)
RETURN
END
```

Appendix D

Creation of the Four-element Square Array Cross Sections from Measured Data

The general procedure for obtaining radar cross sections from measured data given by Lipa and Barrick (1983) is here applied to the four-element square array. A rigorous analysis of the method depends upon the result shown by Barrick and Snider (1977) that the HF sea-echo signal voltages impinging on each element are zero-mean Gaussian random variables. The first step in the procedure is to Fourier transform the voltage time series from each of the four sensors to give frequency spectra, $V(\omega)$. We define the n^{th} sample voltage of such a process for the j^{th} sensor by

$$ {}_nV_j(\omega) = {}_nV_{x_j}(\omega) + i_nV_{y_j}(\omega) \tag{D.1} $$

where $V_{x_j}(\omega)$ and $V_{y_j}(\omega)$ are the real and imaginary parts respectively of $V_j(\omega)$. After Lipa and Barrick (1983), the N-sample-averaged cross spectrum between the j^{th} and ℓ^{th} elements is defined by

$$ {}_NC_{j\ell}(\omega) = \frac{1}{N}\sum_{n=1}^{N} {}_nV_j(\omega)\,{}_nV_\ell^*(\omega) \tag{D.2} $$

where ${}_nV_\ell^*(\omega)$ is the complex conjugate of the n^{th} sample voltage on the ℓ^{th} element i.e.

$$ {}_nV_\ell^*(\omega) = {}_nV_{x_\ell}(\omega) - i_nV_{y_\ell}(\omega)\ . \tag{D.3} $$

For a planar array of P elements, the wide beam cross section (${}_N\sigma(\omega,\psi)$) produced from the cross spectra of equation (D.2) is given in the above reference by

$$ {}_N\sigma(\omega,\psi) = \frac{1}{P^2}\sum_{j=1}^{P}\sum_{\ell=1}^{P} {}_NC_{j\ell}(\omega)e^{-i\vec{k}_\psi\cdot(\vec{r}_j-\vec{r}_\ell)} \; . \tag{D.4} $$

Here, ψ is the scan angle, $\vec{r}_j$ is the position vector of the j^{th} sensor from an arbitrarily chosen reference point and $\vec{k}_\psi$ is the vector defined by

$$ \begin{aligned} \vec{k}_\psi &= (k_0\cos(\psi))\hat{\imath} + (k_0\sin(\psi))\hat{\jmath} \\ &= k_x\hat{\imath} + k_y\hat{\jmath} \end{aligned} \tag{D.5} $$

where $\hat{\imath}$ and $\hat{\jmath}$ are unit vectors in the usual sense and k_0 is the radar wavenumber. By choosing the reference point of the array to be its geometrical centre, we are able to write that $|\vec{r}_1| = |\vec{r}_2| = \cdots = |\vec{r}_P| = r$. Figure 3, p. 23 of the thesis shows the relationships between these various quantities for the four-element square array.

Using the facts that for q complex numbers $Z_1,\ldots,Z_q$, $(Z_1\cdot Z_2\cdot\ldots\cdot Z_q)^* = Z_1^*\cdot Z_2^*\ldots\cdot Z_q^*$ and $(Z_1+Z_2+\ldots+Z_q)^* = Z_1^*+Z_2^*+\ldots+Z_q^*$, it is simple to show that

$$ {}_NC_{j\ell}(\omega) = {}_NC_{\ell j}^*(\omega) \; . \tag{D.6} $$

Then, carrying out the necessary complex algebra, for an array with $P=4$, equation (D.4) becomes

$$ \begin{aligned} {}_N\sigma(\omega,\psi) &= \frac{1}{16}\sum_{j=1}^{4} {}_NC_{jj}(\omega) + \frac{1}{8}\mathrm{Re}\left[{}_NC_{12}(\omega)e^{ir(-k_x+k_y)}\right. \\ &\quad + {}_NC_{13}(\omega)e^{i(2rk_y)} + {}_NC_{14}(\omega)e^{ir(k_x+k_y)} + {}_NC_{23}(\omega)e^{ir(k_x+k_y)} \\ &\quad \left. + {}_NC_{24}(\omega)e^{i(2rk_x)} + {}_NC_{34}(\omega)e^{ir(k_x-k_y)}\right] \; . \end{aligned} \tag{D.7} $$

The form of equation (D.7) lends itself to simple programming. The result expresses the radar cross section of the four-element square array and may be used to develop the radar spectral coefficients of Sections 2.3 and 2.4 which are required for extraction of ocean wave information from sea echo.